UNIVERSIDAD COMPLUTENSE DE MADRID
FACULTAD DE CIENCIAS QUÍMICAS
Departamento de Química Física

TESIS DOCTORAL

Synthesis and Assembly of Uniform Plasmonic Gold Nanostructures for Biomedical Applications

Síntesis y ensamblaje de nanoestructuras plasmónicas de oro uniformes para aplicaciones en biomedicina

MEMORIA PARA OPTAR AL GRADO DE DOCTOR

PRESENTADA

Guillermo González Rubio

Directores

Andrés Guerrero Martínez

Luis M. Liz Marzán

Madrid, 2018

Universidad Complutense de Madrid
Facultad de Ciencias Químicas
Departamento de Química Física I

Synthesis and Assembly of Uniform Plasmonic Gold Nanostructures for Biomedical Applications

Síntesis y Ensamblaje de Nanoestructuras Plasmónicas de Oro Uniformes para Aplicaciones en Biomedicina

Memoria para optar al grado de Doctor presentada por

Guillermo González Rubio

Bajo la dirección de

Andrés Guerrero Martínez, Universidad Complutense de Madrid
Luis M. Liz Marzán, CIC biomaGUNE

Madrid 2017

Tesis Doctoral

Synthesis and Assembly of Uniform Plasmonic Gold Nanostructures for Biomedical Applications

Síntesis y Ensamblaje de Nanoestructuras Plasmónicas de Oro Uniformes para Aplicaciones en Biomedicina

Directores:

Andrés Guerrero Martínez

Investigador Ramón y Cajal

Departamento de Química Física I, Facultad de Ciencias Químicas

Universidad Complutense de Madrid

Luis M. Liz Marzán

Profesor de Investigación Ikerbasque

Asociación Centro de Investigación Cooperativa en Biomateriales, CIC biomaGUNE

Autor:

Guillermo González Rubio

Departamento de Química Física I, Facultad de Ciencias Químicas

Universidad Complutense de Madrid

CIC biomaGUNE

Madrid, 2017

Agradecimientos

Quiero mostrar mi agradecimiento a todas las personas que han participado directamente, aportando sus conocimientos, trabajo y esfuerzo, para que esta tesis se haya hecho realidad.

Especialmente quiero agradecer a mis directores, Luis M. Liz-Marzán y Andrés Guerrero, por haberme brindado la oportunidad de trabajar en con ellos, pero sobretodo porque no me imagino haber podido tener mejores "padres científicos". Por supuesto a Gloria Tardajos quiero darle las gracias por todos sus consejos y tan particulares discusiones.

Quiero también agradecer a todas aquellas personas que han estado conmigo todo este tiempo, amigos y compañeros, fuera y dentro del laboratorio que han hecho la vida mucho más interesante y divertida.

Finalmente, quiero dar mis mayores agradecimientos a aquellos que han estado siempre a mi lado y que me lo han dado todo: a mis padres, mi hermana y María.

Index

List of Most Used Abbreviations

AuNP: Gold nanoparticle

AuNR: Gold Nanorod

AuNS: Gold Nanosphere

CBED: Convergent Beam Electron Diffraction

EF: Enhancement factor

HAADF-STEM: High Angle Annular Dark Field Scanning Transmission Electron Microscopy

LSPR: Localized surface plasmon resonance

NP: Nanoparticle

NIR: Near Infrared Region

SEM: Scanning electronic microscopy

SERS: Surface enhanced Raman scattering

SPP: Surface plasmon polariton

TEM: Transmission electronic microscopy

UPD: under potential deposition

UV-Vis-NIR: Ultraviolet–visible–near infrared

Scope

This thesis work has been carried out in the framework of the project "Reproducible Synthesis and Assembly of Plasmonic Nanostructures for Theranostics (MAT2013-46101-R)", which is focused on the development of novel approaches for the fabrication of plasmonic nanostructures whose optical properties could be used for the simultaneous diagnosis and treatment of various human diseases. More specifically, the thesis was oriented toward several aspects of the fabrication of plasmonic nanostructures and their application into health care: (i) synthesis of uniform plasmonic nanoparticles with tailored optical features; (ii) functionalization with molecules of biological interest; (iii) self-assembly into plasmonic superstructures; and (iv) evaluation of the behavior of nanostructures in biological systems.

In order to achieve such tasks, the thesis was divided in two distinctive but complementary approaches:

- Optimization of the synthesis of plasmonic nanoparticles via colloidal methods for efficient self-assembly, and their application in biological sensing (Chapters 2 and 3).
- Implementation of ultrafast pulse lasers (Chapter 4) as a novel approach to improve NP self-assembly (Chapters 5) and their application to plasmonic photothermal therapy (Chapter 6).

The experimental part was carried out both at the Supramolecular Chemistry Group at the Complutense University of Madrid (UCM) and at the BioNanoPlasmonics Laboratory of CIC biomaGUNE, in San Sebastián. Additionally, part of the results, such as theoretical modeling, ultrafast lasing experiments, and electron microscopy characterization of our systems, arise from external collaborations that invariably contributed to enhance the quality of the research.

As a result the thesis was structured into seven chapters, which are briefly outlined in what follows:

In Chapter 1, we introduce the main concepts that will be addressed throughout the thesis. Initially, we focus on presenting a broad overview of the plasmonic properties of metal nanoparticles, introducing the importance of the assembly to obtain novel optical features, and their use in surface enhanced Raman scattering (SERS) spectroscopy. We continue with a brief

description of the seeded growth method for the synthesis of gold nanoparticles. We then move into the directed self-assembly of gold nanoparticles to produce plasmonic structures with novel optical properties.

Then, in Chapter 2, we demonstrate the development of an optimized synthetic approach for the synthesis of monodisperse gold nanospheres, which are rationally functionalized to obtain large scale pyramidal supercrystals via templated self-assembly.

We describe in Chapter 3 the synthesis and functionalization of gold nanorods to immobilize a model synthetic bacterial prionoid, with the aim of studying the amyloidogenic process of the protein and the formation of the very first oligomers, prior to fibrillation.

Next, in Chapter 4 we provide an overview of fast and ultrafast pulse lasers as tools to induce diverse effects on plasmonic nanoparticles, such as reshaping, fragmentation and self-assembly, as well as the main underlying excitation-relaxation mechanisms.

Using a femtosecond pulse laser, in Chapter 5 we demonstrate control over the directed tip-to-tip self-assembly of gold nanorods, favoring the formation of dimers over other oligomers. Such light-controlled approach allows us to prepare welded species with optical properties in the NIR.

Finally, in Chapter 6 we focus on the directed self-assembly of gold nanorods inside lysosomes of model cancer cells, which allows us to significantly reduce the femtosecond laser power density that is necessary for achieving efficient plasmonic photothermal therapy.

In summary, the thesis presents significant advancements in the synthesis, functionalization and self-assembly of different plasmonic nanostructures with the potential of being used for diagnosis and treatment of human diseases, such as Alzheimer’s and cancer. Furthermore, the use of ultrafast pulse lasers has been proven as a valuable tool to improve assembly aspects for plasmonic gold nanostructures, thereby opening new perspectives that will be dealt with in our future research.

CHAPTER 1

General Introduction

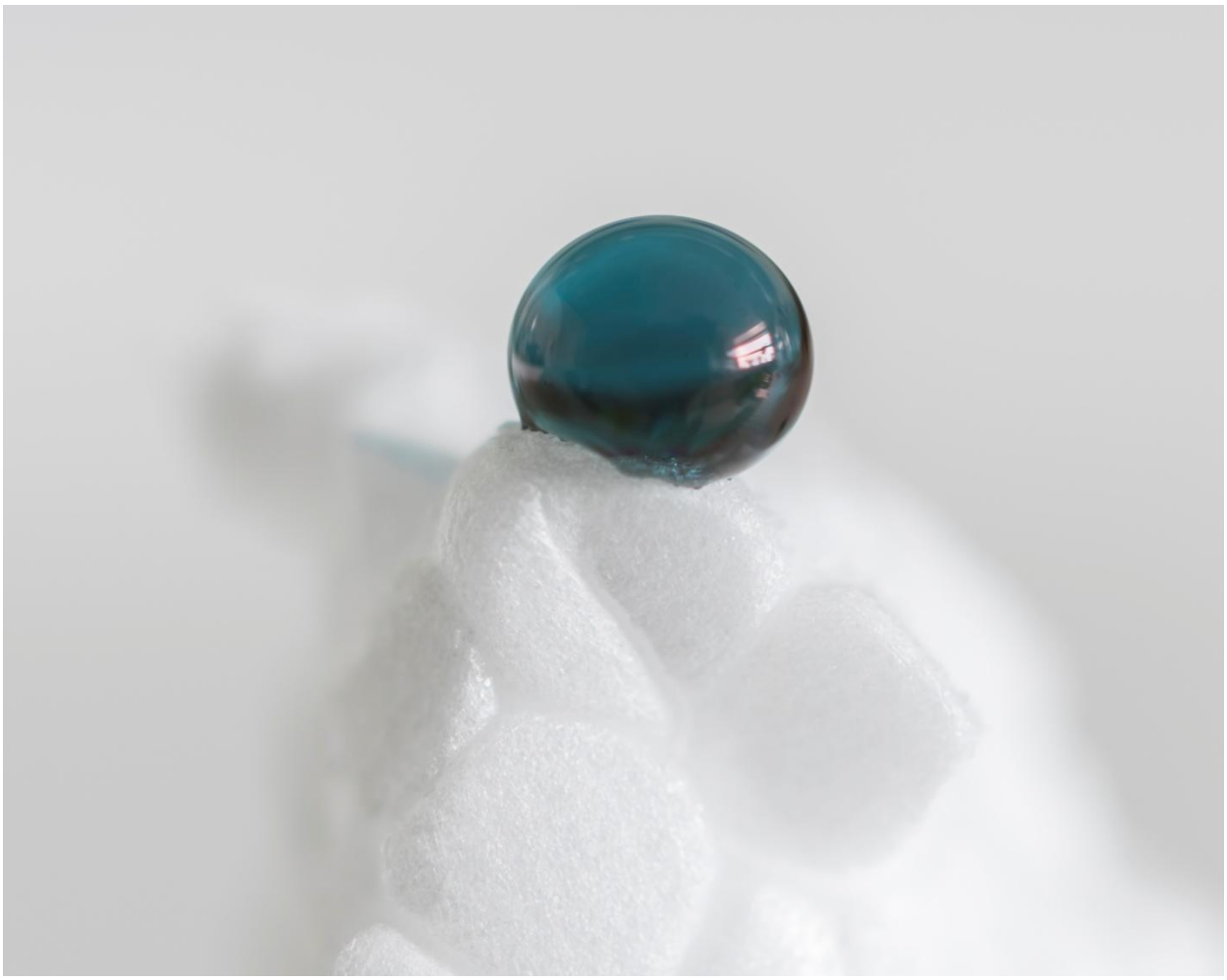

NANOTECHNOLOGY AND THE NANOSCALE

Nanoscience and nanotechnology, fostered by the great potential toward unveiling the secrets that govern our mesocosmos, are expected to address knowledge gaps and provide groundbreaking solutions to many challenges that threaten our future, from energy harvesting, water treatment to human health.[1–5] The term "nano" is used to describe scientific areas and technologies that work with materials possessing at least one dimension of less than 100 nm. For instance, the US committee on Nanoscale Science, Engineering and Technology (NSET) defines nanotechnology as:[6]

"Research and technology development at the atomic, molecular or macromolecular levels, in the length scale of approximately 1-100 nanometer range, to provide a fundamental understanding of phenomena and materials at the nanoscale and to create and use structures, devices and systems that have novel properties and functions because of their small and/or intermediate size. The novel and differentiating properties and functions are developed at a critical length scale of matter typically under 100 nm. Nanotechnology research and development includes manipulation under control of the nanoscale structures and their integration into larger material components, systems and architectures. Within these larger scale assemblies, the control and construction of their structures and components remains at the nanometer scale. In some particular cases, the critical length scale for novel properties and phenomena may be under 1 nm (e.g., manipulation of atoms at ~0.1 nm) or be larger than 100 nm (e.g., nanoparticle reinforced polymers have the unique feature at ~ 200-300 nm as a function of the local bridges or bonds between the nano particles and the polymer)".

Consequently, nanoscience and nanotechnology refer to changes arising from the size of objects, as opposed to classical sciences and technologies, which are identified and classified depending on the specific objects, properties, processes, functions or areas of application. Although the space-relation of nanotechnology implies that it is universal, it was not until 1959 that physicist Richard Feynman introduced the notion of this particular "universe" in his lecture: "*There's plenty of room at the bottom*".[7] Suddenly, a new and unexplored scale was shown, allowing us to produce nanoscopic machines capable of self-replicating, manipulating individual atoms and molecules and, ultimately, ruling the macroscopic world ("*shaping the world atom by*

atom"). Therefore, he foresaw the miniaturization of well-known macroscopic entities and structures.

Eric Drexel and Norio Taniguchi were the first scientists who defined the term nanotechnology.[8,9] With the aim of shaping the definition, they envisioned the concepts of assemblers/disassemblers (nanomachinery capable of carrying out mechanical action to assemble and disassemble objects), replicators (copying mechanism), and nanocomputers (to control the assemblers/disassemblers and replicators).[8] Notwithstanding the strong scientific interest on the nanoscale, nanotechnology cannot be fostered by the simple fact of miniaturizing macroscopic entities and production of molecules and materials by maneuvering atoms. In fact, the above mentioned NSET definition already infers the importance of working at the mesoscale where novel properties and functionalities arise. The physicist Michael Rouke stated:[10]

"Scientists and engineers readily fashion nanostructures on a scale of one to a few hundred nanometers—small indeed, but much bigger than simple molecules. Matter at this mesoscale is often awkward to explore. It contains too many atoms to be easily understood by the straightforward application of quantum mechanics (although the fundamental laws still apply). Yet these systems are not so large as to be completely free of quantum effects; thus, they do not simply obey the classical physics governing the macroworld. It is precisely in this intermediate domain, the mesoworld, which unforeseen properties of collective systems emerge"

Therefore, the need for new properties when reducing the size could be visualized as a boundary between the realms of quantum and the bulk.[11] At the nanoscale, novel laws appear and the classical and hierarchical relation dependence between physics, chemistry and biology become diffuse. Truly, such frontiers never existed in nature and many of its materials and processes exist by extension from the nanoscale to the macroscale. For instance, the movement of some types of bacteria is based on flagella, which are small motors of 20-30 nm in diameter, and many plants possess superhydrophilic nanostructures that allow them to capture water (Figure 1).[12–14]

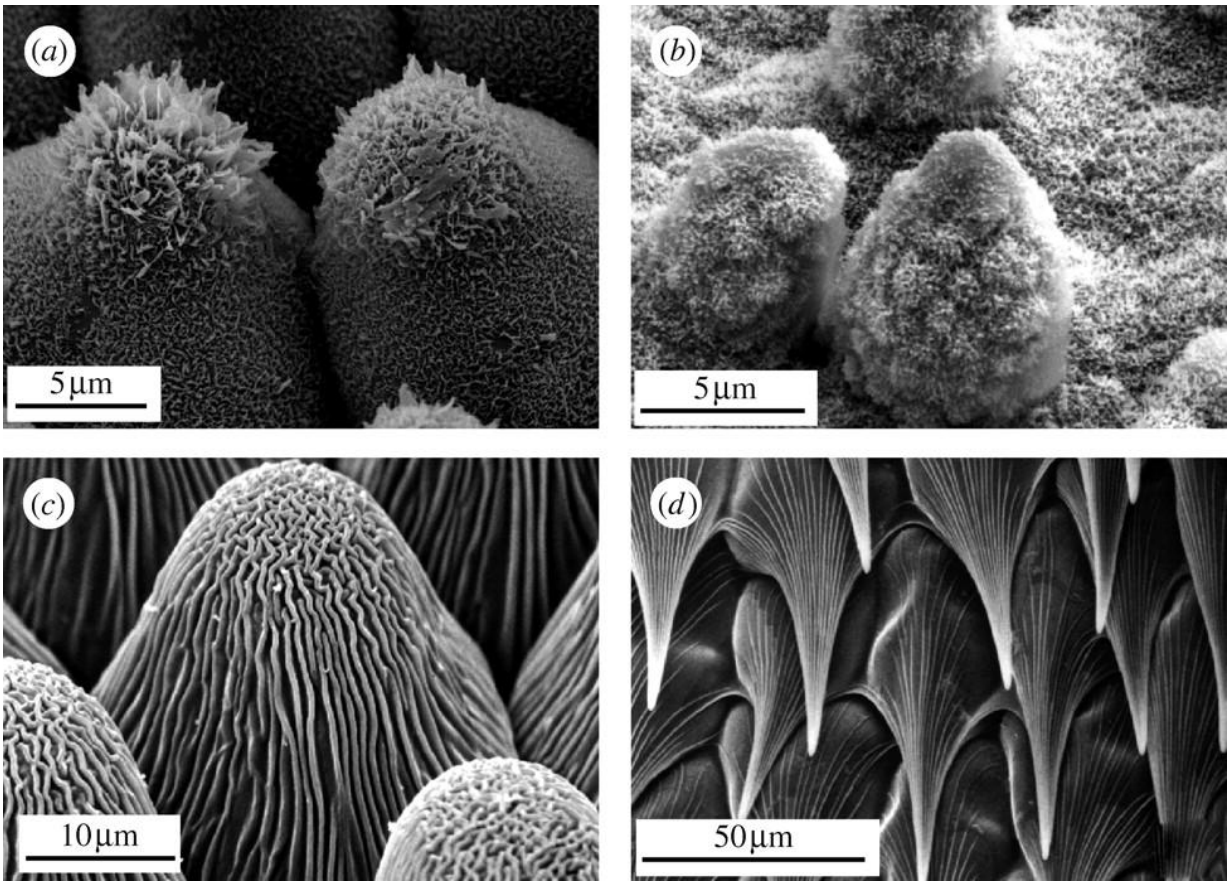

Figure 1. Scanning electron microscopy (SEM) images of hierarchical structures on plant surfaces. (a,b) Double structured plant surfaces with wax crystals on the leaf of (a) *Colocasia esculenta* and (b) *N. nucifera*. (c,d) Convex cells with cuticular folding. (c) The flower leaf of Rosa montana. (d) The cells of the inner side of a tube-like leaf of the carnivorous plant *Sarracenia leucophylla.* Adapted from ref [14].

Interestingly, although fulfilling different bio-functions, they are still based on the same principle: the organization of atoms into molecules and macromolecules, which self-assemble under certain physicochemical conditions, to build functional structures and larger systems with different levels of complexity. Consequently, the arrangement of chemical elements from atoms into one-, two- or three-dimensional complex structures (i.e. clusters, nanoparticles, molecules, amorphous or crystalline solids…) at the nanoscale, not only determines their electrical, optical and magnetic properties but also the behavior as building blocks for the construction of structures with large degree of intricacy.[15–18]

PROPERTIES AT THE NANOSCALE

Since the main subject of this thesis is represented by gold maneuvered at the nanoscale, we present in what follows an overview of its most important size-dependent solid state properties. Intuitively, the major impact of size reduction is observed on the fraction of atoms that are located at the surface with respect to the bulk, which may be explained on the basis of the scaling laws that govern the volume and the surface. They scale with the square and the cubic powers of the radius, respectively, which implies that for spherical particles constituted by 13 and 561 atoms, the relative number of surface atoms decreases from 92% to 45%, respectively (Figure 2).[19,20]

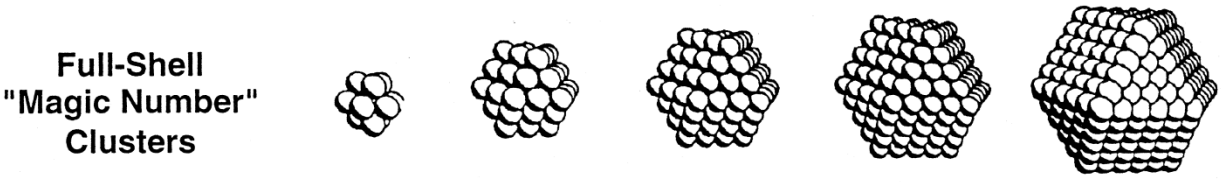

Number of shells	1	2	3	4	5
Number of atoms in cluster	M_{13}	M_{55}	M_{147}	M_{309}	M_{561}
Percentage surface atoms	92%	76%	63%	52%	45%

Figure 2. Idealized representation of hexagonal close-packed full-shell clusters. The fraction of surface atoms decreases as the number of atoms increases. Adapted from ref. [19].

In terms of thermodynamic stability, surface atoms possess poor coordination environment, which renders highly unfavorable binding energies between them. Therefore, considering that thermodynamic and mechanical properties of crystalline materials are determined by the binding energy, the volume-to-surface ratio plays a key role on melting entropy and melting point, Debye temperature, cohesive energy, diffusion activation energy, or amplitude of the thermal vibration, among others.[21–24] Generally, the observed trend points toward a decrease of these parameters according to particle size. Regarding the changes in the melting temperature, the phenomenon is known as *melting point depression*, which has been described for a wide range of materials, from metals to insulators.[21,22,25] Since the surface energy is always higher in the solid compared to the liquid phase, as the fraction of surface atoms

increases the contribution of the surface energy to the overall internal energy is incremented and the melting temperature decreases to compensate it. In the specific case of gold, the melting temperature of a 2 nm nanoparticle is around 700 °C, which is approximately 45% lower than that of the bulk.[26] Lower diffusion activation energies favor the mobility and rearrangement of atoms in the nanostructure (producing the reconstruction of the nanocrystal) and fuel Ostwald ripening effects (small crystal particles dissolve and redeposit onto larger crystals).[27,28] The intrinsic higher internal energy of the surface atoms is behind the catalytic properties and reactivity of many nanostructured materials.[19,29,30]

Nevertheless, changes of the binding energies also have a strong impact on the electronic structure of crystalline solids, inducing novel electrical, magnetic and optical properties of high technological interest. Since the total number of atoms in a nanocrystal is lower compared to the bulk, the density of electronic states is also lower. If we look at an electron confined in an atomic orbital, a physical region around the atomic nucleus, it has a certain discrete value of energy. On the other hand, in an extended solid, the electron is not anymore localized around a single nucleus, meaning that the certainty about its position has decreased. This fact occurs due to strong delocalization around the *n* atoms of the extended crystalline solid. In this case, the energy values are well defined but broadened due to the formation of a continuum of discrete bonding and antibonding molecular orbitals. Each atom added to the structure gives rise to the formation of a molecular orbital, which energy is dependent on its position in the crystal lattice, contributing to the band of energy states. Now, the nature of the atomic orbitals (*s*, *p*, *d*…) and their electron occupancy (empty, partially filled or filled) are translated into the electronic structure of the solid. In the case of alkaline metals, the solid electronic properties are determined by semifilled *s* orbitals, which implies that only half of the molecular orbitals are occupied at a temperature of 0 K. The limit between the highest occupied band (*valence band*) and the lowest unoccupied band (*conduction band*) defines in this case the Fermi level. The characteristic metallic behavior of alkaline elements results from the small energy difference between the conduction and valence band. On the other hand, the semiconductor behavior of elements such as silicon and selenium stems from the formation of a new band of forbidden energy states between the valence band and the conduction band (Figure 3a). The so-called *band gap* has energies up to 4 eV in the case of semiconductors and higher values in insulators.[18,31,32]

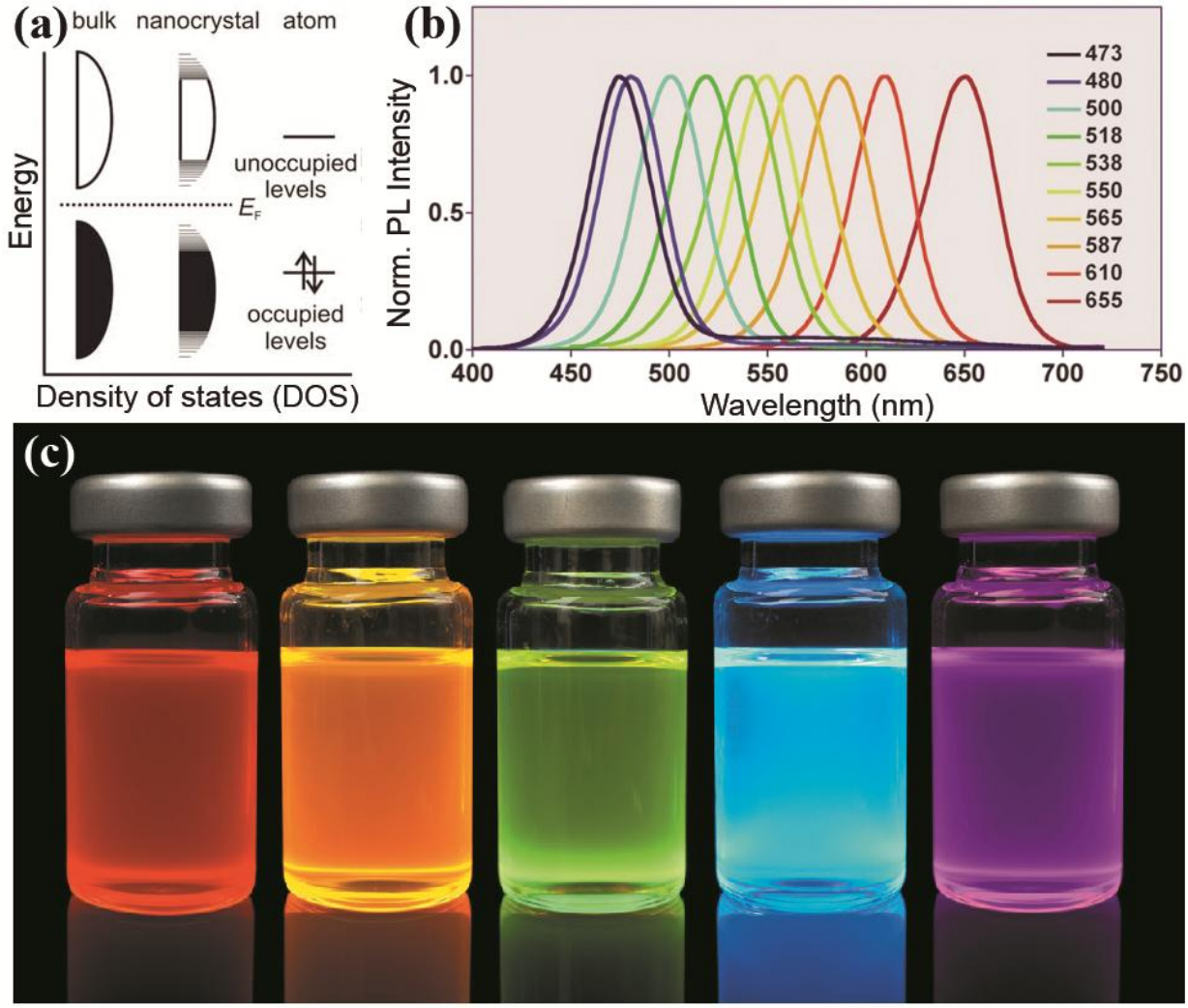

Figure 3. (a) Scheme of the density of states in semiconductors, as a function of their size. The dotted line represents the Fermi energy. Adapted from ref. [33]. (b) Quantum confinement effects on the photoluminescence of CdS quantum dots with sizes ranging from 2.1 to 7.5 nm. Adapted from ref. [34]. (c) Optical image of colloidal quantum dots with decreasing size (from left to right). Adapted from ref. [35].

In nanocrystals, due to the to the confinement of the electrons to few discrete energy levels, the electronic structure resembles what is observed in atoms and molecules with the existence of discrete energy levels (developing first at band edges) (Figure 3a). The scaling laws at which variation of electrical and optical properties are observed for any material is strongly dependent on the energy gap. In the case of semiconductors, where the Fermi level lies between the conduction and valence bands, the optical and electrical properties are dominated by the

edges of the bands, even at relatively large crystal sizes such as 500 nm. Undoubtedly, the most striking effect of size reduction and subsequent quantum confinement in semiconductors is observed on their optical properties: the number of electronic excitations is confined to a few transitions with a larger energy, and therefore the absorption and emission bands blueshift and get narrower (Figure 3b).[31,33,36–38] The intense luminescence properties, together with their tunability upon nanocrystal size and shape modification, are of particular interest for a wide range of applications, from electronic devices and photovoltaics to medicine (Figure 3c).[4,35,39,40]

In metals, where the band gap is negligible even at temperatures of few Kelvin, the optical and electrical properties remain closer to those of the bulk. On the other hand, certain nanosized metals show a unique optical behavior, which is probably one of the most important effects studied in nanotechnology: the emergence of *localized surface plasmons*.[41]

PLASMONIC PROPERTIES

This phenomenon is also related to the electronic structure and the strong delocalization of electrons. The response of a metallic material to an applied static electric field depends on the behavior of the free electrons, which displace toward the positive poles creating positive and negative net charges at the surface of the bulk.[42] Within this context, the permittivity ε is used to measure the response and polarization behavior (electronic, ionic and orientational polarization) of any material to an applied electric field (*Equation 1*). The relative permittivity, also known as dielectric constant ε_r (*Equation 2*), represents the permittivity of a dielectric relative to that of free space,[18]

$$P = \varepsilon_0(\varepsilon - 1)E \qquad \text{(Equation 1)}$$

$$\varepsilon_r = \varepsilon/\varepsilon_0 \qquad \text{(Equation 2)}$$

where ε_0 is the permittivity of vacuum. For insulators the relative permittivity is low, while metals possess high values, which means that electrostatic fields are strongly screened due to electronic polarization, giving rise to a low penetration depth inside the metal.[18]

The above statements are only correct for linear media, not exhibiting spatial or temporal dispersion. Since the interaction of metals with electromagnetic radiations is strongly dependent

on the frequency), the speed and magnitude of the electron response to the oscillating electromagnetic field require the use of complex functions (*Equation 3*).[18]

(*Equation 3*)

The real and imaginary components of the complex dielectric function are related to the refractive index n and the extinction coefficient κ of a material as follows:[18,43]

(*Equation 4*)

(*Equation 5*)

Generally, n dominates the real part of the dielectric function and it accounts for the changes in wavelength $\lambda = \lambda_0/n$ and phase velocity $v = c/n$ of the electromagnetic wave traveling through a medium, as compared with the wavelength λ_0 and speed c in vacuum. On the other hand, the extinction coefficient determines the imaginary part, which is linked to the absorption coefficient α of Beer's law $I(x) = I_0 e^{-\alpha L}$.[43] For example, gold is a metallic material that has high κ values, while transparent materials such as glass BK7 show low values of κ (Figure 4).[44,45]

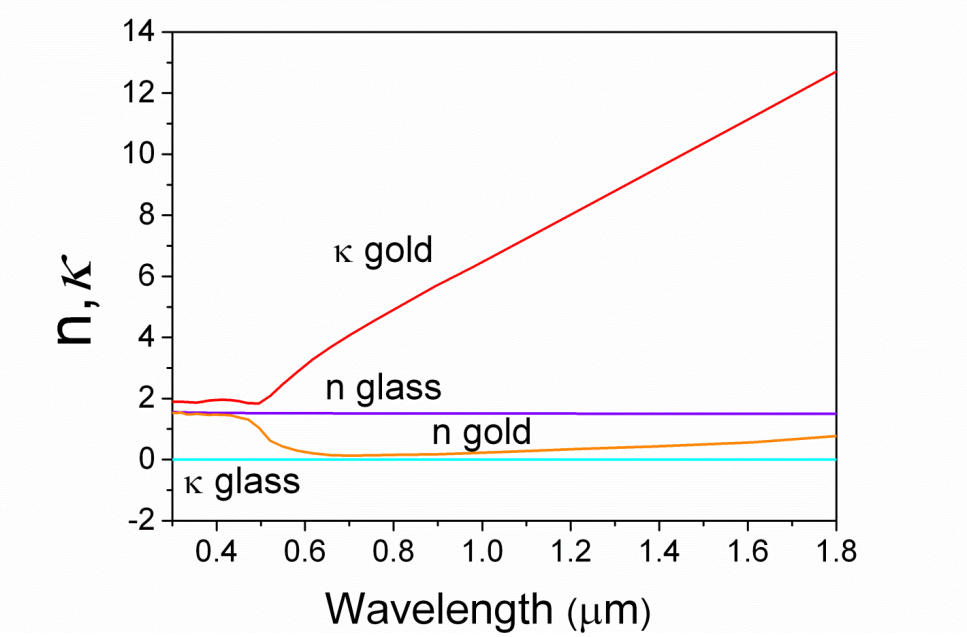

Figure 4. Refractive index (n) and extinction coefficient (κ) of gold and glass BK7. Adapted from ref. [44].

As stated above, the optical properties of metals arise from conduction electrons, which are strongly delocalized and constitute a cloud that moves collectively behind a background of positively charged core atoms. The most accurate model for describing this behavior is the Drude-Sommerfeld model, whose simplified dielectric function (*Equation 6*) describes the way how a light wave of a specific wavelength interacts with an electron plasma,[43,46]

$$\varepsilon_d = 1 - \frac{\omega_p^2}{\omega(\omega - i\gamma)} \qquad \text{(Equation 6)}$$

where γ accounts for the collision of electrons inside the plasma, responsible for damping of the oscillation (10^{14} collisions per second, γ = 100 THz), and ω_p^2 is the plasma frequency (the natural frequency of a free oscillation of the electron cloud). For most metals ω_p is on the order of 5−15 eV, depending on the band structure.[43] For instance, silver is a metal with one electron/atom in the metallic Fermi surface which gives rise to a plasma responsible for its high electrical conductivity, opacity and a large reflectivity below the plasma frequency. On the other hand, silicon is a semiconductor where photons with lower energies with respect to the energy gap propagate without loss, but those with energies above the gap are absorbed, rendering to silicon an increased opacity and reflectance.[18]

The main assumptions of the Drude-Sommerfeld model are that the electrons are the only carriers, the internal restoring force is zero (or the potential is constant), the electron-electron potential is neglected and the relaxation of their motion occurs only via collisions (taken as viscous force). Apart from damping, the electric field is the only external force. Therefore, despite the accuracy of the model for low energy photons, it is limited for those photons of high energy that can promote transitions of bound electrons into the conduction band, as is the case for gold in the visible region of the spectrum.[18,43]

Optical excitation of the electron plasma with frequencies above the plasma frequency renders the emergence of regions with positive and negative net charge due to the displacement of the electrons from the positively charged atom cores. These charge oscillations are known as *plasmon polaritons* and, depending on the propagating plane of the incident electromagnetic radiation respective to the metal, we can distinguish two types: *volume* and *surface plasmon polaritons* (SPPs). Volume surface plasmon polaritons can be excited only with perpendicular

electromagnetic waves, while surface plasmon polaritons couple with transverse electromagnetic waves.[43] SPPs require the presence of a dielectric medium in contact with the metal surface; otherwise the electromagnetic field would be effectively screened inside the material (Figure 5a). This means that charge density waves can only propagate at the interface of a semi-infinite metal surface and a dielectric, vacuum by definition (between a conductor and an insulator). The confinement of the electromagnetic waves at the interface occurs due to greater propagation than in the dielectric, leading to an evanescent decay on both sides of the interface. However, it implies that the momentum of the electromagnetic wave at the interface is higher than that in the dielectric, which in turn means that SPPs cannot be excited directly by light beams (momentum must be conserved).[43,47]

Nevertheless, it is possible to excite the SPPs, for instance, through the use of the Kretschmann geometry, where the metal is sandwiched between low refractive index and high refractive index insulators. When a beam that travels through the high refractive index insulator (a prism ε_p) is reflected at the metal-insulator interface, it will have an in plane momentum which is of the same magnitude as the SPP's momentum at the interface between the metal and the lower-index insulator (air ε_d). The electromagnetic wave travels more easily through insulators with lower index of refraction and consequently the SPP's momentum is lower. Then, the coupling of light with the plasmon generates a wave that tunnels into the low refractive index insulator-metal interface, generating an SPP (Figure 5b,c).[43,48]

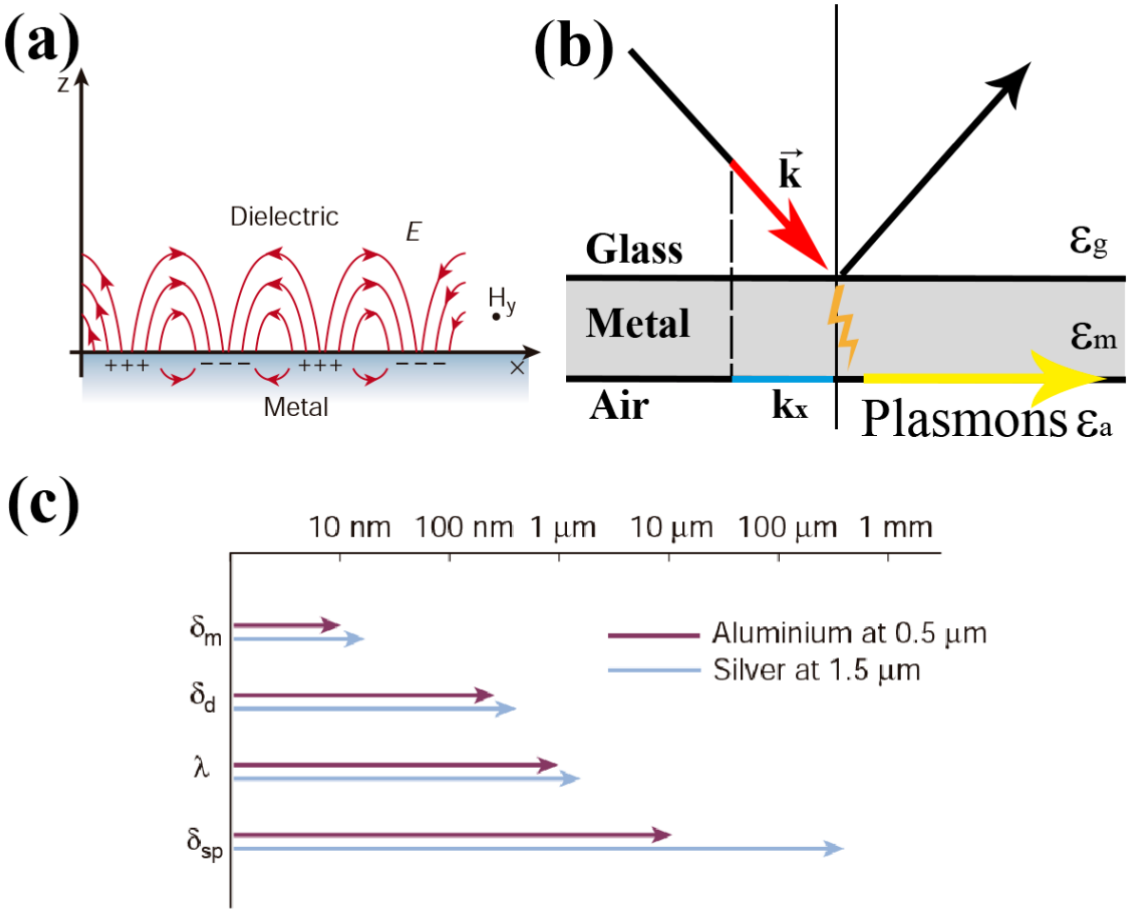

Figure 5. (a) SPP propagation at the interface between a metal and a dielectric. (b) Excitation of SPPs in the Kretschmann geometry. (c) Decay length of the SPP mode in the interface (δ_{SP}), in the dielectric material (δ_d) and in the metal (δ_m) for silver and aluminum (good and poor SPP performance, respectively). Adapted from ref. [47].

Localized Surface Plasmon Resonances

Among other techniques commonly used for SPP excitation, such as grating coupling, highly focused beams or near field excitation, the most striking method for the excitation of surface plasmons consists of reducing the dimension of the metal to the subwavelength scale, where boundary and surface effects become very important. The curved surface of metallic nanospheres induces an effective restoring force on the oscillating electron cloud, which can then fulfill resonance conditions and can be directly excited by light, generating the so-called

Localized Surface Plasmon Resonance (LSPR).[43] When the nanoparticle is irradiated with an electromagnetic wave, the electron gas gets polarized and the restoring force that tries to compensate the polarization forms a non-propagating plasmonic oscillation (Figure 6a).[41,43,46,49] This phenomenon is the origin of the bright colors exhibited by certain metals, such as gold and silver, when they are shaped into nanoparticles, whose plasma frequency lies in the visible region of the electromagnetic spectrum.[50,51]

In order to analyze the LSPR phenomenon, we have to consider that the particle size is much smaller than the wavelength of the incident light, so that we can assume the *quasi-static approximation:* the phase of the electromagnetic field is almost constant over the entire particle. Consequently, the applied field induces dipole emergence due to polarization of the electron cloud of magnitude proportional to the electric field. The polarizability α_{sph} (*Equation 7)* of the sphere related with the dipole formation depends on the dielectric functions of the metal and the surrounding medium, and the volume of the sphere.[43,46,52]

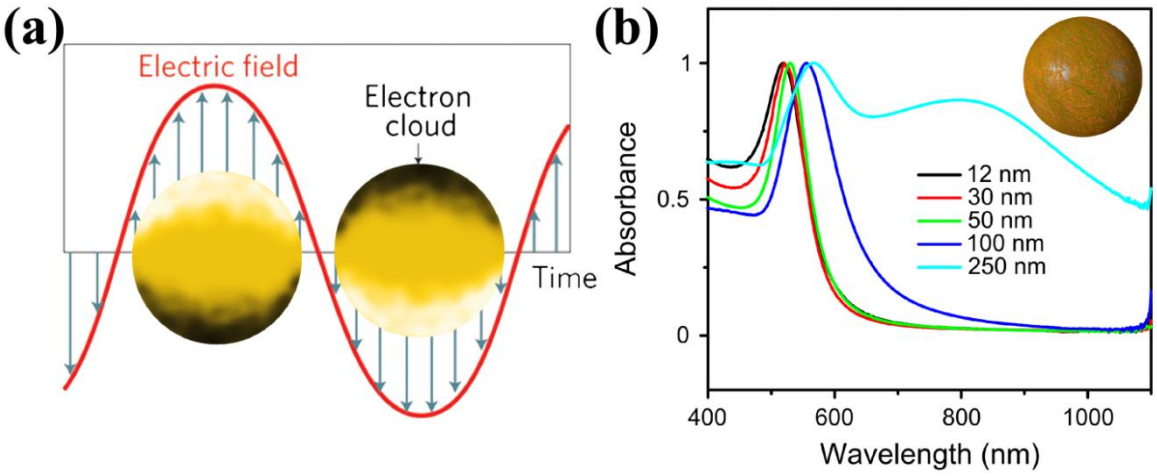

Figure 6. (a) Localized surface plasmon resonance at the surface of metallic nanospheres. (b) Normalized UV-Vis-NIR spectra of spherical gold nanoparticles of different sizes in water: an increase in the diameter induces a larger polarizability, redshift of the LSPR and activation of higher-order resonances, as seen in the case of 250 nm diameter (turquoise line). Adapted from ref. [53].

$$\alpha_{sph} = 3V\varepsilon_0 \frac{l(\varepsilon_{sph} - \varepsilon_{med})}{l\varepsilon_{sph} - (l+1)\varepsilon_{med}} \qquad (\textit{Equation 7})$$

For the dipolar surface plasmon, $l = 1$ and thus when ε_{sph} equals $-2\varepsilon_{med}$ the polarizability reaches a maximum and experiences a resonant enhancement (Fröhlich condition). As a consequence of the resonantly enhanced polarization α, both the efficiency of light absorption and the scattering intensity are increased (Figure 6b).

Now, scattering and absorption are given by the scattering cross section σ_{scatt} (relating to the energy that is sent back to the far-field) (*Equation 8*) and the absorption cross section σ_{abs} (accounting for the energy that is dissipated into lattice vibrations, i.e. phonons) (*Equation 9*):[43,52]

$$\sigma_{scatt} = \frac{k^4}{6\pi}\left|\alpha_{sph}\right|^2 \qquad (\textit{Equation 8})$$

$$\sigma_{abs} = kIm\{\alpha_{sph}\} \qquad (\textit{Equation 9})$$

where k is the wave vector, related to the refractive index, frequency and speed of light in vacuum ($k = n\omega/c$). The extinction coefficients account for both absorption and scattering effects.

Nevertheless, the development of colloid chemistry during the last decade has opened access to a wide variety of plasmonic nanoparticles with different sizes and shapes that differ strongly from the spherical shape assumed so far. In the case of rod-like particles surface plasmons show two different modes that are associated with the relative dimension of the particle: transversal and longitudinal. As the particle elongates, the ratio between the length and width of the nanorod increases and the resonance frequency shifts to longer wavelengths (Figure 7).[46,52,54]

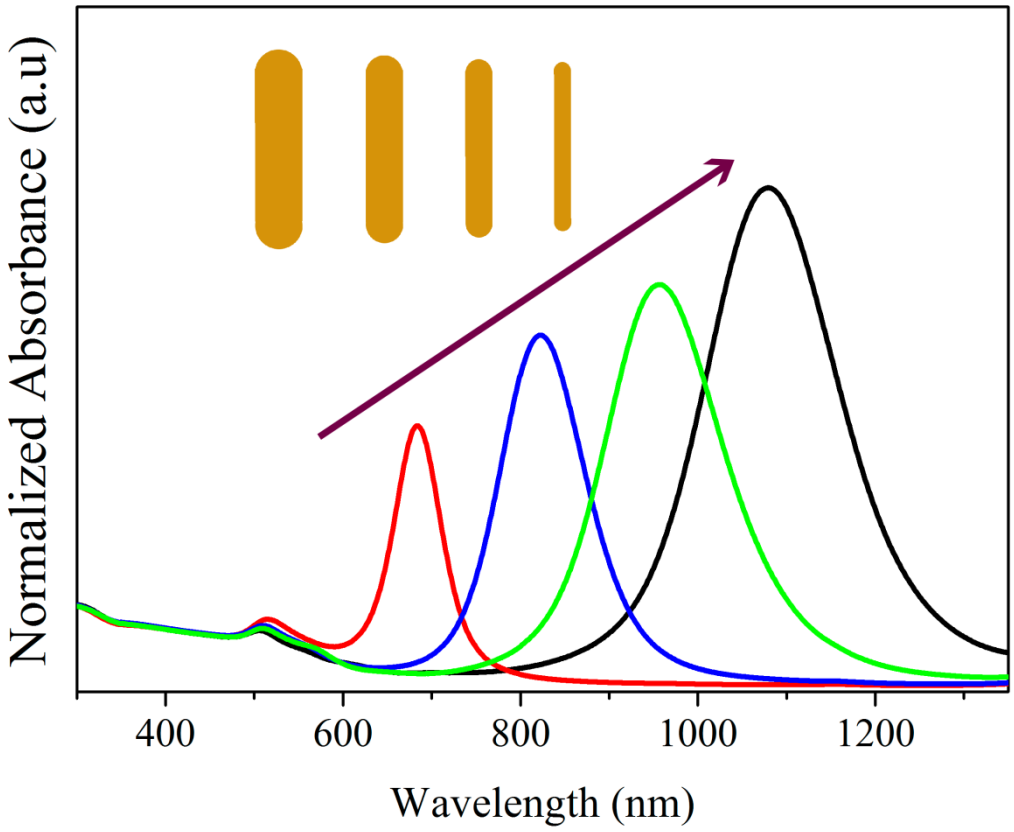

Figure 7. UV-Vis-NIR extinction spectra of gold nanorods at different aspect ratios and fixed length.

Until now, the optical properties of a small metallic particle have been studied, considering a particle radius much smaller than λ. In this particular case, the electric field of the incident light is nearly constant across the nanoparticle. However, when the size of the nanoparticle is larger than 50 nm, the electric field across the nanoparticle varies due to retardation effects and significant phase-changes of the driving field over the particle volume occur. It has been observed experimentally that, the increase of the nanoparticle radius leads to a redshift of the resonance frequency, and radiation losses increase the broadening of the plasmon band. For large particles, the distance between charge poles in a dipolar mode is roughly one particle diameter, which derives into delayed reactions of one end of the nanoparticle to changes in the opposite end, leading to a smaller restoring force and a lower resonance frequency.[43,52]

Within this context, Gustav Mie developed in 1908 a model to understand the behavior of colloidal plasmonic nanoparticles in solution, where the internal and scattered fields are expanded into a set of *normal modes.*[43] Mie took into account several additional parameters such as the *size parameter* (which relates the radius to the free space wavelength), the retardation of the *depolarization field* (damping processes from interband transitions), the enhancement of the polarization (and consequently the strength of the resonance), and also the increase of *radiation damping* (direct radiative decay route of the oscillation into photons, which weakens the strength of the resonance as the particle size increases). An additional term can be included for the appearance of higher multipole modes that emerge at large sizes (Figures 6b and 7).[43,52]

On the other hand, the plasmonic behavior of metal nanoparticles of sizes smaller than 20 nm is affected by other damping processes different from the above mentioned ones. The mean free path of the oscillating electrons is now larger (30-50 nm) than the size of the nanoparticles, and the oscillations are damped due to elastic scattering at the surface particle in a process denominated *chemical interface damping.* Finally, for sizes smaller than 1 nm the coherent oscillation of electrons breaks down and quantum effects dominate the excitation phenomena of the conduction electrons.[43]

Interestingly, the dielectric constant of the medium, particle shape and particle size are not the only parameters affecting the LSPR of plasmonic nanoparticles. In fact, when two nanoparticles are close enough to each other, new hybridized modes appear (in analogy to hybridization in molecular orbitals), by means of coulomb interaction of the localized modes.[46,55] The nature of this interaction in small nanoparticles is essentially dipolar and depends strongly on the interparticle distance. For distances smaller than the nanoparticle radius, the near field dominates the outcome either with a cubic power dependence of the distance, or as an exponential function for distances between 2 nm and 2.5 times the particle diameter. The system can be described as interacting dipoles.[43] When the electromagnetic field is oriented along the longitudinal axes of two coupled particles, a bonding interaction takes place, giving rise to a redshift of the plasmon resonance. Now, the field distribution is strongly localized at the nanosized gap due to suppression of scattering into the far field via excitation of the longitudinal modes. On the other hand, an antibonding interaction occurs when the light polarization is perpendicular to the long axis, producing a small blueshift.[56–58]

Surface Enhanced Raman Scattering

One of the most striking applications of plasmonic nanoparticles is surface enhanced Raman scattering (SERS), a spectroscopic technique capable of detecting molecules that are located in the near field of the plasmonic entity, down to the single molecule limit. The Raman scattering phenomenon in molecules is ascribed to scattering processes where the energy of the scattered photon is different from that of the incident one. The energies involved in the Raman effect derive from the characteristic vibrational modes of the molecule, which in turn implies that excitation of ground states generally leads to scattered radiation photons of energies lower than the original one (Stokes radiation). Meanwhile, already excited states produce scattered photons of higher energy (anti-Stokes radiation). Rayleigh emission occurs when the energy is conserved. Since this phenomenon occurs purely via scattering, without absorption processes, the amount of scattered light scales linearly with the intensity of the excitation beam, and can be expressed as:[59,60]

(*Equation 10*)

being the number of Stokes-active scatterers per irradiated area, the scattering cross section, and the excitation beam intensity. The efficiency of Raman transitions is much weaker than, for instance, fluorescent transitions, ($10^{-31} \leq \leq 10^{-29}$ cm^2/molecule vs. 10^{-16} cm^2/ molecule) even in those cases where the incoming radiation is in resonance with an electronic transition.[43]

Thus, the ability of plasmonic materials to enhance the Raman effect is of prime importance to render SERS a useful sensing and spectroscopic tool. For a constant number of Stokes active scatterers per irradiated area, the only two aspects where a plasmonic substrate can act are σ_{RS} and $I(\nu_L)$. The *chemical* or *electronic* contribution to the enhancement is of the order of 100 and acts on the scattering cross section. Consequently, the main influence on the enhanced Raman scattering is the increase in local electromagnetic field as a result of LSPR excitation. The usually termed *electromagnetic enhancement* leads to an increase of $I(\nu_L)$ on the molecule due to focalization of light at the metal-dielectric interface. Additionally, the photon scattered by the molecule can excite the plasmon dipole and be elastically scattered again, so that it is detected in the far field. Therefore, the SERS emission can be expressed as:[60,61]

$$I_{SERS} = \alpha_{mol}^2 \cdot \left|E_p(\omega_{inc})\right|^2 \cdot \left|E_p(\omega_{inc} - \omega_{vib})\right|^2 \qquad (Equation\ 11)$$

where α_{mol} is the polarizability of the molecule, $E_p(\omega_{inc})$ is the induced plasmonic electric field at the wavelength of the incident light, and $E_p(\omega_{inc} - \omega_{vib})$ is the outgoing electric field generated after the interaction with the probe molecule. When $\omega_{inc} > \omega_{vib,}$ i.e. using green or blue excitation light, the SERS intensity results:[60]

$$I_{SERS} = \alpha_{mol}^2 \cdot \left|E_p(\omega_{inc})\right|^4 \qquad (Equation\ 12)$$

The SERS intensity follows the same cubic power dependence with the distance as the near field does, which indicates that SERS is a truly surface selective effect. Additionally, the Raman profile of the molecule is dependent on the molecule orientation relative to the surface, which is related to the different spatial components of the molecule polarizability.

Probably one of the most challenging problems of SERS spectroscopy is the quantification of the signal enhancement relative to the non-enhanced Raman signal. This would require determination of the SERS and Raman signals per molecule, which in practice turns out to be experimentally complex since it not only requires precise control over the number of molecules per irradiated area, but also a uniform distribution of plasmon resonances giving rise to field enhancements of equal magnitude. The SERS Enhancement Factor (EF) represents the main figure of merit for SERS substrates, and can be expressed as:[60,61]

$$EF = \frac{I_{SERS}/N_{SERS}}{I_{Raman}/N_{Raman}} \qquad (Equation\ 13)$$

For instance, for electric field enhancements in the order of 100, the final Raman intensity scales up to 10^8. In order to reach such values, a widely spread approach consists of assembling plasmonic nanostructures to generate large electromagnetic field enhancements that are strongly localized at the interparticle gaps: *hot spots*.[62] In fact, the EF of colloidal plasmonic nanospheres are on the order of 10^3, while the EF may increase up to 10^{10}-10^{11} inside hot spots. Thus, although the total area conformed by the interparticle regions is very low, the contribution of the molecules located therein reaches 24% of the total SERS signal (i.e. the Raman signal of a single molecule with an EF of 10^{10} is equal to the Raman signal of 10 million molecules with EF of 10^3).[60] The importance of the fabrication of hot spots during the preparation of SERS

substrates for sensing in environmental and medical applications is one of the main motivations for the intense research developed on fabrication, functionalization and self-assembly of colloidal plasmonic metal nanoparticles (Figure 8).[63–65]

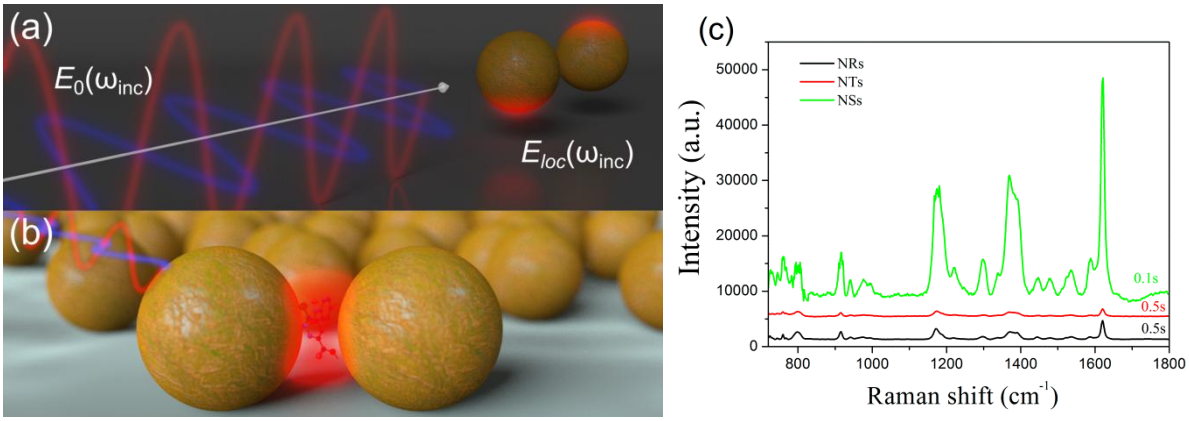

Figure 8. (a) Schematic representation of the induced electric dipole in two gold spheres by an incident electromagnetic radiation. (b) Hot spot formation between two gold spheres separated by a small distance. Molecules placed inside the gap feel an electric field up to ten or more orders of magnitude higher. **(c)** SERS spectra of the molecule Crystal Violet obtained using gold nanospheres (NSs), nanotriangles (NTs) and nanorods (NRs) deposited on a glass substrate as enhancers. As it can be observed the highest enhancement is produced by gold NSs, which indicates that the shape and assembly of the nanoparticles play a key role.

SYNTHESIS OF PLASMONIC GOLD NANOPARTICLES

Historically, the synthesis and application of plasmonic nanoparticles have anticipated their scientific comprehension. The first preparations date back to the beginning of glass development and the quest for its coloration as a symbol of power and wealth, already in Ancient Egypt and Mesopotamia. At that time, one of the most elusive colorings was red and the use of metallic copper was originally employed to produce opaque red glasses.[66] Subsequently, Roman glass workers replaced copper with gold, giving rise to one of the most extraordinary achievements of ancient glass making: the Lycurgus cup (Figure 9a). The unusual optical properties of its dichroic glass, showing ruby color in transmission and green in reflectance are attributed to the presence of silver-gold nanoparticles (7:3 silver-gold ratio and 10% copper), uniformly dispersed in the glass matrix.[67,68] After the fall of the Western Roman Empire, new

references about the use of gold to stained glass are not found until the seventeenth century, when Johann Rudolph Glauber and Johann Kunckel described the production of a purple pigment for glass based on the use of *aqua regia*, gold and tin metallic pieces. [69,70] The chemistry behind the production of the so-called *Purple of Cassius* was elucidated three hundred years later by Richard Zsigmondy. In that work, he demonstrated the existence of gold nanoparticles stabilized by tin hydroxide, both products of the reaction between gold and stannous chloride (1), and the hydrolysis of stannic chloride (2):[69,71]

$$Sn^{2+} + 2Au^{+} \rightleftharpoons Sn^{4+} + 2Au^{0} \quad (1)$$

$$SnCl_4 + 4H_2O \longrightarrow Sn(OH)_4 + 4HCl \quad (2)$$

On the other hand, the first scientific publication on the synthesis of colloidal gold nanoparticles was released by Michael Faraday in 1857.[72] This investigation described the preparation of thin films and colloidal suspensions of gold nanoparticles, and their optical properties. He found the dimensions of the gold particles, the aggregation state and the thickness of the films that were directly responsible for the diverse interactions with light. Nowadays, the gold nanoparticle colloids prepared by Faraday in the 1850's are still on display at the Royal Society in London (Figure 9b).

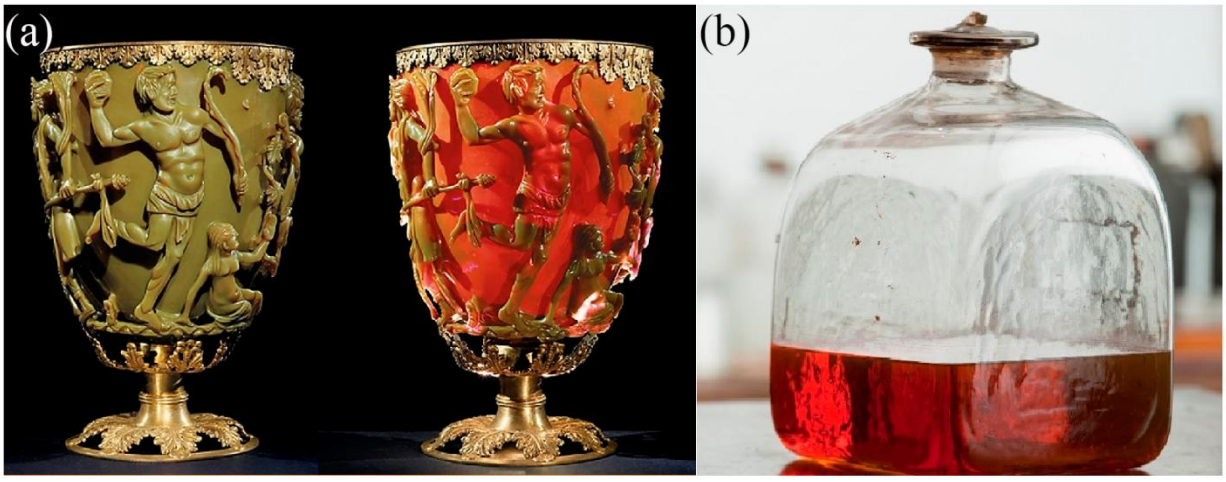

Figure 9 (a) Photographs of the Lycurgus cup (IV century AC), illuminated from the front side (left) and from the back side (right) (conserved in the British Museum) (b) Gold nanoparticles suspension prepared by Michael Faraday (conserved at the Royal society in London). Adapted from ref. (a): [72] and (b): [73].

One of the most interesting aspects of Faraday´s approach for the synthesis of colloidal nanoparticles was the use of water as solvent, and chloroauric acid as the source of gold, which are nowadays common "ingredients" employed in the synthesis of gold nanoparticles. Oppositely, the reducing agent used by Faraday (white phosphorous) has currently been replaced by less toxic reactants such as ascorbic acid or citric acid, among others.[75,76] Moreover, the stabilization of the final colloidal suspension is usually achieved through the use of a wide range of organic ligands, from surfactants to biomolecules.[77–79] Although the fabrication of gold nanocrystals is not limited to aqueous media,[80] the present thesis relies on the use of gold nanoparticles synthesized in water, and therefore from now on we focus exclusively on aqueous nanoparticle colloidal synthesis. Additionally, among the huge body of related literature, we will only show the surfactant based fabrication of gold nanoparticles, which is probably the most versatile and successful method in terms of nanocrystal shape and size control.

Seed Mediated Growth

Despite the importance of the chemical reactants (nature, purity, total concentration, ratios, etc.) toward obtaining the desired gold nanocrystals, the methodology is crucial to determine the uniformity in shape and size of the final metal nanoparticles. In fact, spatial and temporal separation between nanocrystal nucleation and growth has been proven to be the most efficient approach to govern the uniformity and quality of the obtained colloidal nanocrystals, as well as to gain insight into the growth mechanism. First described by Murphy et al. in the early 2000s, the so-called *seed mediated growth method* opened access to an unprecedented variety of shaped metal nanocrystals including rods, wires, stars, cubes, triangles and different polyhedra.[54,81–85] The experimental procedure comprises the preparation of 1-5 nm crystalline seeds, which are then transferred into a growth solution. Throughout fine control of the nature and concentration of the reactants (metal precursor, reducing agent, surfactant, etc.) in the growth solution, the seeds are overgrown into the desired gold nanoparticles. The main advantage of this approach is its versatility regardless of which nanoparticle shape is to be obtained. As a result, the seeded growth method has become the most popular synthetic approach for generating both isotropic and anisotropic metal nanoparticles (including gold, silver, platinum, and palladium nanoparticles).[86–88]

Nevertheless, the complexity of the mixture of surfactant and salts, where nanoparticle growth takes place, makes it difficult to unravel the underlying mechanisms. A wide variety of them have been proposed over the past years to explain the growth of gold nanoparticles and the wide range of morphologies which they can be shaped into. For instance, the role of the surfactant has been claimed to be related to induction of strain favoring anisotropic growth, whereas the presence of crystallographic defects in the seeds is also known to have a large influence.[77,89] Furthermore, the different crystallographic facets of the crystal do not display equal affinity toward adsorption of silver and halide ions, additives that are invariably used due to their ability to tune the final shape of the nanocrystal. The modification of surface energies may favor the growth kinetics of certain facets over others, thereby inducing either the formation of anisotropic particles or the growth of cubic, octahedral or trisoctahedral shapes, among others (Figure 10).[90,91]

The role of halides is of special relevance since quaternary alkylammonium halides, mainly hexadecyltrimethylammonium bromide (CTAB) and its corresponding chloride derivative (CTAC), are the most extensively employed surfactants for gold nanoparticle synthesis.[82,93–96] For this reason, researchers have proposed several possible pathways that generally involve specific binding of halide ions onto the nanoparticles surface (face-specific capping agents), modification of the electrochemical potential of gold ions and interaction with the ancillary reagents (e.g., silver nitrate).[90,97] Moreover, the colloidal properties of surfactants are strongly dependent on the nature and concentration of the halide counterion.[98,99] We leave anisotropic nanoparticles aside for the moment and focus on the effect of silver and halides on the growth of isotropic gold nanocrystals.

Isotropic Gold Nanoparticles

Following up this line of thought, Mirkin et al. studied the use of CTAC versus CTAB and demonstrated that, in combination with silver, it was possible to achieve rational control over the synthesis of a variety of isotropic gold nanoparticles.[100] By looking at the growth kinetics, they proposed that the modulation of the reduction potential of ionic gold, and the passivation of gold nanocrystals surface, were the main mechanisms underlying the effect of halides on the synthesis of truncated bitetrahedra, octahedra, cubes and trisoctahedra (Figure 10a). Larger

halides (e.g., I^-) were found to induce lower growth rates via modification of the reduction potential of $[AuX_2]^-$, and by directly passivating the facets of the growing crystal (Au-I > Au-Br > Au-Cl), giving rise to the formation of gold nanoparticles with lower surface energy facets.

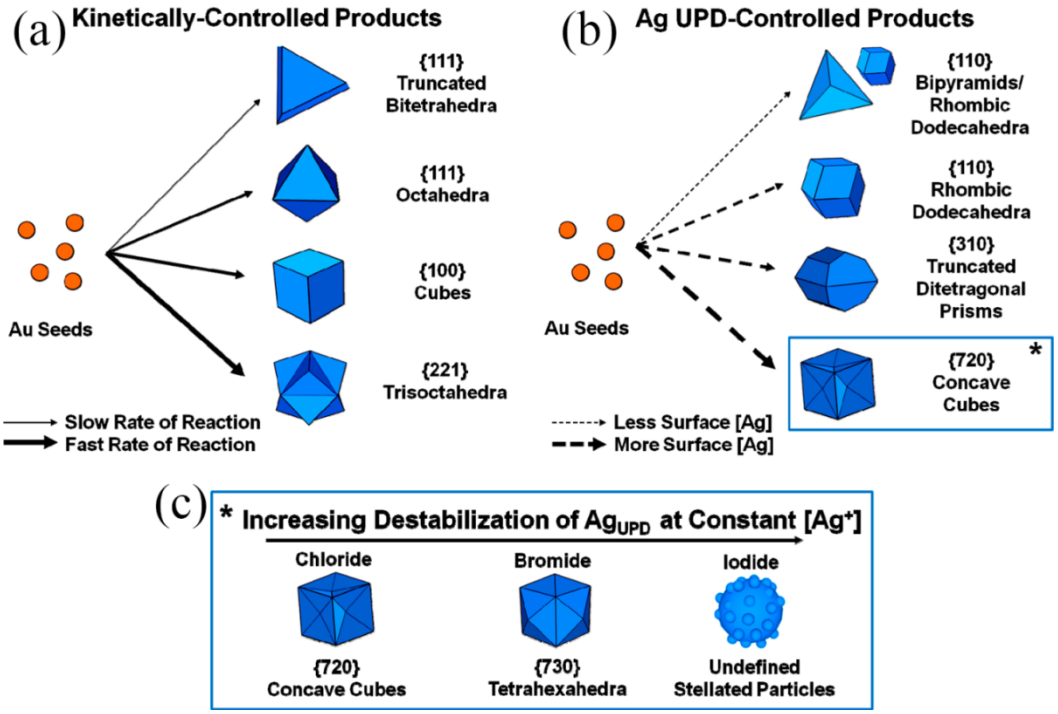

Figure 10. Schematic illustration of the six rules proposed by Mirkin et al. Halides and silver ions direct the growth of gold seeds down different growth pathways, yielding different shaped products. (a) Kinetically controlled products. (b) Ag UPD-controlled products (silver underpotential deposition controls particle shape). (c) Concave cubes, tetrahexahedra, and stellated nanoparticles formed as a result of varying the stability of the silver UPD layer with high concentrations of chloride, bromide, or iodide in the growth solution. Adapted from ref. [100].

A large effect of halides was also observed in the silver assisted seeded-growth synthesis, most probably due to modulation of the extent of silver UPD, which is also affected by silver concentration (Figure 11b-c). In the presence of silver, the rate/stability of silver UPD, which affects the mobility of silver atoms, is responsible for shape control: Ag_{UPD}-Cl > Ag_{UPD}-Br > Ag_{UPD}-I. If the concentration of the larger halide ions is decreased to trace amounts, the stability of the silver UPD layer is decreased, and the formation of higher energy facets is favored. On the other hand, silver deposition is impaired when the concentration of I^- or Br^- is high, thereby

limiting the number of shapes that can be generated. Nevertheless, the role of other crucial parameters such as the seed features, i.e. its size and twinning, were not investigated and consequently, these observations and considerations cannot be fully be generalized to other syntheses.[100] On the other hand, a completely opposite approach was taken by Huang et al., who underlined the growth kinetics to be the main factor exerting shape control, rather than surface passivation by the halides.[85,101,102] The reason behind the growth of high index facets is related to the rate of atom deposition on the crystal, as compared to the rate of atom diffusion on the nanocrystals surface. The reaction proceeds under thermodynamic control when the atoms deposited on the surface of the growing particles are able to diffuse to the lowest energy sites. These phenomena are only possible when the rate of diffusion is faster than that for atom deposition. When the deposition process is the fastest, the shape of the nanocrystals is determined by kinetic control. Nonetheless, it is important to point out that all these studies were performed using hexadecyltrimethyl ammonium halides as surfactant. Therefore, synthesis of gold nanocrystals based on halide free surfactants are not taken into account in the discussion.

Despite the wide variety of shaped isotropic gold nanoparticles that can be produced using the seeded growth method in combination with the above mentioned alkylammonium halide surfactants and silver, the fabrication of monodisperse gold nanospheres of different sizes with a high degree of roundness and sphericity remains challenging.[76,103] Therefore, in Chapter 2 we describe the development of a synthetic approach to produce highly monodisperse gold nanospheres in an efficient and scalable approach, and the subsequent self-assembly into plasmonic superstructures with potential application into sensing and metamaterials.

Anisotropic Gold Nanoparticles: Nanorods

Another important consideration when dealing with the seed mediated synthesis of gold nanoparticles is the crystalline nature and size of the initial seeds, which are strongly interdependent in most cases. The crystalline habit is of major importance as it induces large effects on the final shape of the nanoparticles. Meanwhile the seed size is related to the occurrence of symmetry breaking events, which are required for the formation of anisotropic nanoparticles. The synthesis of gold nanorods is a paradigmatic case of study due to the possibility of varying all of the above mentioned parameters: growth rates, halides and silver,

and the seed effect. Even the addition of organic additives, which intercalate at the surfactant micelles and modify their behavior, can be properly exemplified with gold nanorods synthesis. Furthermore, since gold nanorods have received increasing attention due to their highly tailorable plasmonic properties and their use in a wide range of technological applications (such as catalysis, SERS, biosensing and therapy, etc.), much effort has been made to understand the mechanism behind their formation.[104–113]

In the early 2000´s, two different approaches based on seeded-growth were reported for the synthesis of gold nanorods. Since then, many research articles dealing with the growth mechanism of such nanoparticles have been reported. First of all, the crystal habits of the gold seeds employed in each approach are significantly different in terms of the exposed crystalline facets. When single crystalline nuclei are used, their growth and transformation into gold nanorods require initial dimensions smaller than 2 nm, and the use of silver ions to induce the symmetry breaking.[105,114,115] Ideally, the monodispersity of the seed should be as high as possible, while displaying the same crystallographic habit. To obtain such a good dispersion of nuclei, a strong reducing agent, typically sodium borohydride ($NaBH_4$), is vigorously injected into a solution of gold tetrachloride ions containing CTAB, so that nucleation dominates over growth.[116] On the other hand, when the gold seeds are prepared using sodium citrate as the capping agent, they form with pentatwinned habits and {111} facets. Therefore, preferential growth from these facets yields anisotropic growth and the resulting pentatwinned gold nanorods display pentagonal cross-section, with {100} lateral facets and {111} facets at the tips (Figure 11).[81,117,118] The formation of pentatwinned nanoparticles has been historically less used, as the shape yield was limited to 30%.[54] Only recently, this yield has been significantly improved up to almost 90%.[119] The main advantage of pentatwinned gold nanorods is silver-free synthesis, the access to high aspect ratios, and further elongation into gold and gold-silver nanowires with LSPRs in the near-mid IR.[54,119,120]

Although defect-free and pentatwinned seeds are produced by using different ligands, the formation of rod-like nanoparticles takes places in CTAB solution for both cases. This common feature points out the important role of the surfactant composition. For instance, pentatwinned gold nanorods with larger aspect ratios were synthesized when the number of carbon atoms in the alkyltrimethyl chain was increased from 16 up to 18.[121] On the basis of the existing literature

reporting the formation of elongated CTAB micelles at certain concentrations, a templating effect was proposed as an additional factor for the formation of gold nanorods.[122] Nevertheless, the templating model was recently replaced by the hypothesis that CTAB or CTAB/silver complexes (for the silver assisted synthesis of gold nanorods) are preferentially bound to the lateral faces of the developing gold nanorods. This adsorption may slow down the nanoparticle growth at the sides with respect to the tips. In this context, the role of bromide anions was proposed to be similar to their cationic counterparts, displaying diverse binding affinities upon different crystallographic facets.[99,123,124] Experimental studies about the effect of bromide concentration (initially present in the form of CTAB or KBr) on the growth kinetics of gold nanorods showed an inverse relationship between the concentration of bromide and the growth rate.[106] Atomistic molecular dynamics simulations on the absorption of bromide on gold surfaces showed that they can act as driving forces for the adsorption and stabilization of CTAB micelles on gold surfaces, with stronger adsorption on the {100} and {110} than on {111} facets (Figure 11a).[99] These effects are much less pronounced in the case of chloride, leading to lower surface energy differences between different facets and lower number of surfactant molecules passivating the surface.

The uncertainty on why at a specific size threshold, certain directions start growing preferentially, giving rise to a transition from spherical to elongated shape (symmetry breaking) is still under investigation (Figure 11b).[125] Theoretical studies on the role of the halides and surfactant in the silver assisted synthesis of single crystal gold nanorods reveal that the formed CTAB-AgBr complex has a more efficient absorption on {520} facets than on {100} facets (Figure 11c)[123]. The control over the aspect ratio exerted by silver ions and the Au:Ag ratio in the growth mixture has been recently unraveled by Tong et al. They found that at higher silver concentrations, the seed size at which symmetry breaking occurs is smaller and the aspect ratio of the final particles is higher (Figure 11d).[126] In order to start the anisotropic growth, the nuclei may have some degree of truncation that allows the formation of {110} facets, which only occurs above 4 nm. In fact, these results are in agreement with the structure of single crystalline gold nanorods previously determined by transmission electron microscopy, where {110}, {100} and {520} are the main facets exposed at the sides, while {001} and {111} are present at the tips (Figure 12e).[127] Interestingly, it is possible to control the presence of different high index facets

via modification of the CTAB organization with organic additives or through the use of copper ions, leading to gold nanorods displaying {730}, {511}, {221} or {311} facets, among others.[107,128,129]

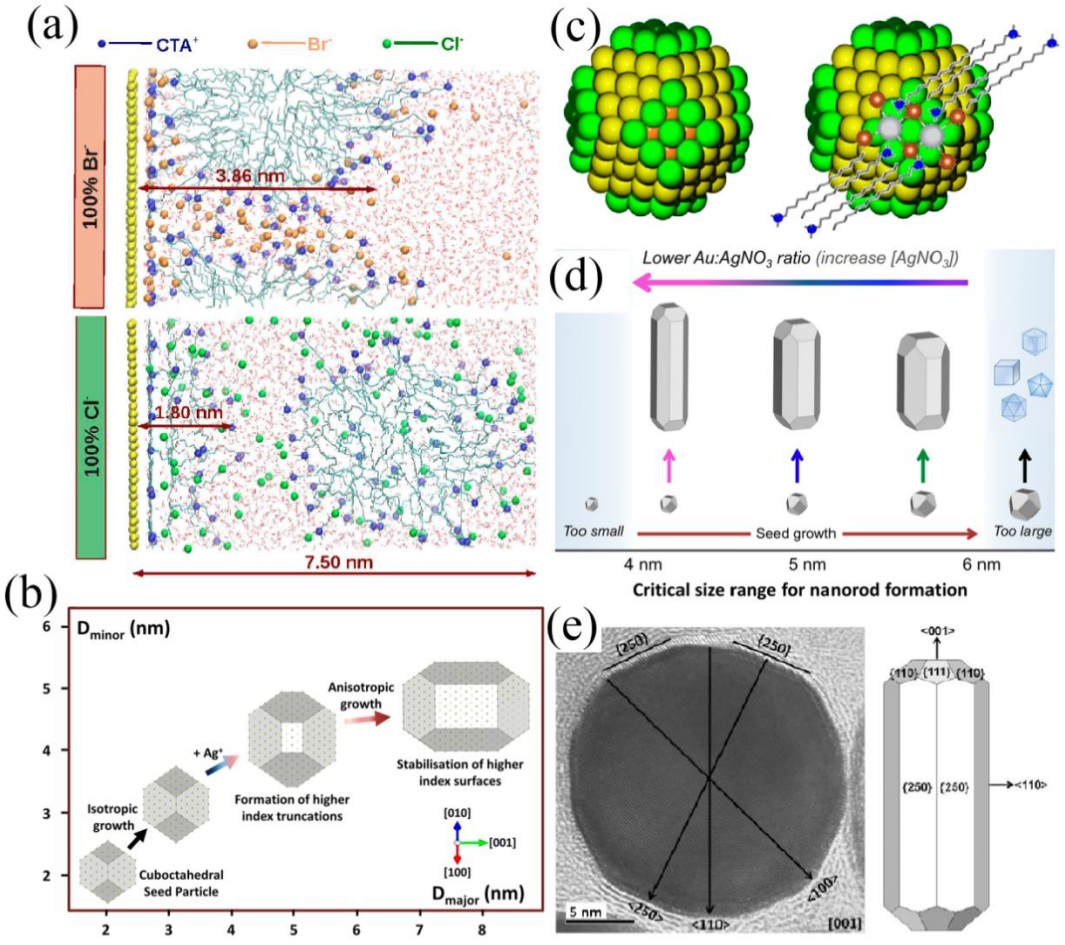

Figure 11. (a) Snapshots from the simulations for 100% CTAB and 100% CTAC on {111} gold facets. (b) Scheme of the proposed symmetry breaking process in single-crystal gold nanorods growth, where truncation occurs only above certain nucleus size. (c) Wulff construction of a gold seed without (left) and with (right) adsorption of CTAB-AgBr complexes, where yellow planes are {111} and green ones are {100} facets. The competition between electrostatic and chain interactions impairs complete coverage of all {100} facets, leading to a cylindrical configuration. (d) Scheme of the proposed symmetry breaking process occurring at different sizes, and leading to gold nanorods of distinct aspect ratios depending on the silver to gold ratio. (e) HRTEM image of a standing gold nanorod, showing the main crystallographic facets {250} (left) and the proposed model (right). Adapted from refs. (a):[99], (b):[125], (c):[123], (d):[115] and (e):[127].

Despite all experimental evidences supporting the importance of bromide for the synthesis of gold nanorods, Ye et al. demonstrated that using a mixture of a alkyltrimethylammonium surfactant with chloride as counterion and sodium oleate as additive, monodisperse suspensions of gold nanorods could be obtained.[130] Since a CTAB capped seed was used, the synthesis cannot be considered completely bromide free, but the concentrations are much lower than the minimum necessary previously reported in the literature. Furthermore, the octagonal prismatic structure enclosed by high index {310} crystal planes was not previously reported for CTAB, suggesting that different facets are stabilized by a CTAC/sodium oleate mixture. In conclusion, the main message is that the stabilization of crystallographic facets is one of the principal directing elements behind anisotropic growth.

Up until this point, the roles of crystalline habits of the seed, halides, silver and surfactant in the synthesis of gold nanorods have been described. All these parameters interplay in a unique manner, where growth is determined by a delicate balance between kinetic and thermodynamic control. It is worth highlighting the distinction between stabilization of crystallographic facets, which takes place under thermodynamic control and anisotropic growth, which is controlled by kinetics.[87,88,131] Therefore, high deposition rates of the gold ions on single crystal nuclei are required to favor the symmetry breaking event, which means it takes place under kinetic control. However, after the formation of the anisotropic nuclei, stabilization and growth require thermodynamic control. In practice, control over aspect ratio is achieved by means of the concentration of silver and the redox potential of the reducing agent. For instance, the reduction potential of ascorbic acid is lower at low pH, giving rise to the formation of higher aspect ratio gold nanorods.[132]

Finally, the synthesis of single crystal rods is the most studied case for the fabrication of gold nanomaterials, due to its higher robustness, large capacity to render particles within a wide range of dimensions (fine tailoring of the LSPRs) and the high shape yield of the synthesis. Therefore, we have taken advantage of the versatility of this method to produce anisotropic nanoparticles with desired surface chemistry features and optical properties (see Chapters 3, 5 and 6).

ASSEMBLY OF GOLD NANOPARTICLES

In analogy to atoms when they get organized to form molecules and crystalline compounds with well-defined physicochemical properties, which are different from those of the isolated atoms, unique optical properties of plasmonic nanoparticles arise when they self-assemble into more complex nanostructures.[31,133–136] As previously explained, coupling of the LSPR modes of individual nanoparticles give rise to new resonance modes and concentration of the electromagnetic field at the gaps between the plasmonic elements.[56,137] Therefore, self-assembly is recognized as one of the most general strategies toward the generation of new ordered nanostructures with potential applications in microelectronics, photonics or near field optics.[53,138,139] The driving force in all cases is the minimization of the free energy of the final assembled structures, which is governed by the balance between attractive and repulsive interactions: van der Waals, Coulomb, hydrogen bonding or hydrophobic interactions, etc.[15,140]

However, the definition of self-assembly may be ambiguous since the boundaries between self-assembly and other phenomena such as molecular recognition, aggregation or complexation are mobile and depend on whoever is using them. As a general definition: *"self-assembly is the autonomous re-organization of pre-existing disordered components into patterns or structures, without human intervention"*.[141] Looking closer into the concept, self-assembly may involve a certain degree of order, at least in one dimension, which is achieved through the balance between attractive and repulsive interactions, i.e. short-range (such as van der Waals, hydrophobic interactions or hydrogen bonding) and long-range (capillarity or flow dragging). The so-called directed self-assembly refers to the rational selection of building blocks to obtain a particular structure, exploiting characteristic properties that are encoded in the building blocks themselves, such as shape, concentration, number of elements and chemistry.[15,140]

Two types of self-assembly processes can be distinguished from a thermodynamic point of view: static and dynamic self-assembly. In the first case, thermodynamic equilibrium is reached, leading to the most stable ordered structure, while in the case of dynamic self-assembly (also called self-organization or dissipative self-assembly) the building blocks interact due to certain driving forces, until these cease. The self-assembly in this type of organizations persists only if the system is dissipating energy and the interaction can arise from external fields, the particles themselves, or entropic forces (tendency to increase entropy).[141,142]

Self-Assembly Mediated by Molecular Interactions

Focusing on systems where gold nanoparticles constitute the building blocks, some of the main driving forces are those arising from interparticle interactions, which are generally directed by molecular interactions at the nanoparticle surface.[15] In the past two decades multiple strategies for the assembly of gold nanoparticles were based on the rational functionalization of the nanoparticle surface with a library of molecules, polymers and biomolecules. Under appropriate stimuli (i.e. temperature, pH, light, electric field, redox reaction, solvent composition, magnetic field, etc.), such ligands assemble the nanoparticles via hydrophobic or electrostatic interactions, depletion attractions, hydrogen bonding, supramolecular interactions, formation of covalent or coordination bonds, etc.[3,79,135,143–149] As a remarkable example, the use of DNA has been widely explored by Mirkin's group to produce gold nanoparticle supercrystals in a programmable artificial fashion, assembling structures that are found in nature (Figure 12).[144,150]

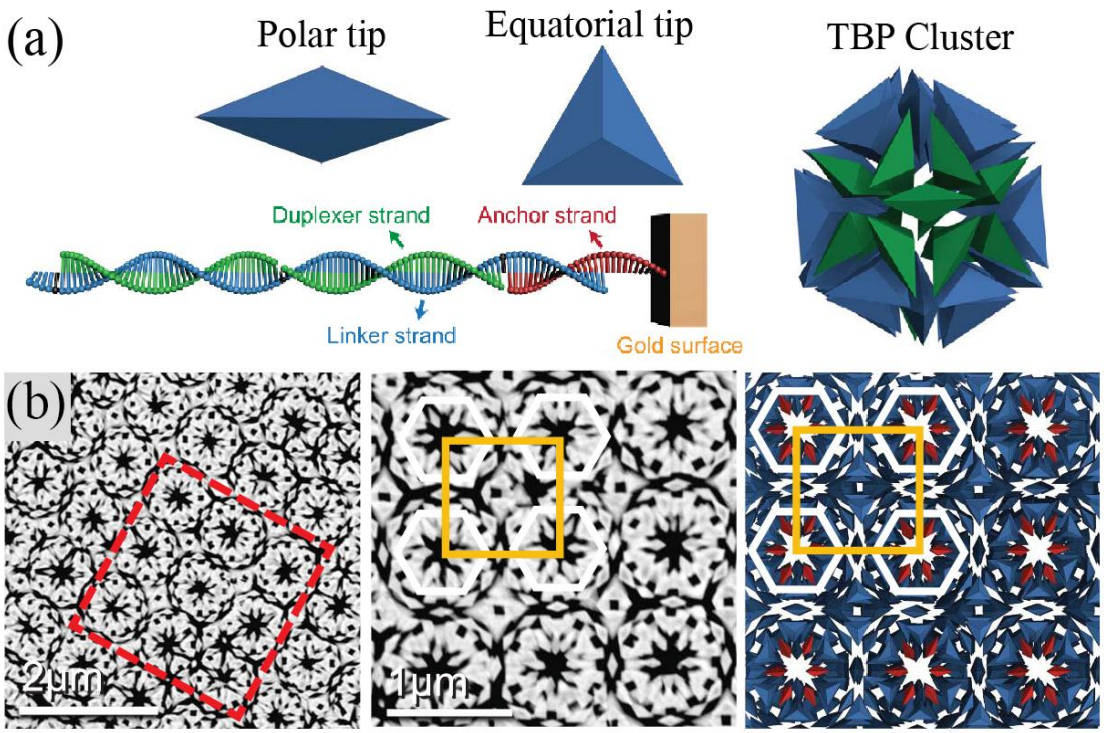

Figure 12. (a) Illustration of triangular bipyramids and clusters formed when they self-assemble via a selected DNA linker. (b) Comparison of electron microscopy images (left), zoom-ins of the red area (middle), and triangular bipyramid cores in the structure model (right) of the obtained clathrate structures. Adapted from ref. [150].

On the other hand, depletion forces have been shown to induce nanoparticle self-assembly sensitive to the geometry, and also to be an important driving force for the formation of free-standing supercrystals made of polyhedral building blocks. In our group, fine modulation of hydrophobic interactions between gold nanoparticles (nanorods, nanostars and nanospheres, among others) by rational functionalization and solvent exchange allowed us to form reversible assemblies with different aggregation numbers and internal organization.[149] Following similar approaches, Kumacheva showed the versatility of hydrophobic forces to drive the self-assembly of gold nanorods into a wide variety of 1D, 2D and 3D structures, ranging from chains and rings to spherical aggregates.[151–153]

Despite of the large amount of reported methods where gold nanoparticles of different sizes and shapes are systematically assembled using the above mentioned forces, the detailed dynamics of such assemblies remain not well understood. This lack of knowledge leads in some cases to low control over the formation of discrete aggregates in high yield. Recently Tan et al. reported an elegant study on the tip-to-tip and side-by-side hydrogen bonding mediated assembly of gold nanorods in solution, monitored by *in situ* time resolved transmission electron microscopy experiments in a liquid cell (Figure 13). They observed that, at low concentration of the molecular linker, tip-to-tip interactions govern assembly, whereas at high concentrations side-by-side assemblies were predominantly formed. In the latter case, the attachment can occur via two parallel prealigned particles or via initial interaction through the tips. [154]

In the thesis, we have demonstrated the assembly of gold nanorods via covalent linkage, to introduce a new concept in the controlled formation of this type of ordered assemblies, based on the femtosecond laser irradiation of plasmonic hot spots (see Chapter 5). In fact, the pH triggered assembly of such nanorods will be used to generate hot spots inside mammalian cancer cells for photothermal therapy purposes (see Chapter 6).

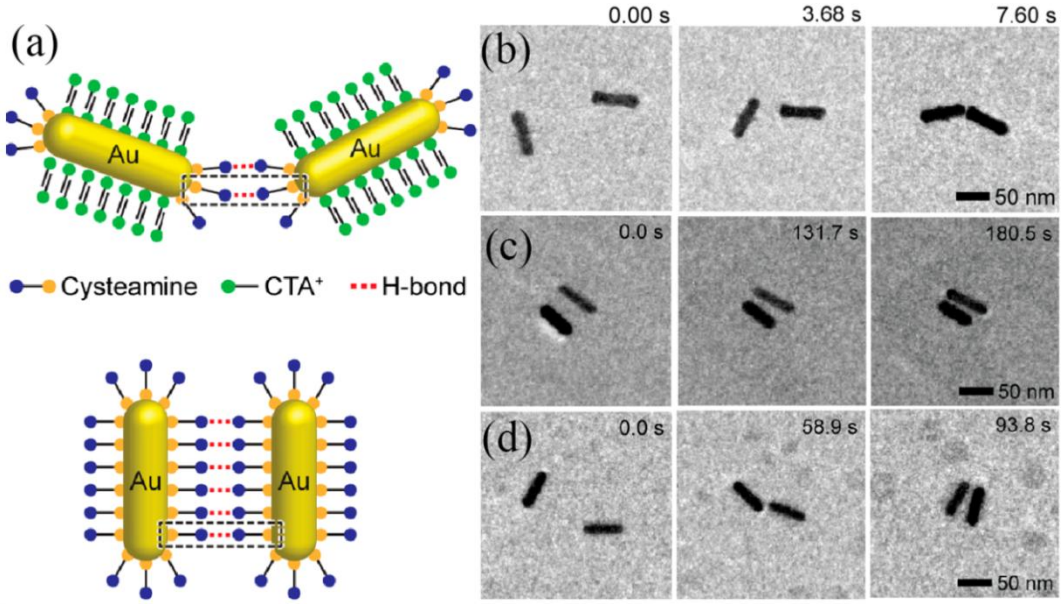

Figure 13. (a) Scheme of tip-to-tip and side-by-side hydrogen bonding mediated assembly of gold nanorods. Time resolved TEM images showing (b) end-to-end and (c,d) the two different pathways of side-to-side assembly Modified from ref. [154].

Evaporative Self-Assembly

On the other hand, the use of evaporative self-assembly combined with confined spaces as templates has gained much attraction due to the improvements in lithography technology.[155,156] First of all, templates are objects that serve as scaffolds in which the nanoparticles can be arranged into a structure that was previously fabricated according to the designer wishes. Therefore, it carries the information on the final position and arrangement of the particles. One of the main advantages of using templates is the flexibility and reproducibility to produce various geometries over large areas. For instance, the use of polymeric chiral fibers as templates for the arrangement of gold nanorods derives into a new material with intense circular dichroism at the NIR, arising from the optical coupling between assembled plasmonic nanorods (plasmonic chirality).[135]

In evaporative self-assembly, the interactions of particles with interfaces are exploited to produce nanoparticle organizations within patterned substrates. Focusing on the nanoparticles packing within the template, rational design of their behavior is required to control effects

derived from particle-particle, particle-surface or particle-solvent interactions. Otherwise, these effects would impair the appropriate self-assembly into the structure with great precision and specificity.[15,140] The nanoparticle has to diffuse and, once the position is reached, it needs to overcome Brownian motion until the system is quenched, e.g. by replacing water by air through an evaporation process. In order for a colloidal nanoparticle to be hold at a certain position, the free energy at a specific location must be minimized. The target or binding sites are potentially well defined by particle–surface interactions: covalent (<1 nm), van der Waals (~1 nm), Coulomb (electrostatic: ~1 nm for polar and ~100 nm for non-polar media), hydrophobic (~1nm) and capillary (~1 mm). These interactions act over different lengths and have different magnitudes, forming minima with different geometries, all of which can influence the self-assembly process. Additionally, the size of the binding site has to be larger than at least one nanoparticle, in order to accommodate just a single object, and much larger in the case of the formation of densely packed hierarchical structures. Therefore, real template-particle systems have complex energy landscapes with multiple secondary minima and kinetic traps, where the geometry of the template, the surface chemistry, size and shape of the nanoparticles play a key role.[140]

In the case of gold colloids, the use of soft templates with micron-sized cavities has been demonstrated to provide control over the hierarchical organization of gold nanoparticles up to the device scale.[157–159] By changing the nanoparticle concentration, the features of the formed supercrystals can be tuned, and in turn the topography of the substrate and the optical properties.[109,160] The precision of this methodology was evidenced by Zhou et al. through the use of elastomeric templates and a selection of the evaporative conditions. They selectively assembled single gold nanoparticles according to their shape and size, and controlled their orientations over several micrometers.[161] Recently, Greybush et al. prepared 2D hexagonal ensembles of ordered gold nanospheres with a variable number of particles per assembly (from 1 to 31). In order to form such plasmonic *metamolecules* they used polygonal topographic templates prepared by electron-beam lithography (Figure 14).[162] Another example is the formation of wrinkles on PDMS substrates, to be used as templates for the alignment of gold nanoparticles into parallel lines over square centimeter areas.[158]

One of the most important issues intrinsically associated with the engineering of building blocks is their size and shape distribution quality. High polydispersity favors an increase in complexity of the energy landscapes, yielding poor control over assembly onto the pattern. Therefore, we will explore the large scale fabrication of highly monodisperse gold nanospheres with different sizes and engineered surface chemistry, to produce large scale assemblies onto patterned surfaces (see Chapter 2).

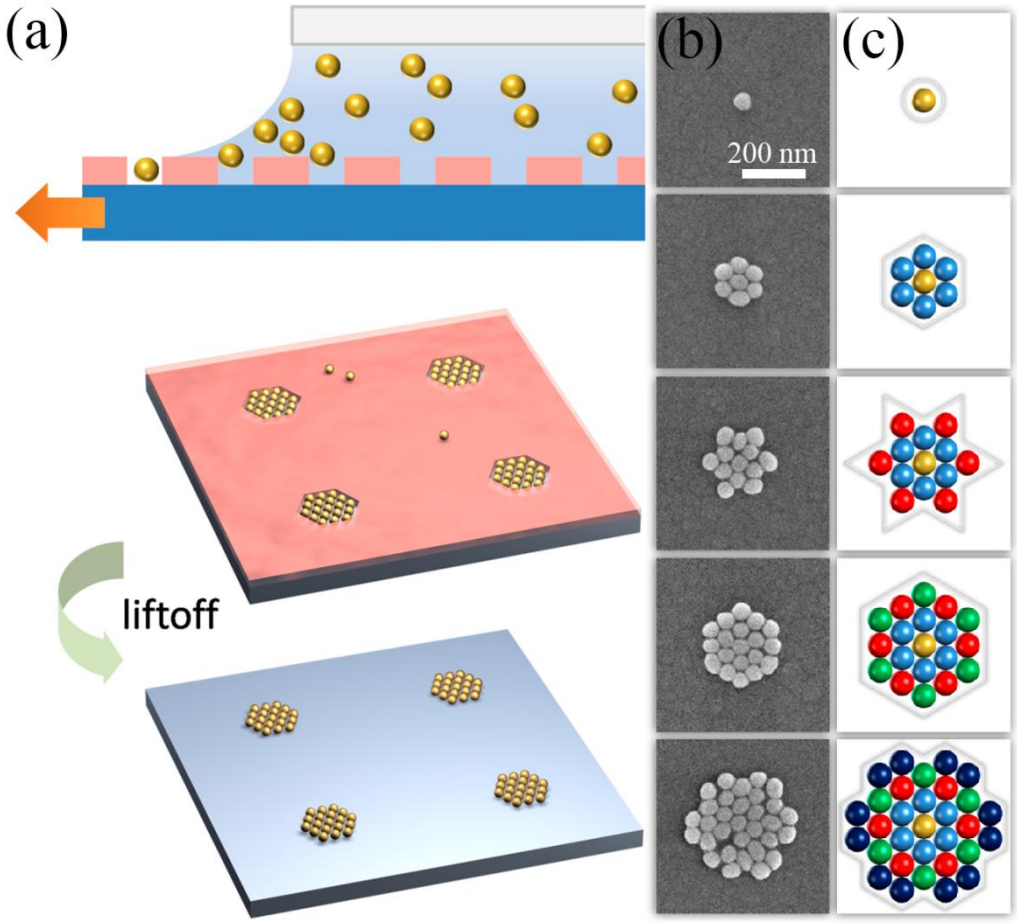

Figure 14. (a) Scheme of the template-assisted self-assembly process. Evaporation of the solvent drives the assembly of nanoparticles within the template. Subsequently, lift-off of the resist layer leaves behind well-defined gold nanosphere assemblies. (b,c) Scanning electron microscopy and scheme of plasmonic oligomer metamolecules assembled within polygonal templates. Modified from ref. [162]

GOLD NANOPARTICLES FOR BIOMEDICAL APPLICATIONS

In 1923, the Dorland's Medical dictionary defined the term "biomedicine" as the *"clinical medicine based on the principles of physiology and biochemistry"*. Nevertheless, the emergence of such field occurred in the middle of 20th century, when the knowledge obtained from biological research and laboratory investigations was applied to clinical medicine.[163] The discovery of the DNA´s structure and biological role led to an understanding of the basic processes that govern life at the molecular level.[164–166] Additionally, the development of new tools, such as electron microscopy techniques or electrophoresis, contributed to the "molecularization" of the biology. Therefore, biomedicine comprised the study of pathophysiological processes from the atomic-molecular level to their consequences at *in vivo* conditions, with the aim of developing new technologies to improve our health.[163]

In this context, gold nanoparticles have been found to be excellent systems for biomedicine. The fruitful combination between the chemical stability of gold with its optical properties at the nanoscale explains the uses of gold nanoparticles on biomedical applications. In fact, the current medical and biological research with gold nanoparticles is very broad and the body of existing information is constantly reviewed.[167–169]

Gold is a transition metal with atomic number 79 that belongs to the group 11 of elements, presenting an electronic configuration [Xe] 4f14 5d10 6s1. In 1979, Pekka Pyykkö and Jean-Paul Desclaux discovered what is now termed relativistic effects in properties of gold: gold shows an unusually large relativistic 6s-orbital stabilization (contraction). As a result, the ionization potential, electron affinity and chemical stability are significantly increased respect to the other elements of group 11: copper and silver.[170] The direct consequence of the low chemical reactivity of gold is its low cytotoxicity, which makes it an ideal material for biomedical applications. Although mild cytotoxic effects of gold nanoparticles have been described, they are mainly ascribed to the nanodimension of the material and unsuitable molecular surface chemistry. [171–174]

Toxic effects of gold nanomaterials can be modulated through the design of the surface functionalization, as well as via shape and size tuning. Moreover, an appropriate functionalization is crucial to control its biological behavior and colloidal stability. In fact, for any desired application, the nature of the molecules and macromolecules attached to the gold

surface determine the biological compatibility and specificity of the nanoparticles. Nowadays, a rich variety of functional molecules and biomolecules can be used depending on the desired purpose.[167,169,175] The coating strategy generally relies on the use of molecular moieties which bond to surface gold atoms. Among other anchoring functionalities, thiol, amine and carboxylate groups are the most commonly exploited linkers. Due to the strength of the S-Au bond that is higher than the Au-Au bond, thiols are employed to firmly attach molecules at the nanoparticles surface.[167,175–177] On the other hand, amine and carboxylate groups are used in those applications where controlled release of the conjugated molecule is desired, i.e. by an external stimuli, pH...[167,169,178,179]

Nevertheless, the use of synthesized molecules is not always necessary, since it is also possible to conduct direct functionalization of biomolecules and biopolymers due to the presence of thiol, amine and carboxylate groups in their structures.[167,180] Therefore, the rich surface chemistry of gold nanoparticles opens up access to the functionalization with a library of biomolecules present in living organisms, allowing a transfer of their biofunctions to the nanoparticles. For instance, controlled delivery of gold nanoparticles to targeted cells requires functionalization with specific antibodies.[169,181] The combination of such powerful tool with the plasmonic properties of gold nanoparticles fuels their uses for a large number of applications that comprise different aspects of diagnostic and therapy, among others.

Gold Nanoparticles for Diagnostic

The use of gold nanoparticles for diagnostic is mainly related to their plasmonic properties: the strong interaction with light, the sensitivity of the plasmonic resonance to changes in the dielectric medium and the aggregation state of the particles, and the Raman signal enhancing properties. One of the most popular techniques for bioimaging is dark field microscopy. First described by El-Sayed´s group, this method is based on the preparation of gold nanoparticles conjugated with tumor-antigen-specific antibodies which preferentially link to cancerous cells surfaces.[182] Subsequently, the tumor can be mapped via dark field microscopy with an accuracy of several cells. Similar approaches can be also applied for detection of bacteria[183] or viruses.[184]Furthermore, since gold is a heavy element, the nanoparticles can be

used for immunoelectron microscopy for the identification of proteins, cancer cells, infectious agents and their surface antigens of cell compartments.[169,185–187]

Detection and recognition of biomacromolecules, such as DNA and proteins, by gold nanoparticles have received also great attention. The so-called sol particle immunoassay was introduced by Leuverin et al. in 1980.[188] Later on, Mirkin et al. developed a new version for the detection of DNA.[189,190] It is based on spectroscopic detection of the plasmon resonance shift induced by biomolecules when they absorb on a surface (the dielectric constant of the medium changes), and by nanoparticle aggregation produced by the analyte. This technique has been implemented for the detection of cancer markers, Alzheimer disease markers etc.[167,169,175] Additionally, it can be complemented with other spectroscopic techniques such as SERS, which can provide structural information at the molecular level.[191,192]

Membrane immunoassays (dot and blot assays) are widely employed in biological and medical analysis. The most common labels are radioactive isotopes (^{125}I, ^{14}C, ^{3}H) and enzymes such peroxidase or alkaline phosphatase. In this context, the use of gold nanoparticles due to their intense coloration has results into faster and cost efficient methods for the detection of proteins with improved detection limits (pM range).[169]

On the other hand, SERS is a powerful vibrational spectroscopy tool that has been implemented for imaging, qualitative and quantitative sensing, and structural analysis. For example, gold nanostars encoded with Raman reporter molecules have been used for multiplexed cell discrimination and cell tracking by SERS imaging (Figure 15).[193] Since the optimized limit of detection is at the single molecule level, this technique has attracted much interest for the fabrication of biosensors.[136,194] Rational design of the gold nanomaterials allows detection and quantification of small molecules,[195] metallic ions,[196] hormones,[197] proteins[198] etc.. Particularly, Parkinson´s and Alzheimer´s diseases have been focus of attention due to their devastating effect on human health. Different SERS biosensors based on gold nanoparticles have been developed in the last decade with the aim of detecting such diseases at early stages.[191,198,199]

In this thesis, we have rationally functionalized gold nanoparticles to induce the controlled formation of amyloid oligomers of a model synthetic bacterial prionoid. Furthermore, we have monitorized and characterized the oligomerization using gold nanoparticle-based immunoelectron microscopy, UV-Vis-NIR and SERS spectroscopy (see Chapter 3).

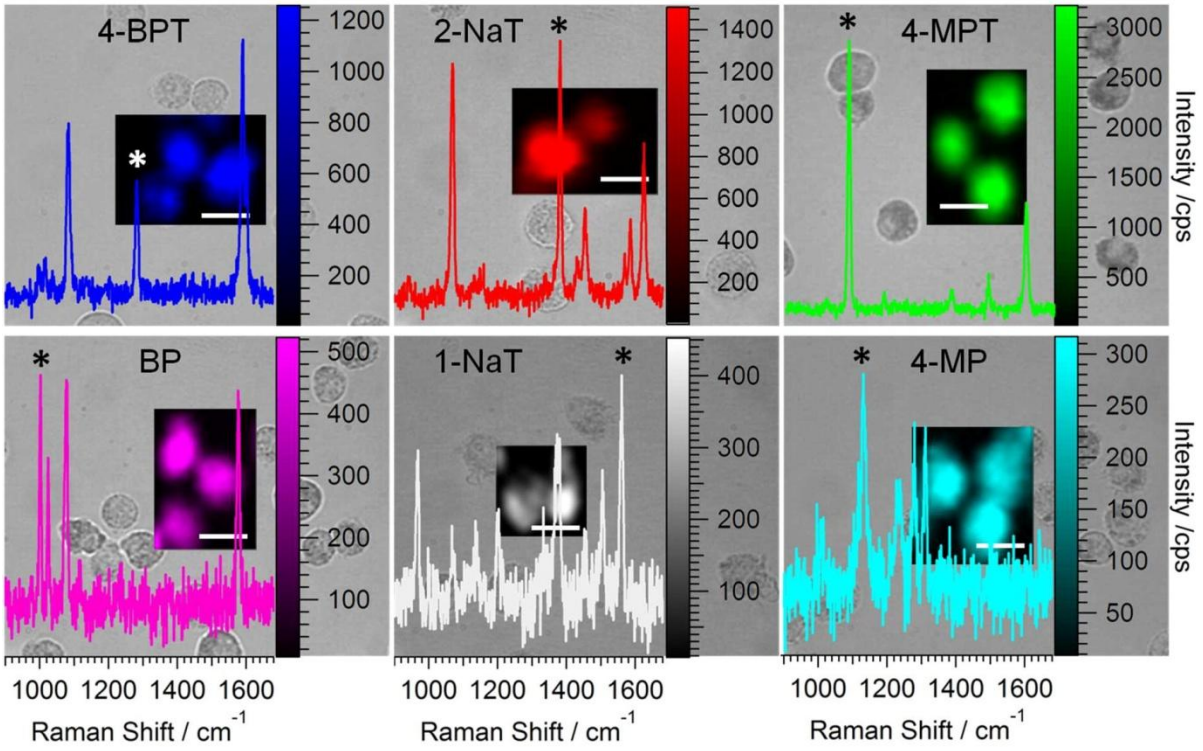

Figure 15. Bright-field optical images of several macrophages which are labeled with six different SERS tags (4-mercaptophenol: 4-MP, 1-naphtalenethiol: 1-NaT, benzenethiol: BT, 4-methylbenzenethiol: 4-MBT, 2-naphtalenethiol: 2-NaT, 4-biphenylthiol: 4-BPT), The corresponding SERS spectra and colored SERS maps are also plotted and overlaid on each image respectively. The specific signals selected for SERS mapping are marked with *. The white scale bars correspond to 20 μm. Adapted from ref. [193]

Gold Nanoparticles for Therapy

There are two main therapeutic uses of gold nanoparticles under intense investigation: drug and gene delivery, and photothermal and photodynamic therapy.[167,169] Drug and gene delivery is based on the targeted delivery of molecular systems such as antitumor preparations, antibiotics and genes. However, since in this thesis we have investigated in photothermal and photodynamic therapy, from now on we will focus on this use of gold nanoparticles.

Photothermal therapy is probably one of the most promising strategies for cancer treatment, which main goal is the generation of high enough local heating inside tumor cells to

induce their death.[200] First described in 2003, the role of plasmonic gold nanoparticles is the conversion of laser light into heat.[201] In order to fulfil such requirements, the localized surface plasmon resonance of the nanoparticles should match the spectral window for biological tissue (700-900 nm).[202] It is to be note that the shape, size, aggregation state and functionalization of the nanoparticles may be optimized with the aim of minimizing toxicity for living cells (Figure 16).[169] Generally, rational surface functionalization with antibodies enables efficient delivery to the cell targets, reducing negative side effects. Colloidal stability is most often achieved via surface co-functionalization with thiolated biocompatible polymers.[203]

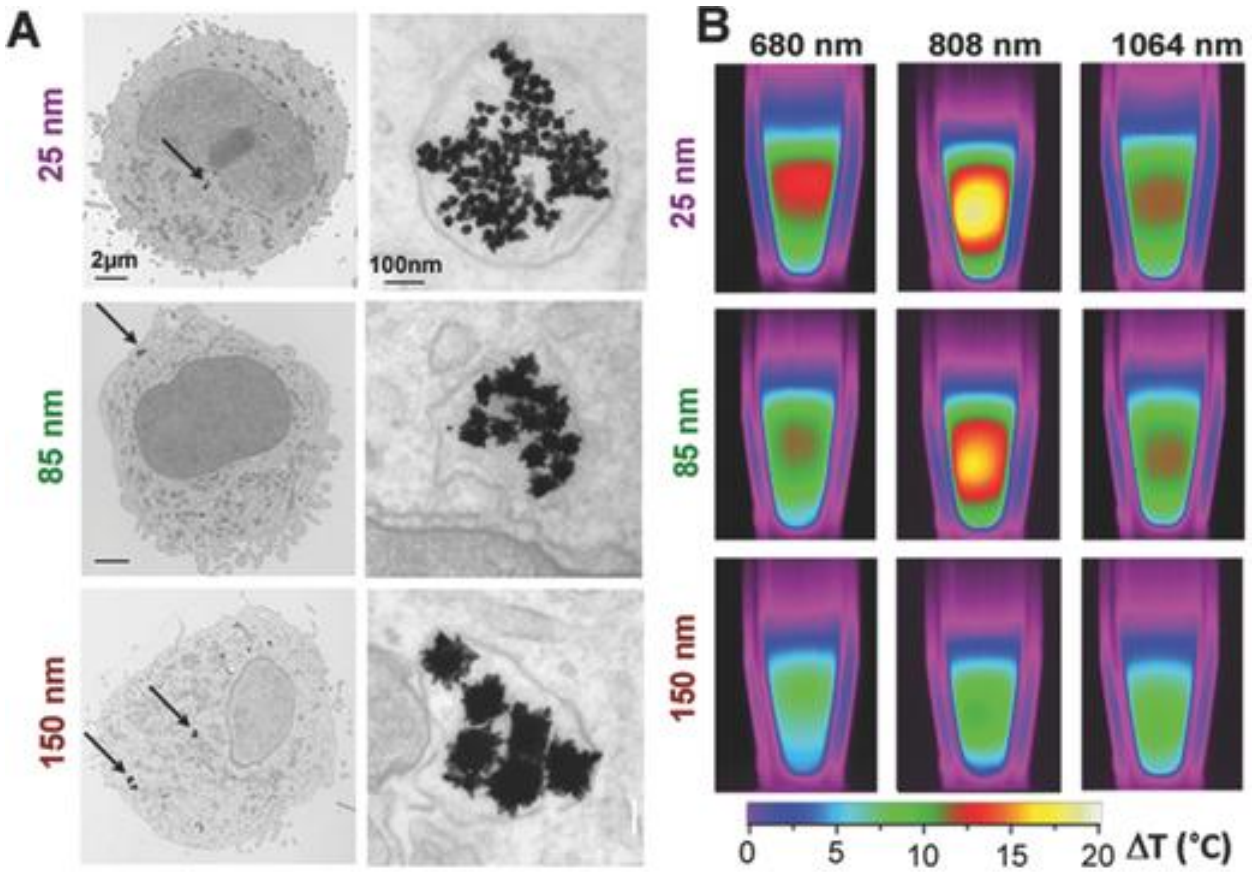

Figure 16. A) TEM images showing the internalization of gold nanostars into cancer cells (scale bars 2 μm and 100 nm). B) Infrared thermal images of the cell samples (150 μL of PBS containing about 15 million cells and gold nanostars). From top to bottom, infrared thermal images showing the effect of 1 min laser irradiation (at 680, 808, and 1064 nm and 1 W cm^{-2}) of cells incubated with gold nanostars of different sizes: 25, 85, and 150 nm. Optimum heating is produced by the 25 and 85 nm stars with laser irradiation at 808 nm Adapted from ref. [202]

The main difference between photothermal and photodynamic therapy, the other commonly researched phototherapy based on gold nanoparticles, is the mechanism whereby cancer cell death is produced. In the case of photodynamic therapy, laser light is used to produce highly toxic oxygen radical species inside the cells.[169,181,204,205] Since the necessary experimental conditions for both therapies are very similar, the boundaries between the effect of heat and radical species generation are sometimes diffuse. Therefore, occasionally, both phenomena may contribute simultaneously to cell death.

However, the underlying mechanisms of photothermal therapy still remain poorly understood. First of all, the nature of the laser irradiation is of main importance, since the effect of continuous, nanosecond and femtosecond pulse lasers are clearly different. For instance, the energy deposited per unit time is much lower in the case of a continuous laser, but more homogenously time distributed.[169,200,206,207] On the other hand, pulse laser generates intense short heating which can produce also the formation of efficient cavitation processes.[208] In any case, researchers aim to induce cell death via apoptotic pathway rather than necrosis, which leads to inflammatory effects on the adjacent tissue.[169,200,206,207]

Despite the numerous publications regarding the synthesis of plasmonic nanostructures (gold nanostars, nanorods, etc..)[168] for efficient photothermal therapy, one of the main drawbacks is the amount of laser energy that may be deposited on the tumor without damaging the healthy adjacent tissue. In Chapter 6, we show a facile method for the self-assembly of gold nanorods inside mammalian breast cancer cells for the optimization of the femtosecond laser photothermal therapy.

REFERENCES

(1) Pradeep, T.; Anshup. Noble Metal Nanoparticles for Water Purification: A Critical Review. *Thin Solid Films* **2009**, *517*, 6441–6478.

(2) Aćimović, S. S.; Ortega, M. A.; Sanz, V.; Berthelot, J.; Garcia-Cordero, J. L.; Renger, J.; Maerkl, S. J.; Kreuzer, M. P.; Quidant, R. LSPR Chip for Parallel, Rapid, and Sensitive Detection of Cancer Markers in Serum. *Nano Lett.* **2014**, *14*, 2636–2641.

(3) Huang, X.; El-Sayed, I. H.; El-Sayed, M. A. Applications of Gold Nanorods for Cancer Imaging and Photothermal Therapy. *Methods Mol. Biol.* **2010**, *624*, 343–357.

(4) Plass, R.; Pelet, S.; Krueger, J.; Grätzel, M.; Bach, U. Quantum Dot Sensitization of Organic−Inorganic Hybrid Solar Cells. *J. Phys. Chem. B* **2002**, *106*, 7578–7580.

(5) Bodelón, G.; Montes-García, V.; López-Puente, V.; Hill, E. H.; Hamon, C.; Sanz-Ortiz, M. N.; Rodal-Cedeira, S.; Costas, C.; Celiksoy, S.; Pérez-Juste, I.; *et al.* Detection and Imaging of Quorum Sensing in Pseudomonas Aeruginosa Biofilm Communities by Surface-Enhanced Resonance Raman Scattering. *Nat. Mater.* **2016**, *15*, 1203–1211.

(6) NSET. NSF's National Nanotechnology Initiative (NNI) - Nanotechnology definition https://www.nsf.gov/crssprgm/nano/reports/omb_nifty50.jsp (accessed Mar 21, 2017).

(7) Feynman, R. P. There's Plenty of Room at the Bottom. *Eng. Sci.* **1960**, *23*, 22–36.

(8) Drexler, K. E. Molecular Engineering: An Approach to the Development of General Capabilities for Molecular Manipulation. *Proc. Natl. Acad. Sci.* **1981**, *78*, 5275–5278.

(9) Taniguchi, N. On the Basic Concept of "Nano-Technology." In *Proc. Intl. Conf. Prod. Eng.*; 1974.

(10) Rouke, M. Plenty of Room Indeed. *Scientif American Special Edition, The edge of Physics*. 2003, pp. 92–100.

(11) Dong, X. *Discovering the Nanoscale*; Baird, D., Nordmann, A., Schummer, J., Ed.; Amsterdam, 2004; Vol. 3.

(12) Zhao, X.; Norris, S. J.; Liu, J. Molecular Architecture of the Bacterial Flagellar Motor in Cells. *Biochemistry* **2014**, *53*, 4323–4333.

(13) Ensikat, H. J.; Ditsche-Kuru, P.; Neinhuis, C.; Barthlott, W. Superhydrophobicity in Perfection: The Outstanding Properties of the Lotus Leaf. *Beilstein J. Nanotechnol.* **2011**, *2*, 152–161.

(14) Koch, K.; Bhushan, B.; Barthlott, W. Diversity of Structure, Morphology and Wetting of Plant Surfaces. *Soft Matter* **2008**, *4*, 1943-1963.

(15) Grzelczak, M.; Vermant, J.; Furst, E. M.; Liz-Marzán, L. M. Directed Self-Assembly of Nanoparticles. *ACS Nano* **2010**, *4*, 3591–3605.

(16) Vigderman, L.; Khanal, B. P.; Zubarev, E. R. Functional Gold Nanorods: Synthesis, Self-Assembly, and Sensing Applications. *Adv. Mater.* **2012**, *24*, 4811–4841.

(17) Yabu, H.; Shimomura, M. Preparation of Self-Organized Mesoscale Polymer Patterns on a Solid Substrate: Continuous Pattern Formation from a Receding Meniscus. *Adv. Funct. Mater.* **2005**, *15*, 575–581.

(18) Tanner, D. B. Optical Effects in Solids. *Department of Physics, University of Florida*, 2013, 6–86.

(19) Aiken, J. D.; Finke, R. G. A Review of Modern Transition-Metal Nanoclusters: Their Synthesis, Characterization, and Applications in Catalysis. *J. Mol. Catal. A Chem.* **1999**, *145*, 1–44.

(20) Schmid, G. Large Clusters and Colloids - Metals in the Embryonic State. *Chem. Rev.* **1992**, *92*, 1709–1727.

(21) Liu, M.; Wang, R. Y. Size-Dependent Melting Behavior of Colloidal In, Sn, and Bi Nanocrystals. *Sci. Rep.* **2015**, *5*, 16353.

(22) Couchman, P. R.; Jesser, W.. Thermodynamic Theory of Size Dependence of Melting Temperature in Metals. *Nature* **1977**, *269*, 481–483.

(23) Henglein, A. Small-Particle Research: Physicochemical Properties of Extremely Small Colloidal Metal and Semiconductor Particles. *Chem. Rev.* **1989**, *89*, 1861–1873.

(24) Yu, X.; Zhan, Z. The Effects of the Size of Nanocrystalline Materials on Their Thermodynamic and Mechanical Properties. *Nanoscale Res. Lett.* **2014**, *9*, 516-522.

(25) Goldstein, A.; Echer, C.; Alivisatos, A. Melting in Semiconductor Nanocrystals. *Science* **1992**, *256*, 1425–1427.

(26) Liu, H. B.; Ascencio, J. A.; Perez-Alvarez, M.; Yacaman, M. J. Melting Behavior of Nanometer Sized Gold Isomers. *Surf. Sci.* **2001**, *491*, 88–98.

(27) Bastús, N. G.; Comenge, J.; Puntes, V. Kinetically Controlled Seeded Growth Synthesis of Citrate-Stabilized Gold Nanoparticles of up to 200 nm: Size Focusing versus Ostwald Ripening. *Langmuir* **2011**, *27*, 11098–11105.

(28) Watt, J.; Hance, B. G.; Anderson, R. S.; Huber, D. L. Effect of Seed Age on Gold Nanorod Formation: A Microfluidic, Real-Time Investigation. *Chem. Mater.* **2015**, *27*, 6442–6449.

(29) Klabunde, K. J.; Stark, J.; Koper, O.; Mohs, C.; Park, D. G.; Decker, S.; Jiang, Y.; Lagadic, I.; Zhang, D. Nanocrystals as Stochiometric Reagents with Unique Surface Chemistry. *J. Phys. Chem.* **1996**, *100*, 12142–12153.

(30) Mukherjee, S.; Libisch, F.; Large, N.; Neumann, O.; Brown, L. V.; Cheng, J.; Lassiter, J. B.; Carter, E. A.; Nordlander, P.; Halas, N. J. Hot Electrons Do the Impossible: Plasmon-Induced Dissociation of H_2 on Au. *Nano Lett.* **2013**, *13*, 240–247.

(31) Alivisatos, A. P. Semiconductor Clusters, Nanocrystals, and Quantum Dots. *Science* **1996**, *271*, 933–937.

(32) Atkins, P. W.; De Paula, J.; Cwi, S. *Química Física*; Médica Panamericana, 2008.

(33) Alivisatos, A. P. Perspectives on the Physical Chemistry of Semiconductor Nanocrystals. *J. Phys. Chem.* **1996**, *100*, 13226–13239.

(34) Smith, A. M.; Nie, S. Chemical Analysis and Cellular Imaging with Quantum Dots. *Analyst* **2004**, *129*, 672.

(35) Lim, B. Y. X. The Nanoscale Rainbow. *Nature News*. 2016, pp. 26–28.

(36) Schlamp, M. C.; Peng, X. G.; Alivisatos, A. P. Improved Efficiencies in Light Emitting Diodes Made with CdSe(CdS) Core/shell Type Nanocrystals and a Semiconducting Polymer. *J. Appl. Phys.* **1997**, *82*, 5837–5842.

(37) Yoffe, A. D. Low-Dimensional Systems: Quantum Size Effects and Electronic Properties of Semiconductor Microcrystallites (Zero-Dimensional Systems) and Some Quasi-Two-Dimensional Systems. *Adv. Phys.* **1993**, *42*, 173–262.

(38) Vossmeyer, T.; Katsikas, L.; Giersig, M.; Popovic, I.; Diesner, K.; Chemseddine, A.; Eychmuller, A.; Weller, H. Cds Nanoclusters-Synthesis, Characterization, Size-Dependent Oscillator Strength, Temperature Shift of the Excitonic-Transition Energy, and Reversible Absorbency Shift. *J. Phys. Chem.* **1994**, *98*, 7665–7673.

(39) Bourzac, K. Quantum Dots Go on Display. *Nature* **2013**, *493*, 283.

(40) Medintz, I. L.; Uyeda, H. T.; Goldman, E. R.; Mattoussi, H. Quantum Dot Bioconjugates for Imaging, Labelling and Sensing. *Nat. Mater.* **2005**, *4*, 435–446.

(41) Willets, K. A.; Van Duyne, R. P. Localized Surface Plasmon Resonance Spectroscopy and Sensing. *Annu. Rev. Phys. Chem.* **2007**, *58*, 267–297.

(42) Myroshnychenko, V.; Rodríguez-Fernández, J.; Pastoriza-Santos, I.; Funston, A. M.; Novo, C.; Mulvaney, P.; Liz-Marzán, L. M.; García de Abajo, F. J. Modelling the Optical Response of Gold Nanoparticles. *Chem. Soc. Rev.* **2008**, *37*, 1792–1805.

(43) Maier, S. a. *Plasmonics : Fundamentals and Applications*; Springer: New York, 2004; Vol. 677.

(44) Johnson, P. B.; Christy, R. W. Optical Constants of the Noble Metals. *Phys. Rev. B* **1972**, *6*, 4370–4379.

(45) Refractiveindex.INFO http://refractiveindex.info (accessed Mar 17, 2017).

(46) Aizpurua, J.; Hillenbrand, R. Localized Surface Plasmons: Basics and Applications in Field-Enhanced Spectroscopy. In *Plasmonics*; Enoch, S.; Bonod, N., Eds.; Springer Series in Optical Sciences; Springer Berlin Heidelberg: Berlin, Heidelberg, 2012; Vol. 167, pp. 151–176.

(47) Benson, O. Assembly of Hybrid Photonic Architectures from Nanophotonic Constituents. *Nature* **2011**, *480*, 193–199.

(48) Gramotnev, D. K.; Bozhevolnyi, S. I. Plasmonics beyond the Diffraction Limit. *Nat.*

Photonics **2010**, *4*, 83–91.

(49) Auguié, B. Optical Properties of Gold Nanostructures, PhD Thesis, University of Exeter, 2009.

(50) Lohse, S. E.; Burrows, N. D.; Scarabelli, L.; Liz-Marzán, L. M.; Murphy, C. J. Anisotropic Noble Metal Nanocrystal Growth: The Role of Halides. *Chem. Mater.* **2014**, *26*, 34–43.

(51) Liz-Marzán, L. M. Tailoring Surface Plasmons through the Morphology and Assembly of Metal Nanoparticles. *Langmuir* **2006**, *22*, 32–41.

(52) Myroshnychenko, V.; Rodríguez-Fernández, J.; Pastoriza-Santos, I.; Funston, A. M.; Novo, C.; Mulvaney, P.; Liz-Marzán, L. M.; García de Abajo, F. J. Modelling the Optical Response of Gold Nanoparticles. *Chem. Soc. Rev.* **2008**, *37*, 1792-1805.

(53) Jiang, L.; Liang, Z.; Sun, J.; Jiang, Y.; Jiang, L. Plasmonic Enhanced Optoelectronic Devices. *Plasmonics* **2014**, *9*, 859–866.

(54) Mayer, M.; Scarabelli, L.; March, K.; Altantzis, T.; Tebbe, M.; Kociak, M.; Bals, S.; Garc, F. J.; Fery, A.; Liz-marza, L. M. Controlled Living Nanowire Growth: Precise Control over the Morphology and Optical Properties of AgAuAg Bimetallic Nanowires. *Nano Lett.* **2015**, *15*, 5427–5437.

(55) Romero, I.; Aizpurua, J.; Bryant, G. W.; García De Abajo, F. J. Plasmons in Nearly Touching Metallic Nanoparticles: Singular Response in the Limit of Touching Dimers. *Opt. Express* **2006**, *14*, 9988–9999.

(56) Jain, P. K.; Huang, W.; El-Sayed, M.. On the Universal Scaling Behavior of the Distance Decay of Plasmon Coupling in Metal Nanoparticle Pairs: A Plasmon Ruler Equation. *Nano Lett.* **2007**, *7*, 2080–2088.

(57) Funston, A. M.; Novo, C.; Davis, T. J.; Mulvaney, P. Plasmon Coupling of Gold Nanorods at Short Distances and in Different Geometries. *Nano Lett.* **2009**, *9*, 1651–1658.

(58) Zuloaga, J.; Prodan, E.; Nordlander, P. Quantum Description of the Plasmon Resonances of a Nanoparticle Dimer. *Nano Lett.* **2009**, *9*, 887–891.

(59) Moskovits, M.; Suh, J. S. Surface Selection Rules for Surface-Enhanced Raman Spectroscopy: Calculations and Application to the Surface-Enhanced Raman Spectrum of Phthalazine on Silver. *J. Phys. Chem.* **1984**, *88*, 5526–5530.

(60) Schlücker, S. Surface-Enhanced Raman Spectroscopy: Concepts and Chemical Applications. *Angew. Chem. Int. Ed.* **2014**, *53*, 4756–4795.

(61) Le Ru, E. C.; Blackie, E. J.; Meyer, M.; Etchegoin, P. G. Surface Enhanced Raman Scattering Enhancement Factors: A Comprehensive Study. *J. Phys. Chem. C* **2007**, *111*, 13794–13803.

(62) Aizpurua, J.; Bryant, G. W.; Richter, L. J.; García De Abajo, F. J.; Kelley, B. K.; Mallouk, T. Optical Properties of Coupled Metallic Nanorods for Field-Enhanced Spectroscopy. *Phys. Rev. B* **2005**, *71*, 235420-235433.

(63) Tian, C.; Deng, Y.; Zhao, D.; Fang, J. Plasmonic Silver Supercrystals with Ultrasmall Nanogaps for Ultrasensitive SERS-Based Molecule Detection. *Adv. Opt. Mater.* **2015**, *3*, 404–411.

(64) Kim, D. S.; Honglawan, A.; Yang, S.; Yoon, D. K. Arrangement and SERS Applications of Nanoparticle Clusters Using Liquid Crystalline Template. *ACS Appl. Mater. Interfaces* **2017**, *9*, 7787-7792.

(65) Zhang, C. L.; Lv, K. P.; Cong, H. P.; Yu, S. H. Controlled Assemblies of Gold Nanorods in PVA Nanofiber Matrix as Flexible Free-Standing SERS Substrates by Electrospinning. *Small* **2012**, *8*, 647–653.

(66) Sciau, P. Nanoparticles in Ancient Materials: The Metallic Lustre Decorations of Medieval Ceramics. In *The Delivery of Nanoparticles*; InTech, 2012; pp. 527–528.

(67) Freestone, I.; Meeks, N.; Sax, M.; Higgitt, C. The Lycurgus Cup — A Roman Nanotechnology. *Gold Bull.* **2007**, *40*, 270–277.

(68) Barber, D.; Freestone, I. An Investigation of the Origin of the Color of the Lycurgus Cup by Analytical Transmission Electron-Microscopy. *Archaeometry* **1990**, *32*, 33–45.

(69) Carbert, J. Gold-Based Enamel Colours: The Constitution and Applications of Purple of Cassius. *Gold Bull.* **1980**, *13*, 144–150.

(70) Hunt, L. B. The True Story of Purple of Cassius: The Birth of Gold-Based Glass and Enamel Colours. *Gold Bull.* **1976**, *9*, 134–139.

(71) Zsigmondy, R. Die Chemische Natur Des Cassiusschen Goldpurpurs; *Justus Liebig's Ann. der Chemie* **1898**, *301*, 361–387.

(72) Faraday, M. The Bakerian Lecture: Experimental Relations of Gold (and Other Metals) to Light. *Philos. Trans. R. Soc. London* **1857**, *147*, 145–181.

(73) Antiquitynow.https//antiquitynow.org/2014/03/06/nanotechnology-and-the-ancient-roman-a.breakthrough-1600-years-in-making/ (accessed Mar 21, 2017).

(74) The Royal Institution. www.rigb.org/our-hystory/iconic-objects/iconic-objets-list/faraday-gold-colloid (accessed Mar 21, 2017).

(75) Bastús, N. G.; Comenge, J.; Puntes, V. Kinetically Controlled Seeded Growth Synthesis of Citrate-Stabilized Gold Nanoparticles of up to 200 Nm: Size Focusing versus Ostwald Ripening. *Langmuir* **2011**, *27*, 11098–11105.

(76) Kim, D. S.; Honglawan, A.; Yang, S.; Yoon, D. K. Arrangement and SERS Applications of Nanoparticle Clusters Using Liquid Crystalline Template. *ACS Appl. Mater. Interfaces* **2017**, *9*, 7787-7792.

(77) Xia, Y.; Xia, X.; Peng, H.-C. Shape-Controlled Synthesis of Colloidal Metal Nanocrystals: Thermodynamic versus Kinetic Products. *J. Am. Chem. Soc.* **2015**, 7947–7966.

(78) Besner, S.; Kabashin, A. V.; Winnik, F. M.; Meunier, M. Synthesis of Size-Tunable Polymer-Protected Gold Nanoparticles by Femtosecond Laser-Based Ablation and Seed Growth. *J. Phys. Chem. C* **2009**, *113*, 9526–9531.

(79) Mirkin, C. A.; Letsinger, R. L.; Mucic, R. C.; Storhoff, J. J. A DNA-Based Method for Rationally Assembling Nanoparticles into Macroscopic Materials. *Nature* **1996**, *382*, 607–609.

(80) Brust, M.; Walker, M., Bethell, D.; Schiffrin, D. J.; Whyman, R. Synthesis of Thiol-Derivatised Gold Nanoparticles in a Two-Phase Liquid-Liquid System. *J. Chem. Soc. Chem. Commun.* **1994**, *7*, 801–802.

(81) Jana, N. R.; Gearheart, L.; Murphy, C. J. Wet Chemical Synthesis of High Aspect Ratio Cylindrical Gold Nanorods. *Phys Chem B.* **2001**, *105*, 4065–4067.

(82) Scarabelli, L.; Coronado-Puchau, M.; Giner-Casares, J. J.; Langer, J.; Liz-Marzán, L. M. Monodisperse Gold Nanotriangles: Size Control, Large-Scale Self-Assembly, and Performance in Surface-Enhanced Raman Scattering. *ACS Nano* **2014**, *8*, 5833–5842.

(83) Guerrero-Martínez, A.; Barbosa, S.; Pastoriza-Santos, I.; Liz-Marzán, L. M. Nanostars Shine Bright for You: Colloidal Synthesis, Properties and Applications of Branched Metallic Nanoparticles. *Curr. Opin. Colloid Interface Sci.* **2011**, *16*, 118–127.

(84) Lee, J.-H.; Gibson, K. J.; Chen, G.; Weizmann, Y. Bipyramid-Templated Synthesis of Monodisperse Anisotropic Gold Nanocrystals. *Nat. Commun.* **2015**, *6*, 7571.

(85) Chung, P. J.; Lyu, L. M.; Huang, M. H. Seed-Mediated and Iodide-Assisted Synthesis of Gold Nanocrystals with Systematic Shape Evolution from Rhombic Dodecahedral to Octahedral Structures. *Chem. Eur. J.* **2011**, *17*, 9746–9752.

(86) Lu, X.; Rycenga, M.; Skrabalak, S. E.; Wiley, B.; Xia, Y. Chemical Synthesis of Novel Plasmonic Nanoparticles. *Annu. Rev. Phys. Chem.* **2009**, *60*, 167–192.

(87) Xia, Y.; Xiong, Y.; Lim, B.; Skrabalak, S. E. Shape-Controlled Synthesis of Metal Nanocrystals: Simple Chemistry Meets Complex Physics? *Angew. Chem. Int. Ed.* **2009**, *48*, 60–103.

(88) Xia, Y.; Gilroy, K. D.; Peng, H.-C.; Xia, X. Seed-Mediated Growth of Colloidal Metal Nanocrystals. *Angew. Chem. Int. Ed.* **2016**, *55*, 2–38.

(89) Langille, M. R.; Zhang, J.; Personick, M. L.; Li, S.; Mirkin, C. A. Stepwise Evolution of Spherical Seeds into 20-Fold Twinned Icosahedra. *Science.* **2012**, *337*, 954–957.

(90) Langille, M. R.; Personick, M. L.; Zhang, J.; Mirkin, C.. Defining Rules for the Shape Evolution of Gold Nanoparticles. *J. Am. Chem. Soc.* **2012**, *134*, 14542–14554.

(91) Park, K.; Drummy, L. F.; Wadams, R. C.; Koerner, H.; Nepal, D.; Fabris, L.; Vaia, R. a. Growth Mechanism of Gold Nanorods. *Chem. Mater.* **2013**, *25*, 555–563.

(92) Xiong, Y.; Xia, Y. Shape-Controlled Synthesis of Metal Nanostructures: The Case of

Palladium. *Adv. Mater.* **2007**, *19*, 3385–3391.

(93) Smith, D. K.; Korgel, B. A. The Importance of the CTAB Surfactant on the Colloidal Seed-Mediated Synthesis of Gold Nanorods. *Langmuir* **2008**, *24*, 644-649.

(94) Xiao, J.; Qi, L. Surfactant-Assisted, Shape-Controlled Synthesis of Gold Nanocrystals. *Nanoscale* **2011**, *3*, 1383–1396.

(95) Fan, F.-R.; Liu, D.-Y.; Wu, Y.-F.; Duan, S.; Xie, Z.-X.; Jiang, Z.-Y.; Tian, Z.-Q. Epitaxial Growth of Heterogeneous Metal Nanocrystals: From Gold Nano-Octahedra to Palladium and Silver Nanocubes. *J. Am. Chem. Soc.* **2008**, *130*, 6949–6951.

(96) O'Brien, M. N.; Jones, M. R.; Brown, K. A.; Mirkin, C. A.; O'Brien, M. N.; Jones, M. R.; Brown, K. A.; Mirkin, C. A. Universal Noble Metal Nanoparticle Seeds Realized through Iterative Reductive Growth and Oxidative Dissolution Reactions. *J. Am. Chem. Soc.* **2014**, *136*, 7603–7606.

(97) Liu, M.; Guyot-Sionnest, P. Mechanism of Silver(I)-Assisted Growth of Gold Nanorods and Bipyramids. *J. Phys. Chem. B* **2005**, *109*, 22192–22200.

(98) Lin, Z.; Cai, J. J.; Scriven, L. E.; Davis, H. T. Spherical-to-Wormlike Micelle Transition in CTAB Solutions. *J. Phys. Chem.* **1994**, *98*, 5984–5993.

(99) Meena, S. K.; Celiksoy, S.; Schäfer, P.; Henkel, A.; Sönnichsen, C.; Sulpizi, M.; Rowan, S. J.; Composto, R. J.; Murray, C. B.; Hammouda, B Hess, B.; Lindahl, E.. The Role of Halide Ions in the Anisotropic Growth of Gold Nanoparticles: A Microscopic, Atomistic Perspective. *Phys. Chem. Chem. Phys.* **2016**, *18*, 13246–13254.

(100) Langille, M. R.; Personick, M. L.; Zhang, J.; Mirkin, C. A. Defining Rules for the Shape Evolution of Gold Nanoparticles. *J. Am. Chem. Soc.* **2012**, *134*, 14542–14554.

(101) Wu, H.-L.; Kuo, C.-H.; Huang, M. H. Seed-Mediated Synthesis of Gold Nanocrystals with Systematic Shape Evolution from Cubic to Trisoctahedral and Rhombic Dodecahedral Structures. *Langmuir* **2010**, *26*, 12307–12313.

(102) Huang, M. H.; Chiu, C.-Y. Achieving Polyhedral Nanocrystal Growth with Systematic Shape Control. *J. Mater. Chem. A* **2013**, *1*, 8081-8087.

(103) Ruan, Q.; Shao, L.; Shu, Y.; Wang, J.; Wu, H. Growth of Monodisperse Gold Nanospheres with Diameters from 20 nm to 220 nm and Their Core/Satellite Nanostructures. *Adv. Opt. Mater.* **2014**, *2*, 65–73.

(104) Scarabelli, L.; Sánchez-Iglesias, A.; Pérez-Juste, J.; Liz-Marzán, L. M. A "Tips and Tricks" Practical Guide to the Synthesis of Gold Nanorods. *J. Phys. Chem. Lett.* **2015**, *6*, 4270–4279.

(105) Park, K.; Drummy, L. F.; Wadams, R. C.; Koerner, H.; Nepal, D.; Fabris, L.; Vaia, R. A. Growth Mechanism of Gold Nanorods. *Chem. Mater.* **2013**, *25*, 555–563.

(106) Bullen, C.; Zijlstra, P.; Bakker, E.; Gu, M.; Raston, C. Chemical Kinetics of Gold Nanorod Growth in Aqueous CTAB Solutions. *Cryst. Growth Des.* **2011**, 3375–3380.

(107) Ye, X.; Zheng, C.; Chen, J.; Gao, Y.; Murray, C. B. Using Binary Surfactant Mixtures to Simultaneously Improve the Dimensional Tunability and Monodispersity in the Seeded Growth of Gold Nanorods. *Nano Lett.* **2013**, *13*, 765–771.

(108) Chen, H.; Shao, L.; Li, Q.; Wang, J. Gold Nanorods and Their Plasmonic Properties. *Chem. Soc. Rev.* **2013**, *42*, 2679–2724.

(109) Hamon, C.; Sanz-Ortiz, M. N.; Modin, E.; Hill, E. H.; Scarabelli, L.; Chuvilin, A.; Liz-Marzán, L. M. Hierarchical Organization and Molecular Diffusion in Gold Nanorod/silica Supercrystal Nanocomposites. *Nanoscale* **2016**, *8*, 7914–7922.

(110) Huang, X.; Neretina, S.; El-Sayed, M. A. Gold Nanorods: From Synthesis and Properties to Biological and Biomedical Applications. *Adv. Mater.* **2009**, *21*, 4880–4910.

(111) Ni, W.; Mosquera, R. A.; Pérez-Juste, J.; Liz-Marzán, L. M. Evidence for Hydrogen-Bonding-Directed Assembly of Gold Nanorods in Aqueous Solution. *J. Phys. Chem. Lett.* **2010**, *1*, 1181–1185.

(112) Pérez-Juste, J.; Pastoriza-Santos, I.; Liz-Marzán, L. M.; Mulvaney, P. Gold Nanorods: Synthesis, Characterization and Applications. *Coord. Chem. Rev.* **2005**, *249*, 1870–1901.

(113) Tsai, M.-F.; Chang, S.-H. G.; Cheng, F.-Y.; Shanmugam, V.; Cheng, Y.-S.; Su, C.-H.; Yeh, C.-S. Au Nanorod Design as Light-Absorber in the First and Second Biological Near-Infrared Windows for *in Vivo* Photothermal Therapy. *ACS Nano* **2013**, *7*, 5330–

5342.

(114) Nikoobakht, B.; El-Sayed, M. A. Preparation and Growth Mechanism of Gold Nanorods (NRs) Using Seed-Mediated Growth Method. *Chem. Mater.* **2003**, *15*, 1957–1962.

(115) Tong, W.; Walsh, M. J.; Mulvaney, P.; Etheridge, J.; Funston, A. M. Control of Symmetry Breaking Size and Aspect Ratio in Gold Nanorods: Underlying Role of Silver Nitrate. *J. Phys. Chem. C* **2017**, *121*, 3549–3559.

(116) Scarabelli, L.; Grzelczak, M.; Liz-Marzán, L. M. Tuning Gold Nanorod Synthesis through Prereduction with Salicylic Acid. *Chem. Mater.* **2013**, *25*, 4232–4238.

(117) Lohse, S. E.; Murphy, C. J. The Quest for Shape Control: A History of Gold Nanorod Synthesis. *Chem. Mater.* **2013**, *25*, 1250–1261.

(118) Garg, N.; Scholl, C.; Mohanty, A.; Jin, R. The Role of Bromide Ions in Seeding Growth of Au Nanorods. *Langmuir* **2010**, *26*, 10271–10276.

(119) Sánchez-Iglesias, A.; Winckelmans, N.; Altantzis, T.; Bals, S.; Grzelczak, M.; Liz-Marzán, L. M. High-Yield Seeded Growth of Monodisperse Pentatwinned Gold Nanoparticles through Thermally Induced Seed Twinning. *J. Am. Chem. Soc.* **2017**, *139*, 107–110.

(120) Jana, N. R.; Gearheart, L.; Murphy, C. J. Wet Chemical Synthesis of High Aspect Ratio Cylindrical Gold Nanorods. *J. Phys. Chem. B* **2001**, *105*, 4065–4067.

(121) Gao, J.; Bender, C. M.; Murphy, C. J. Dependence of the Gold Nanorod Aspect Ratio on the Nature of the Directing Surfactant in Aqueous Solution. *Langmuir* **2003**, *19*, 9065–9070.

(122) Johnson, C. J.; Dujardin, E.; Davis, S. A.; Murphy, C. J.; Mann, S. Growth and Form of Gold Nanorods Prepared by Seed-Mediated, Surfactant-Directed Synthesis. *J. Mater. Chem.* **2002**, *12*, 1765–1770.

(123) Almora-Barrios, N.; Novell-Leruth, G.; Whiting, P.; Liz-Marzán, L. M.; López, N. Theoretical Description of the Role of Halides, Silver, and Surfactants on the Structure of Gold Nanorods. *Nano Lett.* **2014**, *14*, 871–875.

(124) Lohse, S. E.; Burrows, N. D.; Scarabelli, L.; Liz-Marzán, L. M.; Murphy, C. J. Anisotropic Noble Metal Nanocrystal Growth: The Role of Halides. *Chem. Mater.* **2014**, *26*, 34–43.

(125) Walsh, M. J.; Barrow, S. J.; Tong, W.; Funston, A. M.; Etheridge, J. Symmetry Breaking and Silver in Gold Nanorod Growth. *ACS Nano* **2015**, *9*, 715–724.

(126) Tong, W.; Walsh, M. J.; Mulvaney, P.; Etheridge, J.; Funston, A. M. Control of Symmetry Breaking Size and Aspect Ratio in Gold Nanorods: Underlying Role of Silver Nitrate. *J. Phys. Chem. C* **2017**, *121*, 3549–3559.

(127) Carbó-Argibay, E.; Rodríguez-González, B.; Gómez-Graña, S.; Guerrero-Martínez, A.; Pastoriza-Santos, I.; Pérez-Juste, J.; Liz-Marzán, L. M. The Crystalline Structure of Gold Nanorods Revisited: Evidence for Higher-Index Lateral Facets. *Angew. Chem. Int. Ed.* **2010**, *49*, 9397–9400.

(128) Ye, X.; Jin, L.; Caglayan, H.; Chen, J.; Xing, G.; Zheng, C.; Doan-Nguyen, V.; Kang, Y.; Engheta, N.; Kagan, C. R.; Murray,C.B.. Improved Size-Tunable Synthesis of Monodisperse Gold Nanorods through the Use of Aromatic Additives. *ACS Nano* **2012**, *6*, 2804–2817.

(129) Wen, T.; Zhang, H.; Tang, X.; Chu, W.; Liu, W.; Ji, Y.; Hu, Z.; Hou, S.; Hu, X.; Wu, X. Copper Ion Assisted Reshaping and Etching of Gold Nanorods: Mechanism Studies and Applications. *J. Phys. Chem. C* **2013,***117*,25769-25777.

(130) Ye, X.; Gao, Y.; Chen, J.; Reifsnyder, D. C.; Zheng, C.; Murray, C. B. Seeded Growth of Monodisperse Gold Nanorods Using Bromide-Free Surfactant Mixtures. *Nano Lett.* **2013**.

(131) Xiong, Y.; Xia, Y. Shape-Controlled Synthesis of Metal Nanostructures: The Case of Palladium. *Adv. Mater.* **2007**, *19*, 3385–3391.

(132) Miranda, O. R.; Dollahon, N. R.; Ahmadi, T. S. Critical Concentrations and Role of Ascorbic Acid (Vitamin C) in the Crystallization of Gold Nanorods within Hexadecyltrimethyl Ammonium Bromide (CTAB)/Tetraoctyl Ammonium Bromide (TOAB) Micelles. *Cryst. Growth Des.* **2006**, *6*, 2747–2753.

(133) Li, L.; Kolle, S.; Weaver, J. C.; Ortiz, C.; Aizenberg, J.; Kolle, M. A Highly Conspicuous

Mineralized Composite Photonic Architecture in the Translucent Shell of the Blue-Rayed Limpet. *Nat. Commun.* **2015**, *6*, 6322-6330.

(134) Hamon, C.; Novikov, S.; Scarabelli, L.; Basabe-Desmonts, L.; Liz-Marzán, L. M. Hierarchical Self-Assembly of Gold Nanoparticles into Patterned Plasmonic Nanostructures. *ACS Nano* **2014**, *8*, 10694–10703.

(135) Guerrero-Martínez, A.; Auguié, B.; Alonso-Gómez, J. L.; Džolič, Z.; Gómez-Graña, S.; Žinić, M.; Cid, M. M.; Liz-Marzán, L. M. Intense Optical Activity from Three-Dimensional Chiral Ordering of Plasmonic Nanoantennas. *Angew. Chem. Int. Ed.* **2011**, *50*, 5499–5503.

(136) Guerrero-Martínez, A.; Grzelczak, M.; Liz-Marzán, L. M. Molecular Thinking for Nanoplasmonic Design. *ACS Nano* **2012**, *6*, 3655–3662.

(137) Le Ru, E. C.; Etchegoin, P. G. Single-Molecule Surface-Enhanced Raman Spectroscopy. *Annu. Rev. Phys. Chem.* **2012**, *63*, 65–87.

(138) Atwater, H. A.; Polman, A. Plasmonics for Improved Photovoltaic Devices. *Nat. Mater.* **2010**, *9*, 205–213.

(139) Kneipp, K.; Wang, Y.; Kneipp, H.; Perelman, L. T.; Itzkan, I.; Dasari, R.; Feld, M. S. Single Molecule Detection Using Surface-Enhanced Raman Scattering (SERS). *Phys. Rev. Lett.* **1997**, *78*, 1667–1670.

(140) Kraus, T.; Wolf, H. Templated Self-Assembly of Particles. In *Springer Handbook of Nanotechnology*; Springer Berlin Heidelberg: Berlin, Heidelberg, 2010; pp. 187–210.

(141) Whitesides, G. M.; Grzybowski, B. Self-Assembly at All Scales. *Science* **2002**, *295*, 2418–2421.

(142) Fialkowski, M.; Bishop, K. J.; Klajn, R.; Smoukov, S. K.; Campbell, C. J.; Grzybowski, B. A. Principles and Implementations of Dissipative (Dynamic) Self-Assembly. *J. Phys. Chem. B* **2006**, *110*, 2482–2496.

(143) Caswell, K. K.; Wilson, J. N.; Bunz, U. H. F.; Murphy, C. J. Preferential End-to-End Assembly of Gold Nanorods by Biotin−Streptavidin Connectors. *J. Am. Chem. Soc.* **2003**, *125*, 13914–13915.

(144) Macfarlane, R. J.; Lee, B.; Jones, M. R.; Harris, N.; Schatz, G. C.; Mirkin, C. Nanoparticle Superlattice Engineering with DNA. *Science* **2011**, *334*, 204–208.

(145) Ni, W.; Mosquera, R. A.; Pérez-Juste, J.; Liz-Marzán, L. M. Evidence for Hydrogen-Bonding-Directed Assembly of Gold Nanorods in Aqueous Solution. *J. Phys. Chem. Lett.* **2010**, *1*, 1181–1185.

(146) Wang, J.; Zhang, P.; Li, C. M.; Li, Y. F.; Huang, C. Z. A Highly Selective and Colorimetric Assay of Lysine by Molecular-Driven Gold Nanorods Assembly. *Biosens. Bioelectron.* **2012**, *34*, 197–201.

(147) Shibu Joseph, S. T.; Ipe, B. I.; Pramod, P.; Thomas, K. G. Gold Nanorods to Nanochains: Mechanistic Investigations on Their Longitudinal Assembly Using A,ω-Alkanedithiols and Interplasmon Coupling. *J. Phys. Chem. B* **2006**, *110*, 150–157.

(148) Scarabelli, L.; Coronado-Puchau, M.; Giner-Casares, J. J.; Langer, J.; Liz-Marzán, L. M. Monodisperse Gold Nanotriangles: Size Control, Large-Scale Self-Assembly, and Performance in Surface-Enhanced Raman Scattering. *ACS Nano* **2014**, *8*, 5833–5842.

(149) Sánchez-Iglesias, A.; Grzelczak, M.; Altantzis, T.; Goris, B.; Pérez-Juste, J.; Bals, S.; Van Tendeloo, G.; Donaldson, S. H.; Chmelka, B. F.; Israelachvili, J. N.; *Liz-Marzán, L.M.* Hydrophobic Interactions Modulate Self-Assembly of Nanoparticles. *ACS Nano* **2012**, *6*, 11059–11065.

(150) Glotzer, S. C.; Mirkin, C. A. Clathrate Colloidal Crystals. *Science* **2017**, *935*, 931–935.

(151) Lukach, A.; Liu, K.; Therien-Aubin, H.; Kumacheva, E. Controlling the Degree of Polymerization, Bond Lengths, and Bond Angles of Plasmonic Polymers. *J. Am. Chem. Soc.* **2012**, *134*, 18853–18859.

(152) Nie, Z.; Fava, D.; Kumacheva, E.; Zou, S.; Walker, G. C.; Rubinstein, M. Self-Assembly of Metal-Polymer Analogues of Amphiphilic Triblock Copolymers. *Nat. Mater.* **2007**, *6*, 609–614.

(153) Klinkova, A.; Choueiri, R. M.; Kumacheva, E. Self-Assembled Plasmonic Nanostructures. *Chem. Soc. Rev.* **2014**, *43*, 3976-3985.

(154) Tan, S. F.; Anand, U.; Mirsaidov, U. Interactions and Attachment Pathways between

Functionalized Gold Nanorods. *ACS Nano* **2017**, *11*, 1633–1640.

(155) Ofir, Y.; Moran, I. W.; Subramani, C.; Carter, K. R.; Rotello, V. M. Nanoimprint Lithography for Functional Three-Dimensional Patterns. *Adv. Mater.* **2010**, *22*, 3608–3614.

(156) Bagheri, S.; Giessen, H.; Neubrech, F. Large-Area Antenna-Assisted SEIRA Substrates by Laser Interference Lithography. *Adv. Opt. Mater.* **2014**, *2*, 1050–1056.

(157) Henzie, J.; Andrews, S. C.; Ling, X. Y.; Li, Z.; Yang, P. Oriented Assembly of Polyhedral Plasmonic Nanoparticle Clusters. *Proc. Natl. Acad. Sci. U. S. A.* **2013**, *110*, 6640–6645.

(158) Tebbe, M.; Mayer, M.; Glatz, B. A.; Hanske, C.; Probst, P. T.; Müller, M. B.; Karg, M.; Chanana, M.; König, T. A. F.; Kuttner, C.; *et al.* Optically Anisotropic Substrates via Wrinkle-Assisted Convective Assembly of Gold Nanorods on Macroscopic Areas. *Faraday Discuss.* **2015**, *181*, 243–260.

(159) Hanske, C.; Tebbe, M.; Kuttner, C.; Bieber, V.; Tsukruk, V. V.; Chanana, M.; König, T. A. F.; Fery, A. Strongly Coupled Plasmonic Modes on Macroscopic Areas via Template-Assisted Colloidal Self-Assembly. *Nano Lett.* **2014**, *14*, 6863–6871.

(160) Hamon, C.; Postic, M.; Mazari, E.; Bizien, T.; Dupuis, C.; Even-Hernandez, P.; Jimenez, A.; Courbin, L.; Gosse, C.; Artzner, F.; Marchi-Artzner, V. Three-Dimensional Self-Assembling of Gold Nanorods with Controlled Macroscopic Shape and Local Smectic B Order. *ACS Nano* **2012**, *6*, 4137–4146.

(161) Zhou, Y.; Zhou, X.; Park, D. J.; Torabi, K.; Brown, K. A.; Jones, M. R.; Zhang, C.; Schatz, G. C.; Mirkin, C. A. Shape-Selective Deposition and Assembly of Anisotropic Nanoparticles. *Nano Lett.* **2014**, *14*, 2157–2161.

(162) Greybush, N. J.; Liberal, I.; Malassis, L.; Kikkawa, J. M.; Engheta, N.; Murray, C. B.; Kagan, C. R. Plasmon Resonances in Self-Assembled Two-Dimensional Au Nanocrystal Metamolecules. *ACS Appl. Mater. Interfaces* **2016**, DOI: 10.1021/acsnano.6b08189.

(163) Quirke, V.; Gaudiilière, J.-P. The Era of Biomedicine: Science, Medicine, and Public Health in Britain and France after the Second World War. *Med. Hist.* **2008**, *52*, 441–452.

(164) Chargaff, E. Chemical Specificity of Nucleic Acids and Mechanism of Their Enzymatic

Degradation. *Experientia* **1950**, *6*, 201–209.

(165) Levene, P. A. The Structure Of Yeast Nucleic Acid: Iv. Ammonia Hydrolysis. *J. Biol. Chem.* **1917**, 415–424.

(166) Watson, J. D.; Crick, F. H. C. Molecular Structure of Nucleic Acids: A Structure for Deoxyribose Nucleic Acid. *Nature* **1953**, *171*, 737–738.

(167) Dreaden, E. C.; Alkilany, A. M.; Huang, X.; Murphy, C. J.; El-Sayed, M. A. The Golden Age: Gold Nanoparticles for Biomedicine. *Chem. Soc. Rev.* **2012**, *41*, 2740–2779.

(168) Abadeer, N. S.; Murphy, C. J. Recent Progress in Cancer Thermal Therapy Using Gold Nanoparticles. *J. Phys. Chem. C* **2016**, *120*, 4691–4716.

(169) Dykman, L.; Khlebtsov, N. Gold Nanoparticles in Biomedical Applications: Recent Advances and Perspectives. *Chem. Soc. Rev.* **2012**, *41*, 2256–2282.

(170) Pyykko, P.; Desclaux, J. P. Relativity and the Periodic System of Elements. *Acc. Chem. Res.* **1979**, *12*, 276–281.

(171) Pan, Y.; Neuss, S.; Leifert, A.; Fischler, M.; Wen, F.; Simon, U.; Schmid, G.; Brandau, W.; Jahnen-Dechent, W. Size-Dependent Cytotoxicity of Gold Nanoparticles. *Small* **2007**, *3*, 1941–1949.

(172) Murphy, C. J.; Gole, A. M.; Stone, J. W.; Sisco, P. N.; Alkilany, A. M.; Goldsmith, E. C.; Baxter, S. C. Gold Nanoparticles in Biology: Beyond Toxicity to Cellular Imaging. *Acc. Chem. Res.* **2008**, *41*, 1721–1730.

(173) Fratoddi, I.; Venditti, I.; Cametti, C.; Russo, M. V. How Toxic Are Gold Nanoparticles? The State-of-the-Art. Nano Res.2015, 8, 1771-1799.

(174) Alkilany, A. M.; Murphy, C. J. Toxicity and Cellular Uptake of Gold Nanoparticles: What We Have Learned so Far? *J. Nanopart. Res.* **2010**, *12*, 2313–2333.

(175) Giljohann, D. A.; Seferos, D. S.; Daniel, W. L.; Massich, M. D.; Patel, P. C.; Mirkin, C. A. Gold Nanoparticles for Biology and Medicine. *Angew. Chem.-Int. Ed.* **2010**, *49*, 3280–3294.

(176) Xue, Y.; Li, X.; Li, H.; Zhang, W. Quantifying Thiol-Gold Interactions towards the

Efficient Strength Control. *Nat. Commun.* **2014**, *5*, 4348.

(177) Boisselier, E.; Astruc, D. Gold Nanoparticles in Nanomedicine: Preparations, Imaging, Diagnostics, Therapies and Toxicity. *Chem. Soc. Rev.* **2009**, *38*, 1759-1766.

(178) Madhusudhan, A.; Reddy, G.; Venkatesham, M.; Veerabhadram, G.; Kumar, D.; Natarajan, S.; Yang, M.-Y.; Hu, A.; Singh, S. Efficient pH Dependent Drug Delivery to Target Cancer Cells by Gold Nanoparticles Capped with Carboxymethyl Chitosan. *Int. J. Mol. Sci.* **2014**, *15*, 8216–8234.

(179) Yi, Y.; Wang, H.; Wang, X.-W.; Liu, Q.; Ye, M.; Tan, W. A Smart, Photocontrollable Drug Release Nanosystem for Multifunctional Synergistic Cancer Therapy. *ACS Appl. Mater. Interfaces* **2017**, *9*, 5847–5854.

(180) Singh, A. V.; Bandgar, B. M.; Kasture, M.; Prasad, B. L. V.; Sastry, M.; Curtis, A. S. G.; Muhammed, M.; Sastry, M. Synthesis of Gold, Silver and Their Alloy Nanoparticles Using Bovine Serum Albumin as Foaming and Stabilizing Agent. *J. Mater. Chem.* **2005**, *15*, 5115-5121.

(181) El-Sayed, I. H.; Huang, X.; El-Sayed, M. A. Selective Laser Photo-Thermal Therapy of Epithelial Carcinoma Using Anti-EGFR Antibody Conjugated Gold Nanoparticles. *Cancer Lett.* **2006**, *239*, 129–135.

(182) Ivan H. El-Sayed; Xiaohua Huang; Mostafa A. El-Sayed. Surface Plasmon Resonance Scattering and Absorption of Anti-EGFR Antibody Conjugated Gold Nanoparticles in Cancer Diagnostics: Applications in Oral Cancer. *Nanolett.* **2005**, *5*, 829-834.

(183) Xu, X.; Chen, Y.; Wei, H.; Xia, B.; Liu, F.; Li, N. Counting Bacteria Using Functionalized Gold Nanoparticles as the Light-Scattering Reporter. *Anal. Chem.* **2012**, *84*, 9721–9728.

(184) Wan, X.-Y.; Zheng, L.-L.; Gao, P.-F.; Yang, X.-X.; Li, C.-M.; Li, Y. F.; Huang, C. Z. Real-Time Light Scattering Tracking of Gold Nanoparticles- Bioconjugated Respiratory Syncytial Virus Infecting HEp-2 Cells. *Sci. Rep.* **2014**, *4*, 4529-4536

(185) Shirota, K.; Minassian, H.; Jothy, S. Protein G-Gold Immunoelectron Microscopy of Colon Carcinoma: The Effect of Tumor Differentiation on Carcinoembryonic Antigen

Immunostaining. *Exp. Mol. Pathol.* **1988**, *49*, 305–315.

(186) Vreeswijk, J.; Folkers, E.; Wagenaar, F.; Kapsenberg, J. G. The Use of Colloidal Gold Immunoelectron Microscopy to Diagnose Varicella-Zoster Virus (VZV) Infections by Rapid Discrimination between VZV, HSV-1 and HSV-2. *J. Virol. Methods* **1988**, *22*, 255–271.

(187) Geuze, H. J.; Slot, J. W.; van der Ley, P. A.; Scheffer, R. C. Use of Colloidal Gold Particles in Double-Labeling Immunoelectron Microscopy of Ultrathin Frozen Tissue Sections. *J. Cell Biol.* **1981**, *89*, 653–665.

(188) Leuvering, J. H. W.; Thal, P. J. H. M.; Waart, M. van der; Schuurs, A. H. W. M. Sol Particle Immunoassay (SPIA). *J. Immunoassay* **1980**, *1*, 77–91.

(189) Cao, Y. C.; Jin, R.; Mirkin, C. A. Nanoparticles with Raman Spectroscopic Fingerprints for DNA and RNA Detection. *Science* **2002**, *297*,1536-1540.

(190) Taton, T. A.; Mirkin, C. A.; Letsinger, R. L. Scanometric DNA Array Detection with Nanoparticle Probes. *Science* **2000**, *289*,1998-2001.

(191) Kurouski, D.; Sorci, M.; Postiglione, T.; Belfort, G.; Lednev, I. K. Detection and Structural Characterization of Insulin Prefibrilar Oligomers Using Surface Enhanced Raman Spectroscopy. *Biotechnol. Prog.* **2014**, *30*, 488-495

(192) Guerrini, L.; Arenal, R.; Mannini, B.; Chiti, F.; Pini, R.; Matteini, P.; Alvarez-Puebla, R. A. SERS Detection of Amyloid Oligomers on Metallorganic-Decorated Plasmonic Beads. *ACS Appl. Mater. Interfaces* **2015**, *7*, 9420–9428.

(193) Jimenez de Aberasturi, D.; Serrano-Montes, A. B.; Langer, J.; Henriksen-Lacey, M.; Parak, W. J.; Liz-Marzán, L. M. Surface Enhanced Raman Scattering Encoded Gold Nanostars for Multiplexed Cell Discrimination. *Chem. Mater.* **2016**, *28*, 6779–6790.

(194) Chou, I.-H.; Benford, M.; Beier, H. T.; Coté, G. L.; Wang, M.; Jing, N.; Kameoka, J.; Good, T. A. Nanofluidic Biosensing for β-Amyloid Detection Using Surface Enhanced Raman Spectroscopy. *Nano Lett.* **2008**, *8*, 1729–1735.

(195) Rodríguez-Lorenzo, L.; Álvarez-Puebla, R. A.; Pastoriza-Santos, I.; Mazzucco, S.; Stéphan, O.; Kociak, M.; Liz-Marzán, L. M.; García de Abajo, F. J. Zeptomol Detection

Through Controlled Ultrasensitive Surface-Enhanced Raman Scattering. *J. Am. Chem. Soc.* **2009**, *131*, 4616–4618.

(196) Ndokoye, P.; Ke, J.; Liu, J.; Zhao, Q.; Li, X. L-Cysteine-Modified Gold Nanostars for SERS-Based Copper Ions Detection in Aqueous Media. *Langmuir* **2014**, *30*, 13491-13497

(197) Wang, R.; Chon, H.; Lee, S.; Cheng, Z.; Hong, S. H.; Yoon, Y. H.; Choo, J. Highly Sensitive Detection of Hormone Estradiol E2 Using Surface-Enhanced Raman Scattering Based Immunoassays for the Clinical Diagnosis of Precocious Puberty. *ACS Appl. Mater. Interfaces* **2016**, *8*, 10665-10672.

(198) Zengin, A.; Tamer, U.; Caykara, T. A SERS-Based Sandwich Assay for Ultrasensitive and Selective Detection of Alzheimer's Tau Protein. *Biomacromolecules* **2013**, *14*, 3001–3009.

(199) Choi, I.; Huh, Y. S.; Erickson, D. Ultra-Sensitive, Label-Free Probing of the Conformational Characteristics of Amyloid Beta Aggregates with a SERS Active Nanofluidic Device. *Microfluid. Nanofluidics* **2012**, *12*, 663–669.

(200) Melamed, J. R.; Edelstein, R. S.; Day, E. S. Elucidating the Fundamental Mechanisms of Cell Death Triggered by Photothermal Therapy. *ACS Nano* **2015**, *9*, 6–11.

(201) Hirsch, L. R.; Stafford, R. J.; Bankson, J. a; Sershen, S. R.; Rivera, B.; Price, R. E.; Hazle, J. D.; Halas, N. J.; West, J. L. Nanoshell-Mediated near-Infrared Thermal Therapy of Tumors under Magnetic Resonance Guidance. *Proc. Natl. Acad. Sci. U. S. A.* **2003**, *100*, 13549–13554.

(202) Espinosa, A.; Silva, A. K. A.; Sánchez-Iglesias, A.; Grzelczak, M.; Péchoux, C.; Desboeufs, K.; Liz-Marzán, L. M.; Wilhelm, C. Cancer Cell Internalization of Gold Nanostars Impacts Their Photothermal Efficiency In Vitro and In Vivo: Toward a Plasmonic Thermal Fingerprint in Tumoral Environment. *Adv. Healthc. Mater.* **2016**, *5*, 1040–1048.

(203) Oh, E.; Susumu, K.; Mäkinen, A. J.; Deschamps, J. R.; Huston, A. L.; Medintz, I. L. Colloidal Stability of Gold Nanoparticles Coated with Multithiol-Poly(ethylene Glycol) Ligands: Importance of Structural Constraints of the Sulfur Anchoring Groups. *J. Phys.*

Chem. C **2013**, *117*, 18947–18956.

(204) Pérez-Hernández, M.; Del Pino, P.; Mitchell, S. G.; Moros, M.; Stepien, G.; Pelaz, B.; Parak, W. J.; Gálvez, E. M.; Pardo, J.; De La Fuente, J. M. Dissecting the Molecular Mechanism of Apoptosis during Photothermal Therapy Using Gold Nanoprisms. *ACS Nano* **2015**, *9*, 52–61.

(205) Lin, J.; Wang, S.; Huang, P.; Wang, Z.; Chen, S.; Niu, G.; Li, W.; He, J.; Cui, D.; Lu, G.; Chen X.; Nie Z. Photosensitizer-Loaded Gold Vesicles with Strong Plasmonic Coupling Effect for Imaging-Guided Photothermal/photodynamic Therapy. *ACS Nano* **2013**, *7*, 5320–5329.

(206) Pérez-Hernández, M.; del Pino, P.; Mitchell, S. G.; Moros, M.; Stepien, G.; Pelaz, B.; Parak, W. J.; Gálvez, E. M.; Pardo, J.; de la Fuente, J. M. Dissecting the Molecular Mechanism of Apoptosis during Photothermal Therapy Using Gold Nanoprisms. *ACS Nano* **2015**, *9*, 52–61.

(207) Ali, M. R. K.; Wu, Y.; Han, T.; Zang, X.; Xiao, H.; Tang, Y.; Wu, R.; Fern??ndez, F. M.; El-Sayed, M. A. Simultaneous Time-Dependent Surface-Enhanced Raman Spectroscopy, Metabolomics, and Proteomics Reveal Cancer Cell Death Mechanisms Associated with Gold Nanorod Photothermal Therapy. *J. Am. Chem. Soc.* **2016**, *138*, 15434–15442.

(208) Ju, H.; Roy, R. A.; Murray, T. W. Gold Nanoparticle Targeted Photoacoustic Cavitation for Potential Deep Tissue Imaging and Therapy. *Biomed. Opt. Express* **2013**, *4*, 66–76.

CHAPTER 2

Large-Scale Plasmonic Pyramidal Supercrystals via *Templated Self-Assembly of Monodisperse Gold Nanospheres*

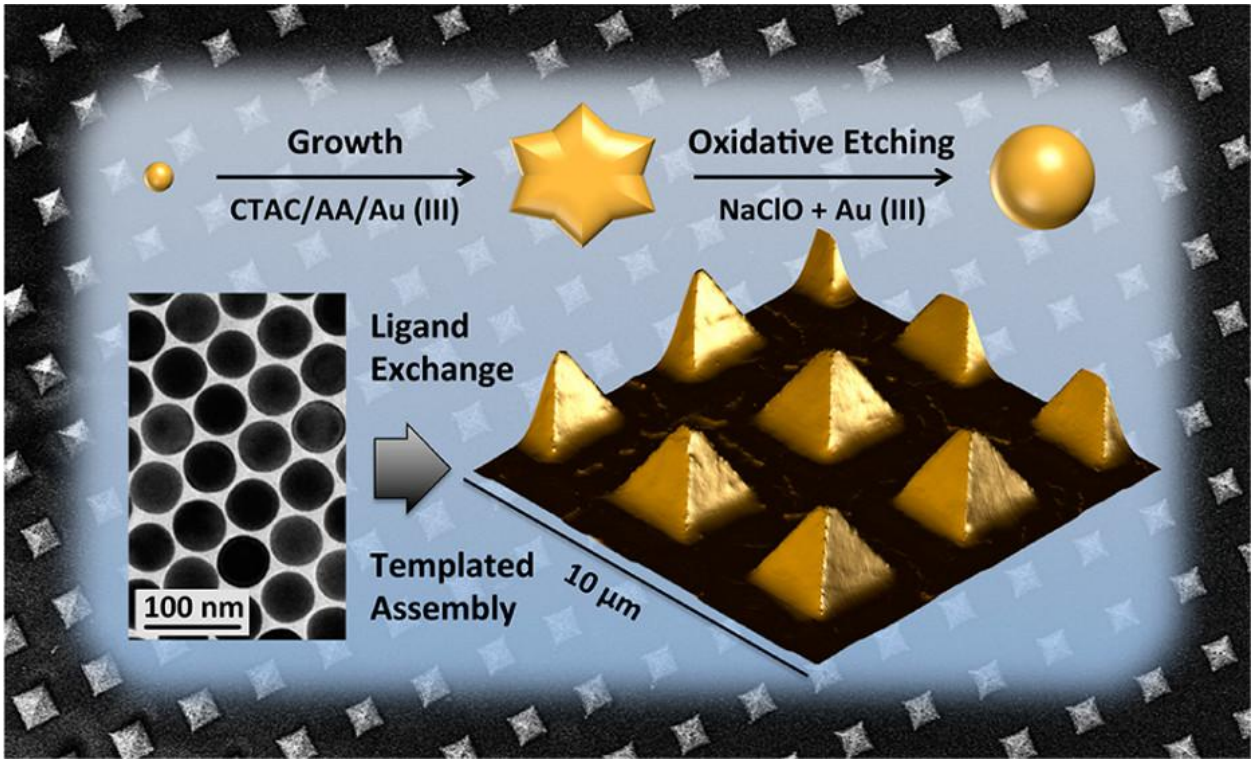

http://pubs.acs.org/doi/abs/10.1021/acs.jpcc.6b12161

Chapter 2
Large-Scale Plasmonic Pyramidal Supercrystals via Templated Self-Assembly of Monodisperse Gold Nanospheres

ABSTRACT

Three-dimensional supercrystals of plasmonic nanoparticles are a novel class of materials with exciting applications in technologies such as light harvesting or metamaterials. However, their realization relies on extraordinarily regular colloidal building blocks and accurate self-assembly methods. We present here a simple and up-scalable protocol for the synthesis of smooth gold nanospheres with high monodispersity in size and sphericity. The synthesis involves rapid growth up to the desired size and subsequent removal of surface roughness via an efficient etching step, so that nanospheres with diameters ranging between 10 and 110 nm can be obtained in large quantities. Upon functionalization with thiolated polyethylene glycol and low surfactant concentration, Au nanospheres were employed as building blocks to produce uniform arrays of micron-sized 3D pyramidal supercrystals over large areas, by means of a template-assisted approach. Focused ion beam cutting and SEM characterization revealed a face-centered cubic lattice within individual pyramidal supercrystals.

CHAPTER 3

Nucleation of Amyloid Oligomers by RepA-WH1-Prionoid-Functionalized Gold Nanorods

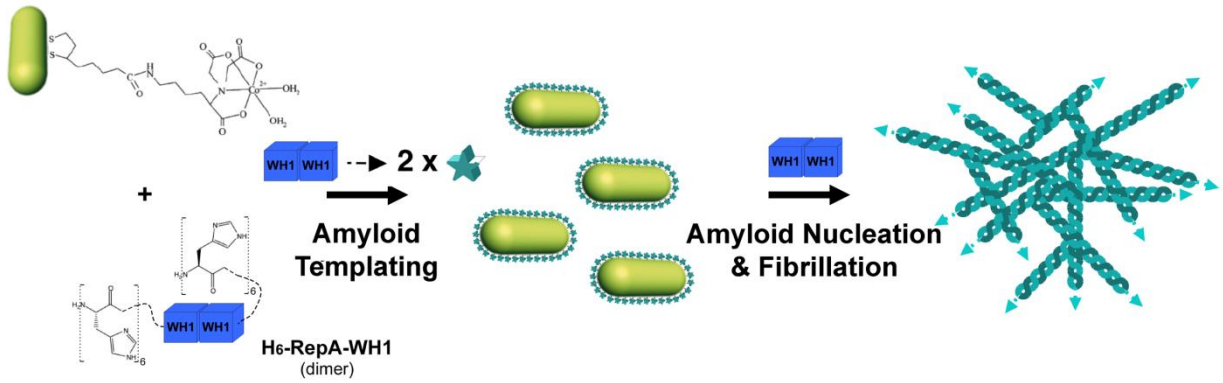

http://onlinelibrary.wiley.com/doi/10.1002/anie.201604970/abstract

ABSTRACT

Understanding protein amyloidogenesis is an important topic in protein science, fueled by the role of amyloid aggregates, especially oligomers, in the etiology of a number of devastating human degenerative diseases. However, the mechanisms that determine the formation of amyloid oligomers remain elusive due to the high complexity of the amyloidogenesis process. For instance, gold nanoparticles promote or inhibit amyloid fibrillation. We have functionalized gold nanorods with a metal-chelating group to selectively immobilize soluble RepA-WH1, a model synthetic bacterial prionoid, using a hexa-histidine tag (H6). H6-RepA-WH1 undergoes stable amyloid oligomerization in the presence of catalytic concentrations of anisotropic nanoparticles. Then, in a physically separated event, such oligomers promote the growth of amyloid fibers of untagged RepA-WH1. SERS spectral changes of H6-RepA-WH1 on spherical citrate-AuNP substrates provide evidence for structural modifications in the protein, which are compatible with a gradual increase in β-sheet structure, as expected in amyloid oligomerization.

CHAPTER 4

Introduction to Reshaping, Fragmentation, And Assembly of Gold Nanoparticles Assisted By Pulse Lasers

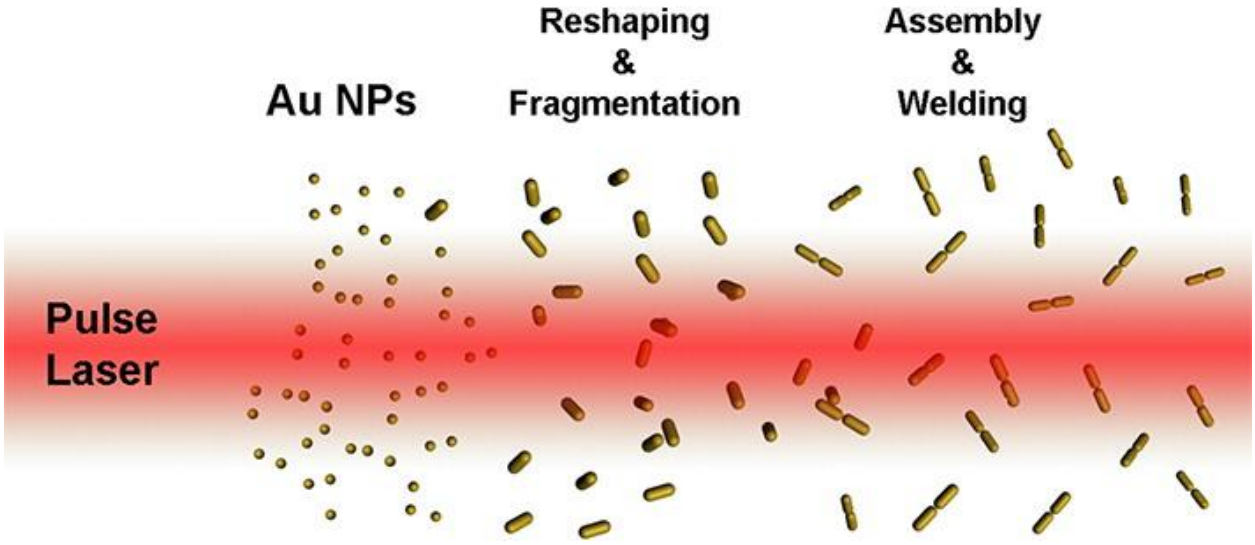

http://pubs.acs.org/doi/abs/10.1021/acs.accounts.6b00041

http://pubs.acs.org/doi/suppl/10.1021/acs.accounts.6b00041

CONSPECTUS

The vast majority of the outstanding applications of metal nanoparticles (NPs) developed during the last two decades have arisen from their unique optical properties. Within this context, rational synthesis and assembly of gold NPs have been the main research focus, aiming at the design of nanoplasmonic devices with tailored optical functionalities. The progress made in this field is thus to be ascribed to the understanding of the origin of the interaction between light and such gold nanostructures, the dynamics of which have been thoroughly investigated with significant contributions from short and ultrashort pulse laser technologies.

We focus this Account on the potential of pulse lasers to provide new fundamental insights into the electron dynamics involved in the interaction of light with the free conduction electrons of Au NPs, that is, localized surface plasmon resonances (LSPRs). The excitation of LSPRs with a femtosecond pulse laser is followed by thermalization of the Au NP electrons and the subsequent relaxation of the nanocrystal lattice and the surrounding environment, which generally results in surface melting. By contrast, nanosecond irradiation usually induces AuNP fragmentation and uncontrolled melting due to overlapping excitation and relaxation phenomena. These concepts have been exploited toward the preparation of highly monodisperse gold nanospheres via pulse laser irradiation of polyhedral nanocrystal colloids, or in the fabrication of nanostructures with "written-in" optical properties. The applicability of pulsed coherent light has been extended toward the direct synthesis and manipulation of Au NPs. Through ablation of a gold target in a liquid with pulse lasers, spherical Au NPs can be synthesized with no need of stabilizing ligands, which is a great advantage in terms of reducing toxicity, rendering these NPs particularly suitable for medical applications. In addition, femtosecond laser irradiation has been proven a unique tool for the controlled welding of plasmonic gold nanostructures by electromagnetic field enhancement at the hot spots of assembled Au NPs. The combination of such nanostructures with pulse lasers promises significant chemical and biochemical advances, including the structural determination of organic reaction intermediates, the investigation of phase transitions in inorganic nanomaterials at mild reaction conditions, or the efficient photothermal destruction of cancer cells avoiding damage of surrounding tissue.

CHAPTER 5

Femtosecond Laser-Controlled Tip-to-Tip Assembly and Welding of Gold Nanorods

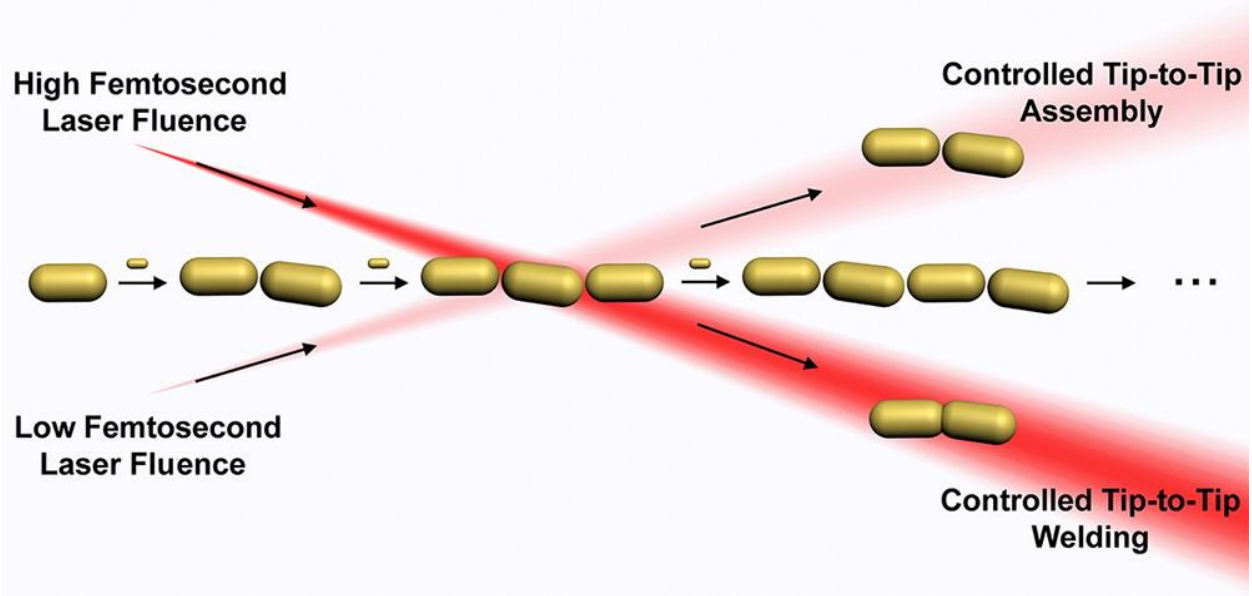

http://pubs.acs.org/doi/abs/10.1021/acs.nanolett.5b03844

ABSTRACT

Directed assembly of gold nanorods through the use of dithiolated molecular linkers is one of the most efficient methodologies for the morphologically controlled tip-to-tip assembly of this type of anisotropic nanocrystals. However, in a direct analogy to molecular polymerization synthesis, this process is characterized by difficulties in chain-growth control over nanoparticle oligomers. In particular, it is nearly impossible to favor the formation of one type of oligomer, making the methodology hard to use for actual applications in nanoplasmonics. We propose here a light-controlled synthetic procedure that allows obtaining selected plasmonic oligomers in high yield and with reaction times in the scale of minutes by irradiation with low fluence near-infrared (NIR) femtosecond laser pulses. Selective inhibition of the formation of gold nanorod *n*-mers (trimers) with a longitudinal localized surface plasmon in resonance with a 800 nm Ti:sapphire laser, allowed efficient trapping of the (n – 1)-mers (dimers) by hot spot mediated photothermal decomposition of the interparticle molecular linkers. Laser irradiation at higher energies produced near-field enhancement at the interparticle gaps, which is large enough to melt gold nanorod tips, offering a new pathway toward tip-to-tip welding of gold nanorod oligomers with a plasmonic response at the NIR. Thorough optical and electron microscopy characterization indicates that plasmonic oligomers can be selectively trapped and welded, which has been analyzed in terms of a model that predicts with reasonable accuracy the relative concentrations of the main plasmonic species.

CHAPTER 6

Intracellular pH-Induced Tip-to-Tip Assembly of Gold Nanorods for Enhanced Plasmonic Photothermal Therapy

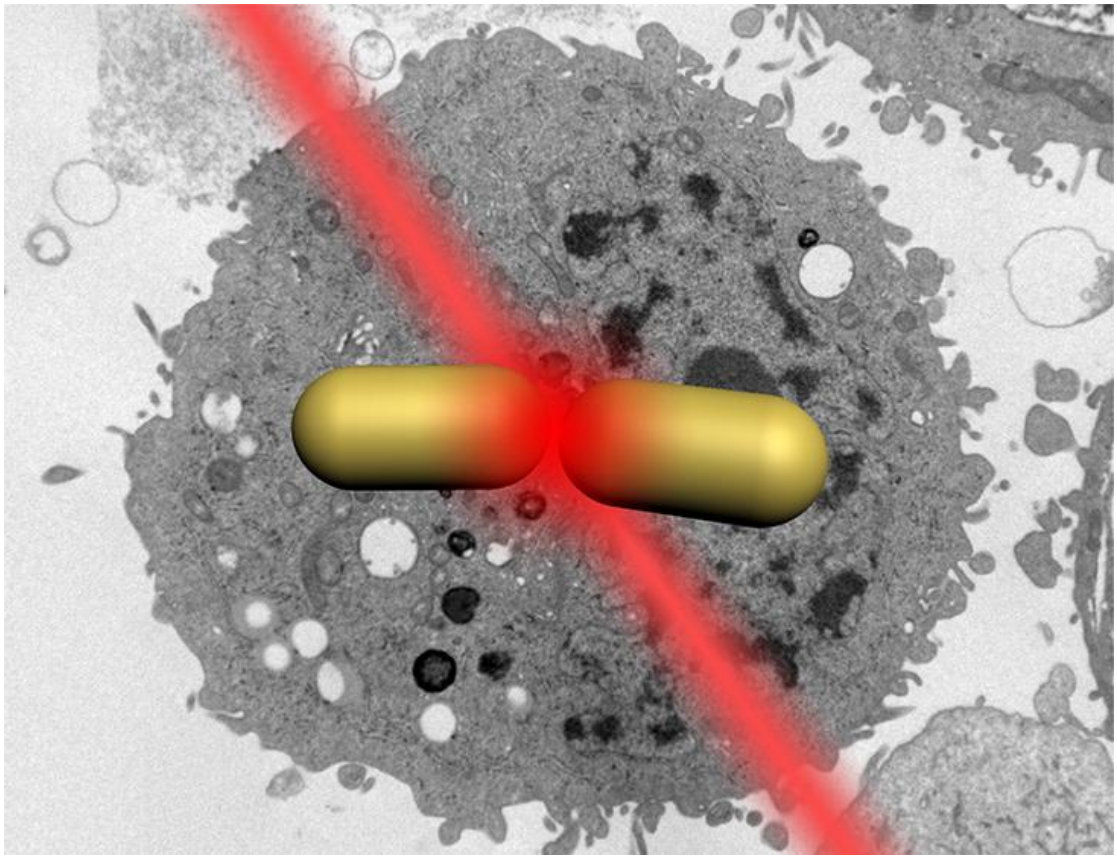

http://pubs.acs.org/doi/abs/10.1021/acsomega.6b00184

Chapter 6
Intracellular pH-Induced Tip-to-Tip Assembly of Gold Nanorods for Enhanced Plasmonic Photothermal Therapy

ABSTRACT

The search for efficient plasmonic photothermal therapies using nonharmful pulse laser irradiation at the near-infrared (NIR) is fundamental for biomedical cancer research. Therefore, the development of novel assembled plasmonic gold nanostructures with the aim of reducing the applied laser power density to a minimum through hot spot-mediated cell photothermolysis is an ongoing challenge. We demonstrate that gold nanorods (AuNRs) functionalized at their tips with a pH-sensitive ligand assemble into oligomers within cell lysosomes through hydrogen-bonding attractive interactions. The unique intracellular features of the plasmonic oligomers allow us to significantly reduce the femtosecond laser power density and AuNR dose while still achieving excellent cell killing rates. The formation of gold tip-to-tip oligomers with longitudinal localized surface plasmon resonance bands at the NIR, obtained from low-aspect-ratio AuNRs close in resonance with 800 nm Ti:sapphire 90 fs laser pulses, was found to be the key parameter for realizing the enhanced plasmonic photothermal therapy.

CHAPTER 7

Conclusions

Chapter 7
Conclusions

Nanoscience and nanotechnology are expected to deal with many challenges that threaten our future, from energy harvesting to biomedicine. Within this context, gold nanoparticles are especially appealing because they offer a unique combination of tunable optical properties (localized surface plasmon resonances, LSPRs), and high chemical stability with controlled reactivity. Among the wide variety of topics covered by gold nanoparticles, their uses in sensing, diagnosis and treatment of human diseases will be probably those with a higher impact on the society.

In the thesis presented here and entitled "Synthesis and Assembly of Uniform Plasmonic Gold Nanostructures for Biomedical Applications", we have investigated the development of novel approaches for the synthesis of plasmonic nanostructures that could be used for diagnostics and therapy of various human diseases, such as Alzheimer and cancer. Specifically, the fundamental aspects of this thesis are the synthesis of gold nanoparticles with desired optical properties, and their subsequent functionalization and self-assembly, with the aim of exploiting them for studying and sensing amyloidogenesis, as well as for photothermal therapy. One of the main innovations presented in this work is the implementation of ultrashort pulse lasers as a valuable tool for controlling some of the above mentioned aspects.

As a first approach, we synthesized gold nanospheres with high monodispersity and directed their self-assembly into patterned substrates by rational functionalization with thiolated polyethylenglycol, in the presence of small concentrations of cationic surfactant (Chapter 2). Following the concept of designed synthesis and functionalization, we fabricated and stabilized gold nanorods with the model prionoid RepA-WH (Chapter 3). This approach allowed us to induce the formation of amyloid oligomers, toxic species that play a key role in the etiology of a number of devastating human degenerative diseases. Moreover, we used the LSPR sensitivity and the molecular Raman enhancing properties of gold nanoparticles to monitor the process.

In a second approach, we took advantage of the strong interaction of plasmonic nanoparticles with femtosecond pulse lasers for the synthesis and self-assembly of anisotropic gold nanoparticles, as well as for their use in photothermal therapy.

Therefore, we first carried out a critical review of the most relevant uses of pulse lasers for reshaping, fragmentation and assembly of gold nanoparticles, as well as the main mechanisms of interaction (Chapter 4). Then, we demonstrated that by femtosecond pulse laser

irradiation, we are capable of controlling the self-assembly of gold nanorods when molecular dithiolated linkers were used as the assembly driving force (Chapter 5). Additionally, we synthesized welded species with optical LSPR modes in the NIR at high fluences of irradiation.

Finally, we synthesized and functionalized gold nanorods in such a manner that they were programed to self-assemble within lysosomes of model cancer cells. The corresponding plasmonic nanostructures were used for efficient photothermal therapy via femtosecond pulse laser irradiation (Chapter 6).

In conclusion, this thesis presents a significant advancement in the synthesis, functionalization and self-assembly of different plasmonic nanoparticles, but also shows interesting research in several aspects of biomedical applications, such as amyloidogenesis research and cancer photothermal therapy.

Summary

Throughout this thesis work we have dealt with diverse aspects of the plasmonic gold nanoparticle cosmos. Even though specific conclusions have been extracted in each chapter, they can be summarized in what follows:

Synthesis and assembly of monodisperse gold nanospheres: An optimized synthetic protocol was devised for the synthesis of highly monodisperse and smooth spherical gold nanoparticles of various sizes, with the aim of avoiding time-consuming intermediate centrifugation steps and consumption of expensive gold salt in such a manner that fast production of large volumes on the liter scale would be easily obtained. By means of this method, the so-produced high quality colloids were employed as building blocks for the fabrication of super-structures by evaporative templated self-assembly. Taking advantage of the uniformity of the building blocks, in combination with rational surface chemistry functionalization, we demonstrated the suitability of this system for the large-scale assembly and production of plasmonic supercrystals, which are of interest for applications in biosensing and metamaterials design.

Gold nanoparticles for nucleation and sensing of amyloid oligomers: We synthesized plasmonic nanoparticles to study the amyloidogenic process in the model synthetic bacterial prionoid RepA-WH1. Firstly, we demonstrated the ability of gold nanorods to promote the stable oligomerization, from the native protein to the amyloid conformation, via rational functionalization with a metal-chelating group which selectively immobilizes soluble RepA-WH1. Furthermore, the enhanced sensitivity of the LSPR of gold nanorods toward the surrounding medium was exploited to monitor the very initial stages of the process. In a second step, the structural conformational changes of the protein were evidenced by SERS spectroscopy, where gold nanospheres were used as enhancers to show the gradual increase of the Raman peak associated with the β-sheet structure (a characteristic feature of amyloid oligomerization). Finally, we studied the promoted growth of amyloid fibers RepA-WH1 in the presence of gold nanorods functionalized with such oligomers

Summary

In the following work we benefit from the interaction of plasmons with femtosecond pulse laser radiation to assembly gold nanorods, as well as for photothermal therapy enhanced by assembled plasmonic aggregates.

Tip-to-tip assembly and welding of gold nanorods: We envisage the assembly of gold nanorods via dithiolated molecular linkers to form plasmonic dimers, where the control over self-assembly can be achieved by the activation of hot spots of undesired species, i.e. trimers. The activated hot spots would lead to photothermal decomposition of the interparticle molecular linkers. Following this idea, we synthesized gold nanorods with LSPR at 600 nm, i.e. matching the LSPR of the trimers with the fs laser emission (800 nm). We were able to demonstrate effective control of the assembly, where the laser pulse fluence was found to be the most important parameter. Additionally, we showed that irradiation with high fluence led to such a temperature increase at the particle gaps that the nanoparticles were welded into new species with plasmonic resonances in the NIR.

Self-assembly of gold nanorods for photothermal therapy: Following a similar concept as that described in the previous chapter, we prepared gold nanorods that after self-assembly would display an LSPR matching the emission of a fs laser (800 nm). With the aim of introducing such aggregates into cancer cells for efficient photothermal therapy, we functionalized the gold nanorods surface so that oligomerization would occur inside the cell lysosomes. The formation of massive tip-to-tip assemblies was likely to occur due to pH and a confinement effect of the lysosomes membrane confinement. Subsequent activation of the hot spots with fs laser irradiation not only promoted cell death but also increased the efficiency of the treatment, allowing significant reduction of the femtosecond laser power density and AuNR dose while still achieving excellent cell killing rates.

APPENDIX 1: Large-Scale Plasmonic Pyramidal Supercrystals via Templated Self-Assembly of Monodisperse Gold Nanospheres

http://pubs.acs.org/doi/suppl/10.1021/acs.jpcc.6b12161

Appendix 1
Large-Scale Plasmonic Pyramidal Supercrystals via Templated Self-Assembly of Monodisperse Gold Nanospheres

Oxidation of Faceted AuNPs with NaClO

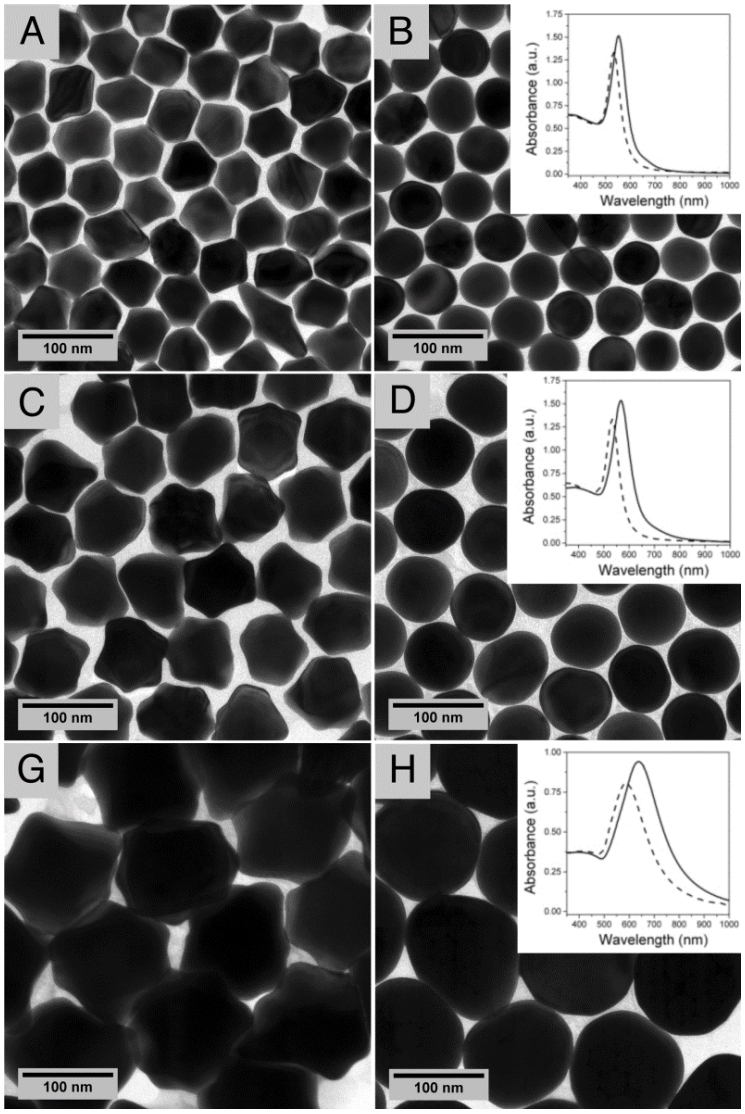

Figure S1. TEM images of AuNPs of various sizes obtained using different volumes of 10 nm seed solution: 25 μL (A), 10 μL (C) and 2.5 μL (E); and the effect of the addition of 10 μL of NaClO solution to A,C and E, respectively (B, D, F). The insets show the changes in the extinction spectra of faceted AuNPs nanoparticles (solid lines) after addition of NaClO solution (dashed lines). LSPR blue shifts: from 552 nm to 533 nm (B inset), from 566 nm to 543 nm (D inset) and from 640 to 596 nm (F inset). Partial AuNPs oxidation by NaClO occurs in the presence of CTAC due to modification of the reduction potential of AuCl2 upon complexation with CTA+ As a result of the multistep process, monodisperse quasi-spheres with average diameters of 55 nm (SD: 3), 77 nm (SD: 4) and 123 nm (SD: 13) (Figure 2B, D, F) were obtained.

APPENDIX 2: Nucleation of RepA-WH1 Amyloid Oligomers by Prionoid Functionalized-Gold Nanorods

http://onlinelibrary.wiley.com/doi/10.1002/anie.201604970/abstract

Materials

All the starting materials were obtained from commercial suppliers and used without further purification: Hexadecyltrimethylammonium bromide (CTAB, ≥99%), Hexadecyltrimethylammonium chloride (CTAC, 25% w/w in water), 5-bromosalicylic acid (technical grade, 90%), hydrogen tetrachloroaurate trihydrate (HAuCl4·H2O, ≥99.9%), silver nitrate (AgNO3, ≥99.0%), L-ascorbic acid (≥99%), sodium borohydride (NaBH4, 99%), poly(ethylene glycol) methyl ether thiol (PegSH, Mn 6000), (±)-α-Lipoic acid (0≥98.0%), Nα,Nα-Bis(carboxymethyl)-L-lysine hydrate (ANTA, ≥97.0%, TLC), cobalt(II) chloride hexahydrate (ACS reagent, 98%), N-(3-Dimethylaminopropyl)-N′-ethylcarbodiimide hydrochloride (EDC, purum, ≥98.0% (AT)), N-Hydroxysuccinimide (NHS, 98%) were purchased from Aldrich. Nanopure water (resistivity 18.2 MΩ cm at 25 °C) was used in all experiments.

Synthesis and characterization of AuNRs

The seeds were prepared by the standard CTAB/$NaBH_4$ procedure: 25 μL of a 0.05 M $HAuCl_4$ solution was added to 4.7 mL of 0.1 M CTAB solution; 300 μL of a freshly prepared 0.01 M $NaBH_4$ solution was then injected under vigorous stirring. Excess borohydride was consumed by keeping the seed solution for 30 min at room temperature prior to use. Gold nanorods were prepared, with some modifications, as previously described by Murray and co-workers. In a typical synthesis of a 50 mL nanorod solution, 45 mg of 5-bromosalicylic acid was added to 50 mL of 0.05 M CTAB. The solution was mildly stirred for 15 min until complete dissolution, and 480 μL of 0.01 M $AgNO_3$ and 500 μL of 0.05 M $HAuCl_4$ solutions were added to the mixture. After 40 min, 130 μL of 0.1 M ascorbic acid solution was added under vigorous stirring, followed by 80 μL of seed solution. The mixture was left undisturbed at room temperature for at least 4 h. The resulting gold nanorods presented a LSRP with an absorption maximum at 760 nm (Figure S1A). Typically, the mixture was centrifuge (7000 rpm, 30 min) and finally, nanorods were redispersed in 10 mL of 2 mM CTAB solution.

UV/Vis/NIR absorption spectra of the resulting AuNRs were registered using a Cary 5000 UV-Vis-NIR (Figure S1A). All experiments were carried out at 298 K, using quartz

APPENDIX 3: Femtosecond Laser-Controlled Tip-to-Tip Controlled Assembly and Welding of Gold Nanorods

http://pubs.acs.org/doi/suppl/10.1021/acs.nanolett.5b03844

MEEP calculations

Optical response and near-field enhancements were calculated using the FDTD method, as implemented in the free software package MEEP.[216] In this method Maxwell equations are solved by a second order approximation. Space is divided into a discrete grid, the Yee grid,[217] and the fields are evolved in time using discrete time steps. A schematic representation of the geometry used for the calculation is shown in Figure S1. Simulations were performed for the polarizations parallel and perpendicular to the structure axis. In all calculations we used spatial resolution of 0.5 nm.

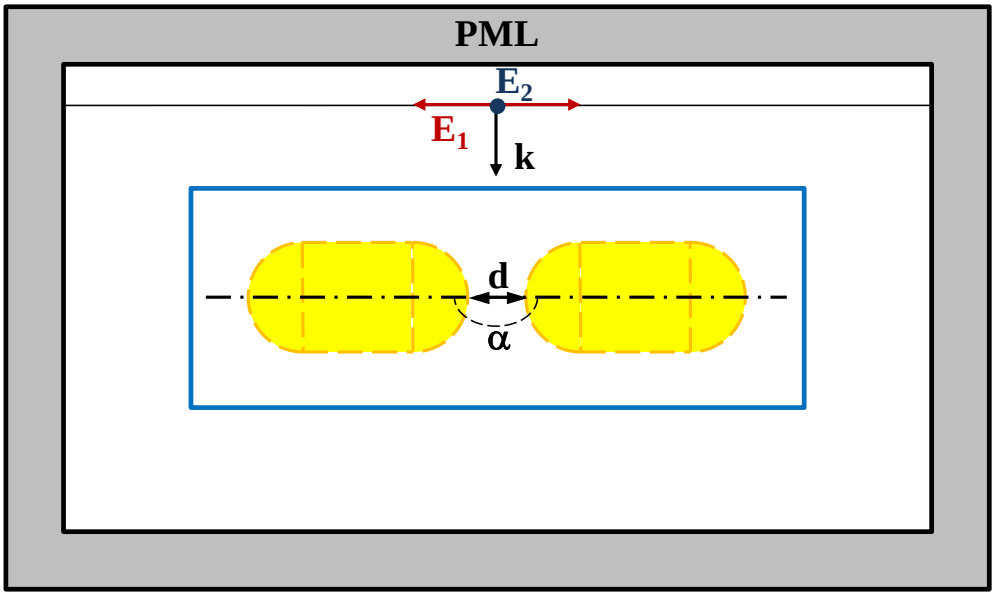

Figure S1. Schematic representation of the geometry used for the FDTD calculations. The dimer structure is surrounded by flux planes (blue lines), in order to calculate the far-field response. Calculations are performed for light polarized parallel (red) and perpendicular (dark blue) to the structure axis. The entire cell is surrounded by a perfectly matched layer, in order to simulate an infinitum space.

Characterization techniques

***Transmission electron microscopy*:** TEM images were obtained with a JEOL JEM-1400PLUS transmission electron microscope, operating at an acceleration voltage of 120 kV. High Resolution TEM images were recorded using a JEOL2010F FE-TEM instrument operating at 200 kV. Carbon-coated 400 square mesh copper grids were used. All the samples were centrifuged at least once before blotting on the grid.

APPENDIX 4: Intracellular pH-Induced Tip-to-Tip Assembly of Gold Nanorods for Enhanced Plasmonic Photothermal Therapy

http://pubs.acs.org/doi/suppl/10.1021/acsomega.6b00184

Appendix 4
Intracellular pH-Induced Tip-to-Tip Assembly of Gold Nanorods for Enhanced Plasmonic Photothermal Therapy

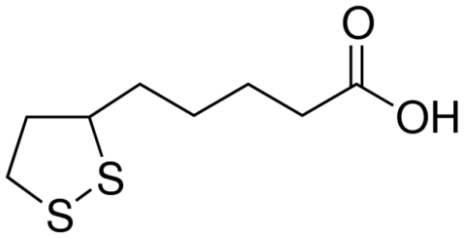

Figure S1. (±)-α-Lipoic acid chemical structure. Also known as thioctic acid is an organosulfur compound derived from octaonic acid.

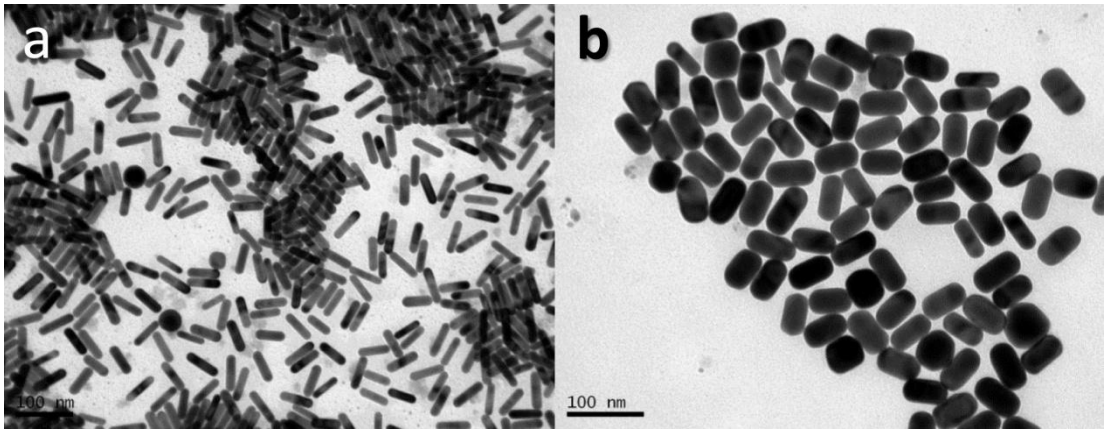

Figure S2. Transmission electron microscopy images of the AuNRs. (a) The resulting CTAB-stabilized AuNRs with L-LSPR band at 803 nm presented a length and diameter of 56 ± 4 nm and 16 ± 2 nm, respectively, and an aspect ratio of 3.5, as determined from TEM images. (b) The resulting CTAB-stabilized AuNRs with L-LSPR band at 604 nm presented a length and diameter of 58 ± 4 nm and 34± 4 nm, respectively, and an aspect ratio of 1.7.

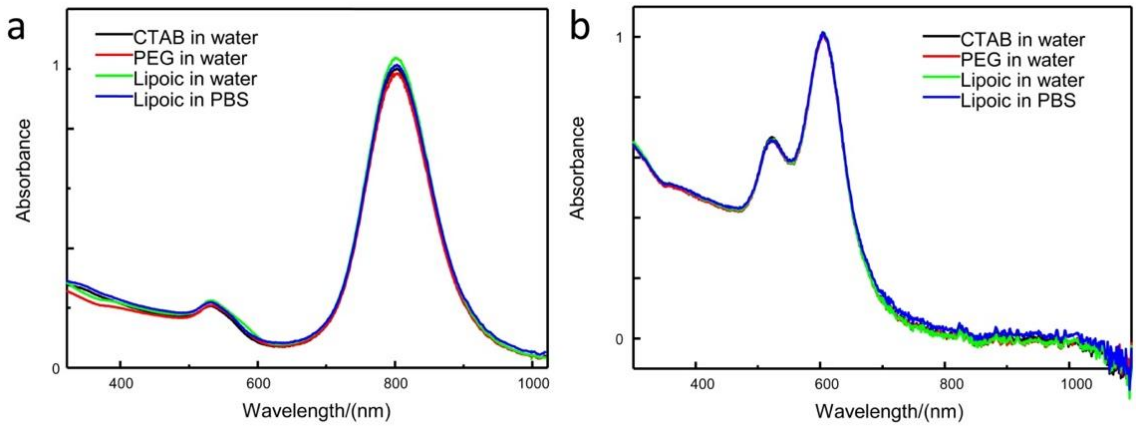

Figure S3. UV-Vis-NIR spectra of AuNRs with LSPR bands at 803 nm (a) and 604 nm (b), stabilized with CTAB (black), PEG-SH (red), and lipoic acid (green) in water, and lipoic acid in PBS buffer (blue).

Resumen

INTRODUCCIÓN

De la nanociencia y la nanotecnología se espera que sean capaces de encontrar respuestas a numerosos vacíos de conocimiento y proporcionar soluciones para muchos de los problemas que amenazan nuestro futuro, desde el tratamiento de aguas, la captación de energía solar, el transporte o incluso la cura de enfermedades.[1–5] El término "nano" se emplea para describir campos y tecnologías que trabajan con materiales donde al menos una de sus dimensiones es menor de 100 nm.[6] Sin embargo, el interés científico por la nanoescala no puede residir en el mero hecho de miniaturizar cualquier entidad macroscópica, o la fabricación de materiales mediante la manipulación de sus componentes atómicos. Es la aparición de nuevas propiedades (eléctricas, ópticas y magnéticas) y funcionalidades en los materiales al reducir sus dimensiones, lo que en verdad hace tremendamente atractiva la investigación en la nanoescala. Así pues, la generación de nuevas propiedades al reducir el tamaño podría visualizarse como un nuevo límite difuso entre los dominios atómico y macroscópico.[7]

Si nos centramos más específicamente en el caso de los metales como el oro o la plata, la reducción de sus dimensiones a la escala nanoscópica da lugar a cambios bruscos en sus propiedades ópticas. Esta modificación de su interacción con la luz es uno de los efectos más importantes estudiados en la nanotecnología: la aparición de *resonancias de plasmones superficiales localizados (LSPR)*.[8,9] Cuando una nanopartícula metálica plasmónica es excitada con una radiación electromagnética, su nube de electrones se polariza y la fuerza que intenta compensar la polarización da lugar a una oscilación plasmónica localizada. (Figura 1).[10] Este fenómeno es el origen de los colores brillantes que exhiben ciertos metales, como por ejemplo el oro y la plata, cuando se preparan en forman de nanopartículas, cuya frecuencia de excitación se encuentra en la región visible del espectro electromagnético.[9] El metal, el medio en el que se encuentre, el tamaño, la forma y el estado de agregación de las nanopartículas son parámetros que determinan dicha frecuencia de excitación (Figura 1).[12] Por lo tanto, mediante el control de dichos parámetros es posible diseñar y fabricar sistemas nanoplasmónicos con propiedades ópticas predefinidas.

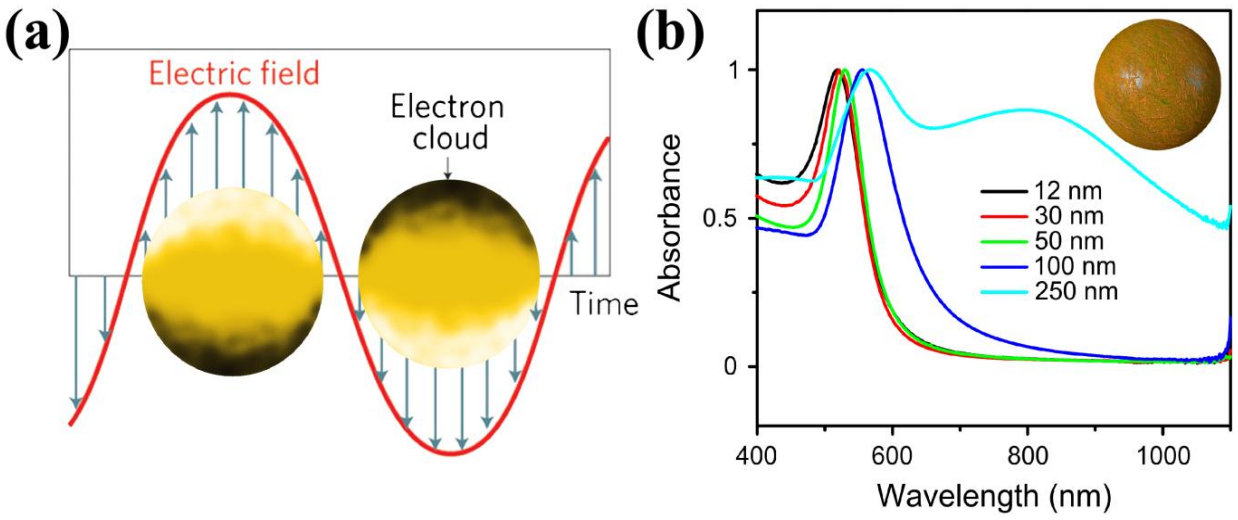

Figura 1. (a) Plasmón superficial localizado en nanoesferas metálicas. (B) Espectros normalizados de extinción UV-Vis de nanopartículas esféricas de diferentes tamaños en agua: un aumento en el diámetro induce mayor polarizabilidad y desplazamiento hacia el rojo de la LSPR. Adaptado de ref. [11]

La primera publicación científica relacionada con la síntesis de nanopartículas plasmónicas la realizó Michael Faraday en 1857, cuando describió la preparación de nanoesferas de oro dispersas en una fase líquida.[13] Siguiendo dicha aproximación, actualmente la síntesis coloidal es probablemente la más popular para la fabricación de nanocristales metálicos plasmónicos.[14] Además, de entre todas las metodologías coloidales descritas, la que combina el empleo de surfactantes con la separación entre la formación de semillas y su crecimiento (*crecimiento mediado por semillas*), es sin duda la que más éxito ha tenido. Esto es debido a su gran versatilidad y al elevado control sobre la forma y tamaño, para una gran variedad de metales como plata, oro, paladio, platino, etc.[15–19]

Por otra parte, y en analogía con los átomos cuando se organizan para formar moléculas y compuestos cristalinos con propiedades fisicoquímicas diferentes de las partes constituyentes, el auto-ensamblaje de nanopartículas plasmónicas origina propiedades ópticas únicas.[21–24] Hoy en día, una de las aplicaciones más interesantes de las nanopartículas plasmónicas es su uso en espectroscopia Raman aumentada en superficies (SERS), una técnica mediante la cual es posible detectar incluso moléculas individuales que se encuentran en el campo cercano de la nanopartícula.[25] En esta técnica, el auto-ensamblaje de las nanopartículas es crucial para obtener aumentos significativos de la señal Raman.[26] Por lo tanto, el interés hacia estos sistemas

ensamblados es enorme, pues presenta un gran potencial en campos como la fotónica o la biomedicina.

La fuerza motriz del auto-ensamblaje es, en todos los casos, la minimización de la energía libre de la estructura final, que se rige por el equilibrio entre interacciones atractivas y repulsivas: van der Waals, Coulomb, enlace de hidrógeno o interacciones hidrófobas entre otras.[27,28] Aunque existen diversas formas para ensamblar nanopartículas, una de las más interesantes reside en explotar dichas interacciones moleculares para dirigir el proceso.[28] Durante las dos últimas décadas, se han desarrollado múltiples estrategias para el ensamblaje de nanopartículas de oro, basadas en la funcionalización de la superficie de las nanopartículas con una amplia batería de (bio)moléculas y (bio)polímeros que luego, bajo estímulos apropiados (temperatura, pH, luz, ...), inducen el ensamblaje de las nanopartículas a través de interacciones hidrófobas o electrostáticas, enlaces de hidrógeno (Figura 2), formación de enlaces covalentes, uniones por ADN, anticuerpo-antígeno, etc.[3,24,29–36]

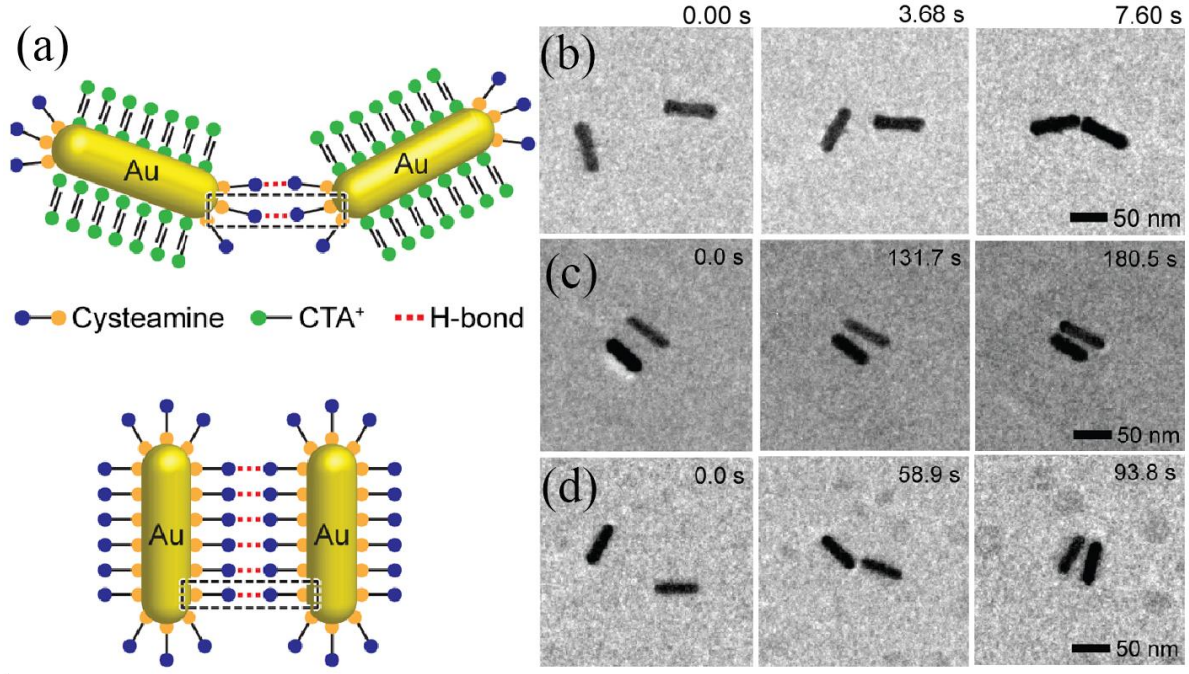

Figure 2. (a) Esquema y (b) imágenes de TEM del ensamblaje de nanovarillas de oro mediante enlaces de hidrógeno a través de las puntas y de los lados.

Otra técnica reside en el uso de moldes previamente diseñados, que contienen información sobre la posición final y la disposición de las nanopartículas, que serán ensambladas

generalmente mediante evaporación del disolvente. Una de las principales ventajas del uso de estas plantillas es su gran flexibilidad para producir diversas geometrías en grandes áreas. La versatilidad de este método hacia la preparación de estructuras con distintos tipos de nanopartículas (p.ej. ensamblados en líneas, monocapas, supercristales…) es una de sus características más relevantes.[27,37–42]

OBJETIVOS

Este trabajo de tesis se ha llevado a cabo en el marco del proyecto "Síntesis Reproductible y Ensamblado de Nanoestructuras Plasmónicas para la Teranóstica (MAT2013-46101-R)", que se centra en el desarrollo de nuevos enfoques para la fabricación de nanoestructuras plasmónicas cuyas propiedades ópticas puedan utilizarse para el diagnóstico y tratamiento simultáneo de diversas enfermedades humanas. Más específicamente, la tesis se orientó hacia varios aspectos de la fabricación de nanoestructuras plasmónicas y su aplicación en biomedicina: (i) síntesis de nanopartículas plasmónicas uniformes con características ópticas optimizadas; (ii) funcionalización con moléculas de interés biológico; (iii) auto-ensamblaje en superestructuras plasmónicas con propiedades ópticas predefinidas; y (iv) evaluación de su comportamiento en sistemas biológicos.

Para lograr estos objetivos, la tesis se organizó en base a dos enfoques distintos pero complementarios:

• Optimización de la síntesis de nanopartículas plasmónicas a través de métodos coloidales para el auto-ensamblaje eficiente y su aplicación en detección biológica (Capítulos 2 y 3).

• Implementación de láseres de pulsos ultrarrápidos (Capítulo 4), como un nuevo enfoque para mejorar sus ensamblajes (Capítulos 5) y para su aplicación en la terapia fototérmica plasmónica (Capítulo 6).

La parte experimental se realizó tanto en el Grupo de Química Supramolecular de la Universidad Complutense de Madrid (UCM) como en el Laboratorio de Bionanoplasmónica de CIC biomaGUNE, en San Sebastián. Las investigaciones se complementaron con periodos de estancia en el Centro de Nanotecnología Aplicada de Hamburgo y en el Instituto Laue Langevin de Grenoble. Además, parte de los resultados, tales como interpretaciones teóricas, experimentos con láseres ultrarrápidos y caracterización por microscopía electrónica de los sistemas desarrollados, surgen de colaboraciones externas y que invariablemente han contribuido a mejorar la calidad de la investigación realizada.

RESULTADOS

FORMACIÓN DE SUPERCRISTALES PIRAMIDALES PLASMÓNICOS A GRAN ESCALA MEDIANTE EL AUTO-ENSAMBLAJE EN MOLDES DE ESFERAS DE ORO MONODISPERSAS

Un desafío central en la construcción de supercristales plasmónicos bien definidos con orden tridimensional es la producción de nanopartículas de oro (AuNPs) uniformes en grandes cantidades como es, por ejemplo, el caso de las nanoesferas (AuNSs).[43] A pesar de que las AuNPs de mayores dimensiones (> 75 nm) son interesantes desde un punto de vista plasmónico, su empleo está limitado por las dificultades existentes en su síntesis en grandes cantidades y con calidades adecuadas. En el caso específico de esferas, aunque se han descrito varios protocolos para su preparación, muchos de ellos requieren un consumo elevado de tiempo y reactivos, que eventualmente complican el escalado potencial a grandes volúmenes.[44,45]

En esta tesis presentamos un nuevo procedimiento que combina los conceptos de crecimiento rápido sobre semillas y ataque oxidativo de las nanopartículas preparadas en presencia de cloruro de hexadeciltrimetil amonio (CTAC) para, de este modo, llevar a cabo la fabricación reproducible de AuNSs esféricas y lisas, con tamaños entre 10 y 110 nm.

El crecimiento mediado por semillas comienza con esferas de entre 1 y 3 nm, que posteriormente se sobrecrecen en otra disolución hasta alcanzar los 10 nm. A partir de estas se crecen el resto de partículas de distintos tamaños. Las imágenes de microscopía electrónica de transmisión (TEM) de las AuNPs crecidas a partir de semillas de 10 nm (Figura 3) revelaron la formación de partículas con caras y aristas bien definidas, semejantes a nanotrisioctaedros.[46] Posteriormente, el uso de NaClO seguido de una pequeña cantidad de Au (III)[47] permitió eliminar caras y aristas para formar esferas lisas. El tamaño final de las AuNSs se controló de manera efectiva a través de la cantidad de semillas de 10 nm añadida a la mezcla de crecimiento. Además, la preparación en grandes volúmenes para su uso en ensamblajes no mermó su calidad.

Para llevar a cabo su ensamblado en supercristales se emplearon sustratos de PDMS con patrones piramidales como plantillas. Las AuNSs se funcionalizaron con polietilenglicol de 5000 Da de peso molecular para, en combinación con una pequeña concentración del surfactante empleado en la síntesis (CTAC), incrementar la afinidad de las partículas hacia el vidrio. De este

modo, durante la evaporación se evitaron efectos de secado que habitualmente dan lugar a deposiciones no homogéneas (Figura 4). La dispersión de partículas se depositó directamente sobre el sustrato de PDMS, el cual se cubrió a continuación con otro de vidrio recién hidrofilizado. Una vez evaporada el agua, la caracterización a través de imágenes SEM de baja ampliación confirmó que el patrón periódico del molde se había reproducido con alta fidelidad sobre casi la totalidad de la superficie del substrato (varios mm^2). Este procedimiento se repitió con éxito para partículas de 52 y 105 nm. Las imágenes de SEM permitieron demostrar el empaquetamiento compacto de las esferas en los moldes piramidales, con estructura cúbica compacta centrada en las caras. Mediante la técnica de litografía por haz de iones focalizado (FIB), se realizó un corte transversal en una de las pirámides y se pudo visualizar que el orden cristalino también se mantenía en el interior de la estructura.

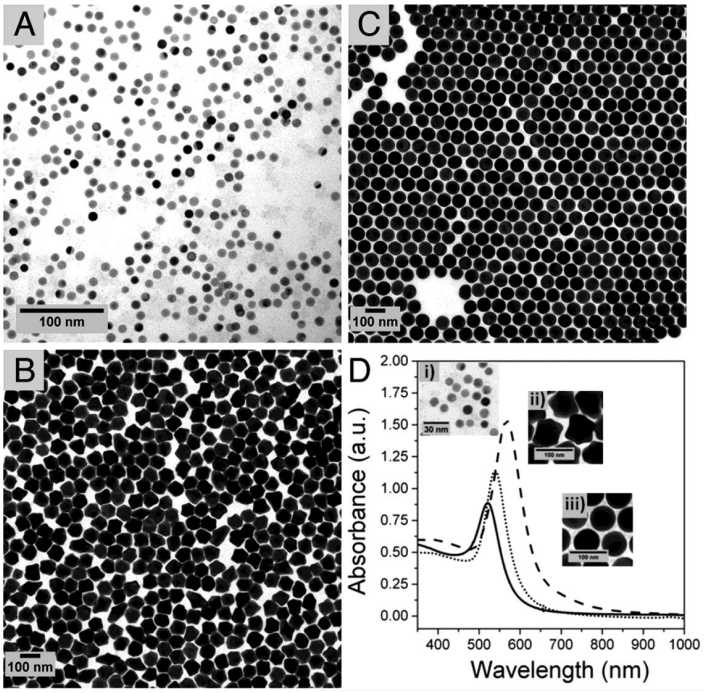

Figure 3. Imágenes TEM de las AuNPs de 10 nm (A) utilizadas como semillas para el crecimiento de AuNPs con aristas y caras (B), que pueden posteriormente transformarse en AuNSs monodispersas, lisas y altamente esféricas (C) mediante ataque oxidativo. (D) Espectros UV-vis-NIR de las semillas (línea continua, imagen i), AuNPs rugosas (línea punteada, imagen ii) y AuNSs lisas (línea punteada, imagen iii). Barras de escala en (D): 30 nm (imagen i) y 100 nm (imágenes ii y iii).

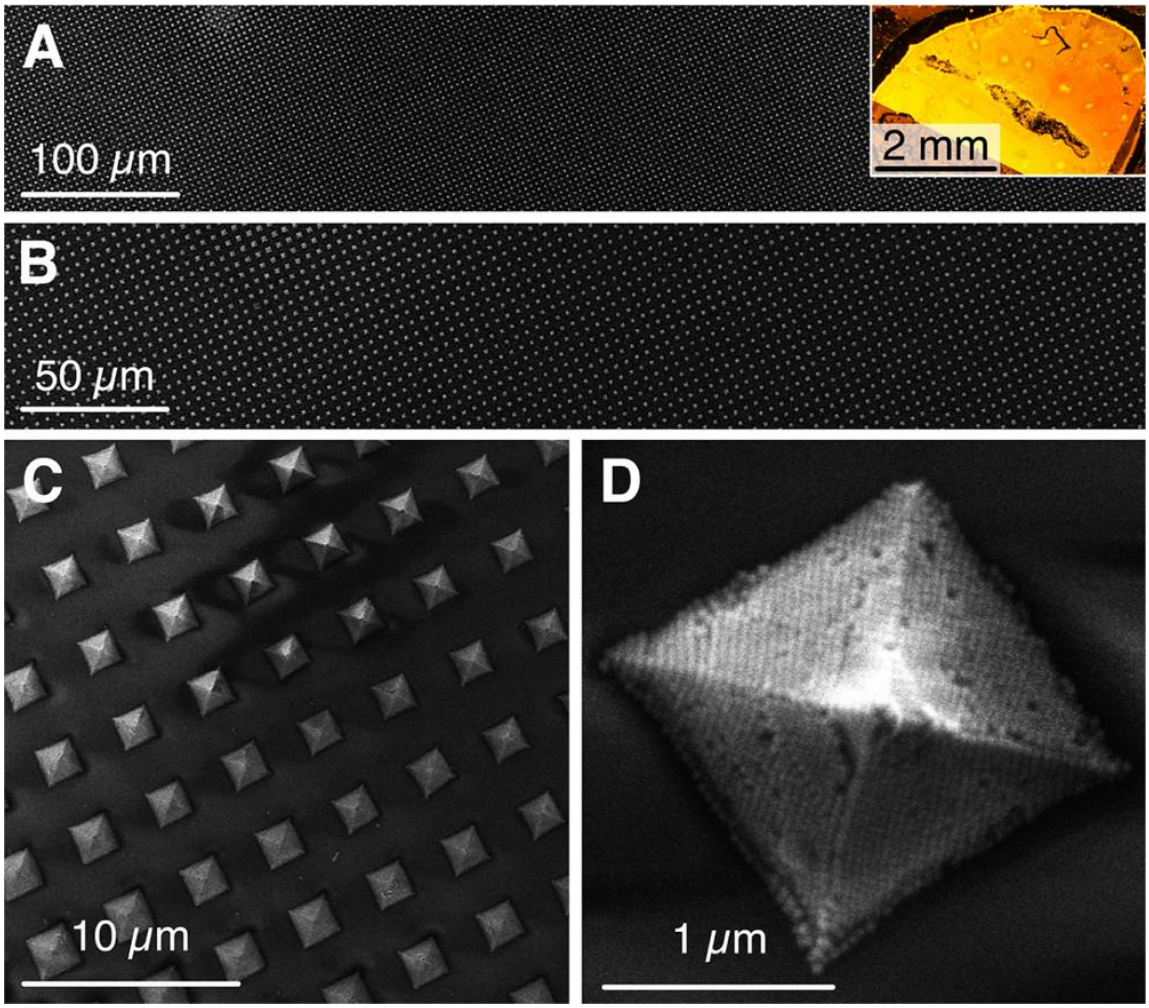

Figure 4. (A,B) Caracterización a distintas escalas de los supercristales tridimensionales producidos por el ensamblaje dirigido de AuNSs monodispersas. (C,D) Imágenes a mayor magnificación que muestran una excelente regularidad de las estructuras piramidales (C) así como un alto grado de orden en sus caras laterales densamente empaquetadas (D). Macroscópicamente, la muestra presenta iridiscencia bajo iluminación lateral (A, fotografía interior).

Por lo tanto, concluimos que las estructuras auto-ensambladas obtenidas son efectivamente supercristales, que se han obtenido gracias al desarrollo de un método optimizado de síntesis de AuNSs de alta calidad en grandes volúmenes y en combinación con una funcionalización superficial específica para mejorar su ensamblaje.

NUCLEACIÓN DE OLIGÓMEROS AMILOIDES MEDIANTE NANOVARILLAS DE ORO FUNCIONALIZADAS CON EL PRIONOIDE RepA-WH1

La comprensión de la amiloidogénesis proteica es de gran relevancia en la ciencia de proteínas, debido principalmente al papel de los oligómeros y agregados amiloides en la etiología de una serie de devastadoras enfermedades degenerativas humanas.[48,49] Sin embargo, los mecanismos que determinan la formación de dichos oligómeros amiloides siguen siendo desconocidos debido a la alta complejidad del proceso de amiloidogénesis.[50] En este contexto, las nanopartículas de oro pueden tanto promover como inhibir la fibrilación amiloide.[51–53]

En este capítulo se describe la formación de oligómeros amiloides con diferentes pesos moleculares, inducidos por nanovarillas de oro (AuNRs) funcionalizadas con el prionoide H6-RepA-WH1 (A31V). Además, se usaron dichos oligómeros para activar el crecimiento de superestructuras de fibras amiloides. Las AuNRs fueron elegidas en lugar de las más comúnmente utilizadas AuNSs debido a su mayor sensibilidad a pequeños cambios en su entorno y reactividad localizada en las puntas, lo cual facilitó su funcionalización molecular y el seguimiento del proceso.[54]

Las AuNRs se funcionalizaron primero con polietilenglicol tiolado (para proporcionar estabilidad coloidal en medio tampón) y luego se co-funcionalizaron con ácido lipoico, que posteriormente se haría reaccionar con un complejo nitrilotriacético de cobalto (ANTACo).[55] Gracias a este complejo situado en la superficie de las partículas y a una cadena de histidinas incluidas en la proteína prionoide, se pudo unir la RepA-WH1 (A31V) a las AuNRs. Durante el proceso de incubación de la RepA-WH1 (A31V) con las AuNRs se observó un desplazamiento de 5 nm del máximo del plasmón superficial localizado (LSPR) de las partículas, como consecuencia de la unión de la proteína a la superficie del oro (Figura 5A).[56,57]

Para verificar el recubrimiento de las AuNRs por la H6-RepA-WH1 (A31V), se realizó un ensayo de inmuno-microscopia electrónica (iEM) utilizando un anticuerpo policlonal anti-WH1.[58] Se pudieron encontrar anticuerpos secundarios (previamente conjugados con AuNSs de 10 nm) en las proximidades de las AuNRs (7:1), lo que indudablemente demuestra la presencia de nuestra H6-RepA-WH1 (A31V) en torno a las mismos (Figura 5B). Además, con el paso del tiempo y tras largos períodos de almacenamiento (hasta 4 semanas) a 4 ºC, se observó la presencia de varias especies oligoméricas con pesos moleculares progresivamente más altos de

H6-RepA-WH1 (A31V). La presencia de estos oligómeros, resistentes además a condiciones desnaturalizantes, apuntaba claramente a la presencia de especies oligoméricas pre-amiloides. (Figura 5C)

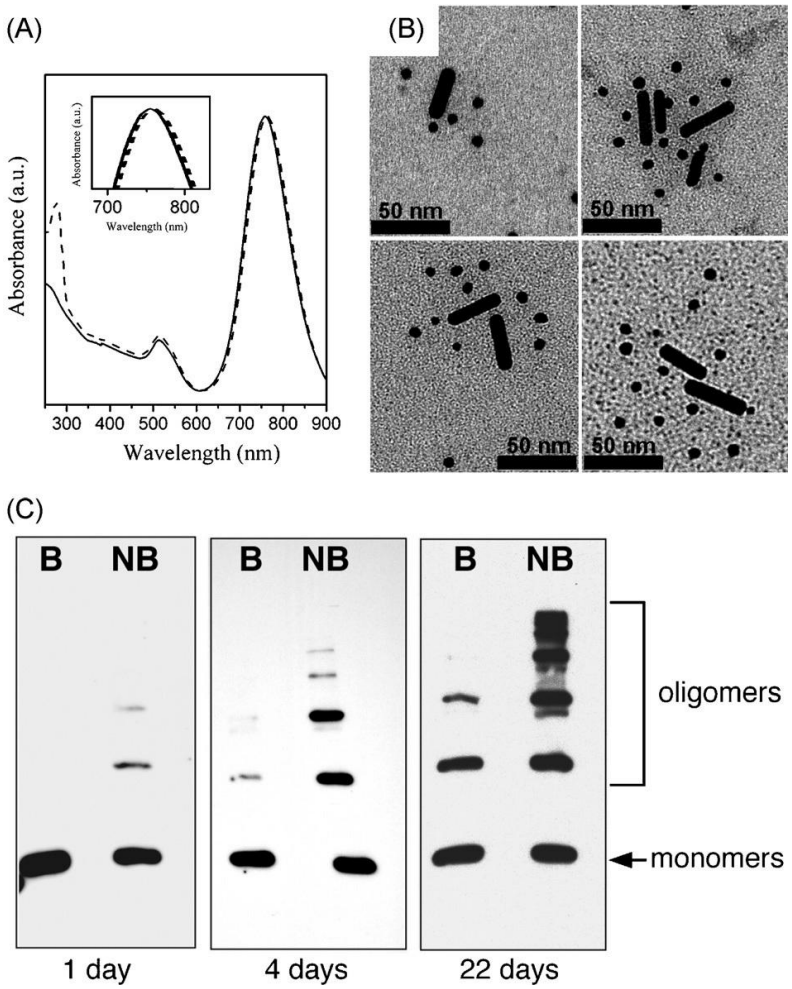

Figura 5. (A) Espectro UV/Vis de AuNRs en ausencia (línea continua) y en presencia (línea de trazos) de H6-RepA-WH1 (A31V), después de 24 h de incubación ($1:10^5$ AuNR:H6-RepA-WH1 (A31V)). El cuadro interior muestra un detalle del desplazamiento hacia el rojo (5 nm) observado durante la incubación. (B) iEM de AuNRs incubadas con H6-RepA-WH1 (A31V) en (A) y el anticuerpo primario (anti-WH1), unido a clones secundarios de anticuerpos conjugados con AuNSs. (C) SDS-PAGE más western-blotting (anti-WH1) de las AuNRs en (B). Pistas B: muestras hervidas; Pistas NB: no hervidas. La proteína experimenta la oligomerización sobre las partículas, indicando la transición a un estado pre-amiloide.

Mediante la técnica de inmunotransferencia con un anticuerpo especifico de la forma amiloide, se pudo confirmar la naturaleza amiloidogénica de estos agregados. Además, mediante la técnica SERS, se evidenció la transición desde la estructura nativa rica en estructura

secundaria tipo α-hélice hacia una amiloide rica en laminas β (Figura 6). Para obtener dichos espectros se emplearon AuNSs de 60 nm, debido a su gran eficiencia plasmónica en SERS, una vez agregadas sobre un sustrato.[59,60] Por último, en analogía a los procesos amiloidogénicos, se observó que dichas AuNRs funcionalizadas con oligómeros amiloides de H6-RepA-WH1 (A31V) actuaron como núcleos para el crecimiento de fibras amiloides en ensayos de fibrilación. Podemos concluir que el uso de AuNRs funcionalizadas con el prionoide H6-RepA-WH1 (A31V) resulta de utilidad para la reproducción controlada *in vitro* de procesos amiloidogénicos y acceder así a sistemas modelo para el estudio de dichas enfermedades.

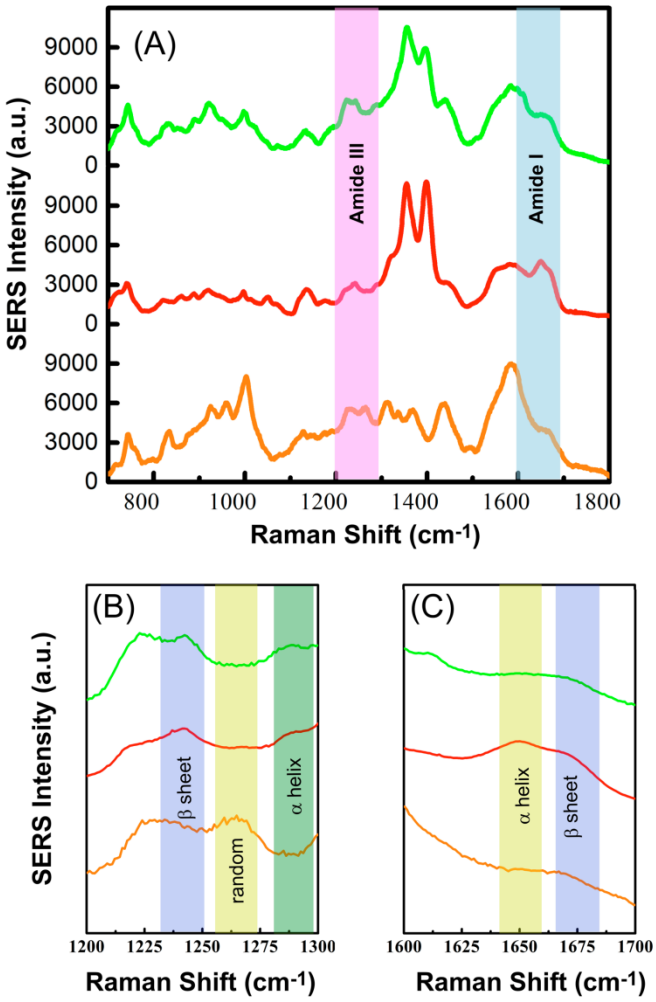

Figure 6. (A) Espectros de SERS de la proteína nativa (línea inferior) y oligómeros amiloides de pesos moleculares bajos (línea media) y altos (línea superior), excitados a 785 nm. (B,C) Ampliación de las regiones amida III y I, respectivamente

INTRODUCCIÓN A LOS LÁSERES PULSADOS PARA LA REESTRUCTURACIÓN, FRAGMENTACIÓN Y ENSAMBLAJE DE NANOPARTÍCULAS DE ORO

La gran mayoría de las aplicaciones de las AuNPs que se han desarrollada durante las dos últimas décadas han surgido de sus propiedades ópticas. En este contexto, la síntesis y ensamblaje racionales de las AuNPs han sido el principal foco de investigación, con el objeto de diseñar dispositivos nanoplasmónicos con funcionalidades ópticas específicas. El progreso realizado en este campo puede atribuirse a la comprensión del origen de la interacción entre la luz y las nanoestructuras de oro, cuya dinámica ha sido investigada en detalle gracias a la significativa contribución de las tecnologías láser de pulsos cortos y ultracortos.[61–63]

Así pues, la excitación de LSPRs con láseres pulsados de femtosegundos da lugar a una termalización de los electrones de las AuNPs y su posterior relajación a través de la red nanocristalina y su entorno, que finalmente deriva en la fusión de la superficie de la nanopartícula. (Figura 7).[61,63–65]. Por el contrario, la irradiación con pulsos de duraciones situadas en el rango de los nanosegundos suele inducir la fragmentación de las AuNPs y su fusión incontrolada debido a la superposición temporal de los fenómenos de excitación y relajación.[66–68] Estos conceptos se han explotado, por ejemplo, para la preparación de nanoesferas de oro altamente monodispersas a partir de AuNPs poliédricas o en la fabricación de nanoestructuras capaces de almacenar información.[69] Además, el uso de pulsos laser se ha extendido hacia la síntesis directa y la manipulación de AuNPs. Por ejemplo, a través de la ablación de un blanco de oro en una fase líquida se pueden preparar AuNSs que no requieren ligandos estabilizadores, lo cual presenta ventajas en términos de baja toxicidad de cara a aplicaciones médicas.[70,71] Además, la irradiación con láseres de femtosegundos ha demostrado ser una herramienta única para la soldadura controlada de nanoestructuras plasmónicas de oro,[72] y para el control del ensamblaje de nanopartículas (ver siguiente apartado). La combinación de dichas nanoestructuras con láseres pulsados promete importantes avances químicos y bioquímicos, incluyendo la determinación estructural de productos intermedios en reacciones orgánicas, la investigación de transiciones de fase en nanomateriales inorgánicos en condiciones de reacción suaves o la destrucción fototérmica eficiente de células cancerosas evitando daños en el tejido circundante.

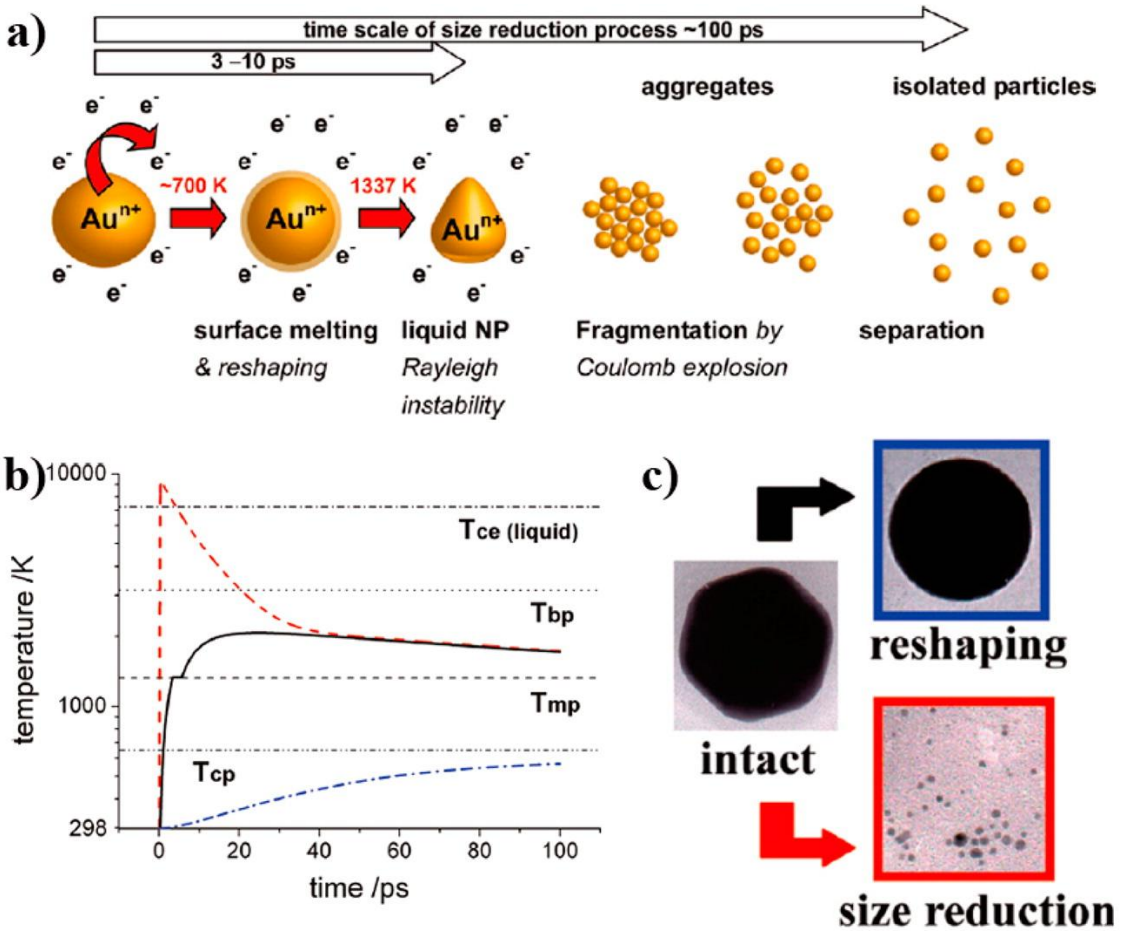

Figura 7. (a) Proceso propuesto para la fragmentación inducida por un láser de femtosegundo. (b) Evolución temporal de la temperatura electrónica (curva roja discontinua); Temperatura del la red cristalina (curva negra continua); Temperatura máxima del agua en la interfase superficie de NP-agua (curva azul), para una nanoesfera de oro de 60 nm de diámetro y un solo pulso láser de 400 nm a 150 fs y fluencia de 12,3 mJ/cm^2. (c) Imágenes TEM que representan la reestructuración y reducción de tamaño a fluencias bajas y altas, para una cuasi-esfera de 60 nm. Reproducido con permiso de la ref. [65].

ENSAMBLAJE Y FUSIÓN A TRAVÉS DE LAS PUNTAS DE NANOVARILLAS DE ORO POR MEDIO DE PULSOS LÁSER DE FEMTOSEGUNDOS.

Cuando la distancia entre dos AuNPs es suficientemente corta, aparecen nuevos modos plasmónicos híbridos debido al acoplamiento de las LSPR,[73] de tal manera que la intensidad de la interacción resultante está controlada por la distancia entre las partículas.[74,75] En el caso de las AuNRs, el ensamblaje a través de las puntas da lugar a un desplazamiento significativo del LSPR hacia el rojo y un aumento de la polarizabilidad efectiva. Esto da lugar a elevados aumentos del campo electromagnético en el espacio entre partículas respecto al campo incidente, y que generalmente son conocidos como *puntos calientes*.[12]

El ensamblaje controlado de nanovarillas de oro mediante el uso de conectores moleculares ditiolados es una de las metodologías más eficientes para obtener ensamblaje punta-punta.[34] Sin embargo, en una analogía directa con la polimerización molecular, este proceso se caracteriza por grandes dificultades en el control del crecimiento de la cadena de oligómeros de las nanopartículas. En particular, es casi imposible favorecer la formación de un tipo determinado de oligómero, haciendo la metodología difícil de usar para aplicaciones reales en nanoplasmónica.

En este trabajo hemos optimizado un procedimiento sintético controlado por luz que permite obtener oligómeros plasmónicos con alto rendimiento y con tiempos de reacción en la escala de minutos. Mediante la irradiación con pulsos láser de femtosegundos en el infrarrojo cercano (NIR) de baja fluencia, conseguimos la inhibición selectiva de la formación de trímeros de oro con LSPR en resonancia con el láser (Ti:zafiro de 800 nm). De este modo, pudimos obtener eficientemente los dímeros (Figura 9). El fenómeno transcurre a través de la activación selectiva de los puntos calientes de los trímeros, produciendo la descomposición fototérmica de los conectores ditiolados que mantenían unidas las partículas. Además, la irradiación con láser a energías más altas dio lugar a un aumento del campo cercano en los espacios entre partículas lo suficientemente grande como para poder fundir las puntas de nanovarillas de oro, ofreciendo así una vía hacia nuevas especies de oro con respuesta plasmónica en el NIR (Figuras 8 y 9).

En conclusión, hemos demostrado que la radiación con láser de femtosegundos es una poderosa herramienta para controlar el ensamblaje de AuNRs, donde la fluencia de pulso láser

determina el control de la formación de dímeros o su fusión a través de las puntas para formar nuevas especies plasmónicas con bandas en el NIR.

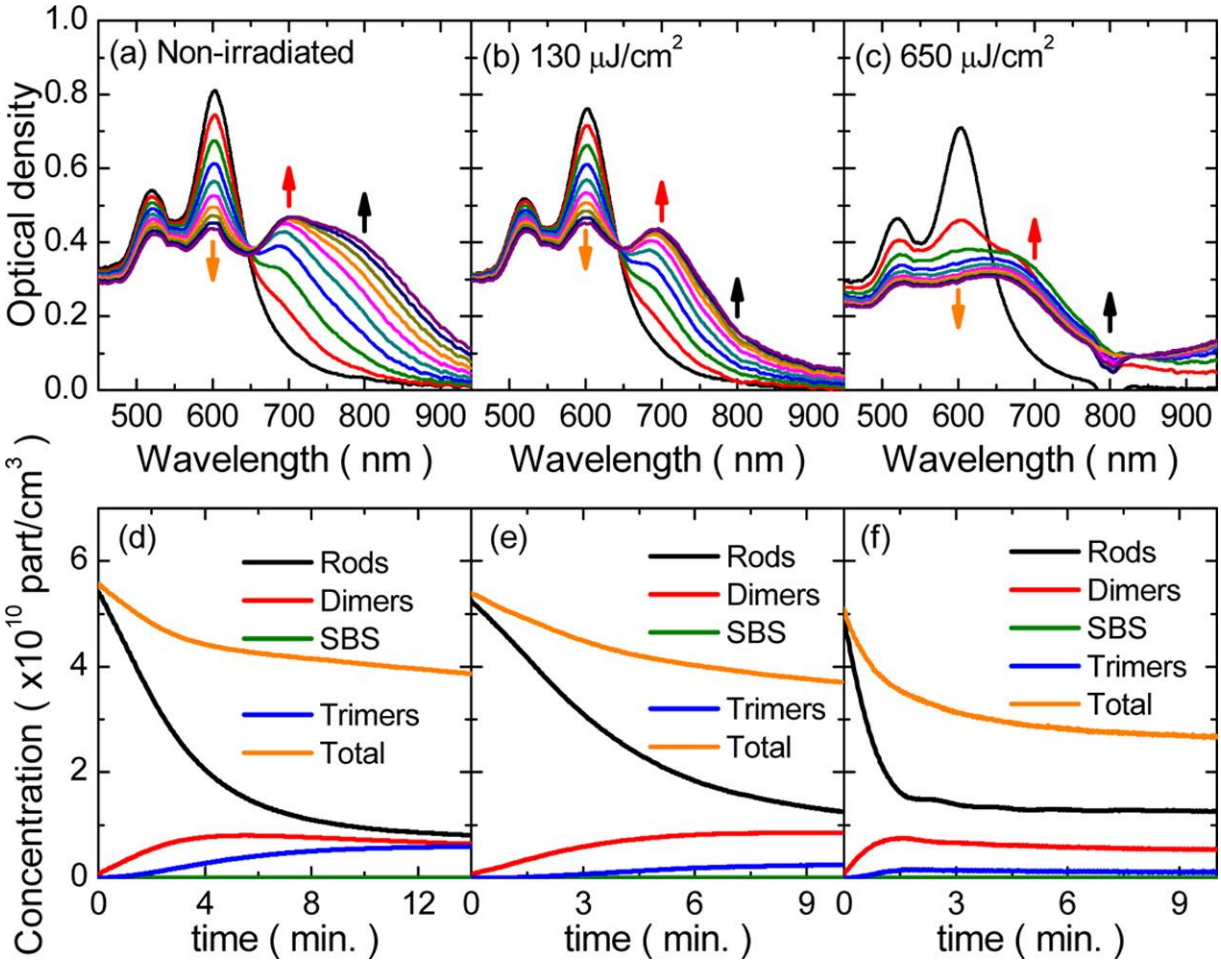

Figura 8. Evolución del proceso de auto-ensamblaje punta a punta de AuNRs para diferentes condiciones de irradiación. (a-c) Espectros de extinción a intervalos de 20 s durante 10 min. (a) sin irradiación con láser, (b) 130 μJ/cm^2 por pulso a 1 kHz, y (c) 650 μJ/cm^2 por pulso a 1 kHz. Las flechas apuntan a la región espectral en los máximos de LSPR para el monómero (naranja), dímero (rojo) y trímero (negro). La concentración de dímeros unidos a través de los lados (SBS, líneas verdes) producidos por el ajuste es muy próxima a cero. (d-f) Concentración de monómeros, dímeros y trímeros de AuNRs obtenidos de los ajustes para fluencias: (d) sin irradiar, (e) 130 μJ/cm^2 y (f) 650 μJ/cm^2.

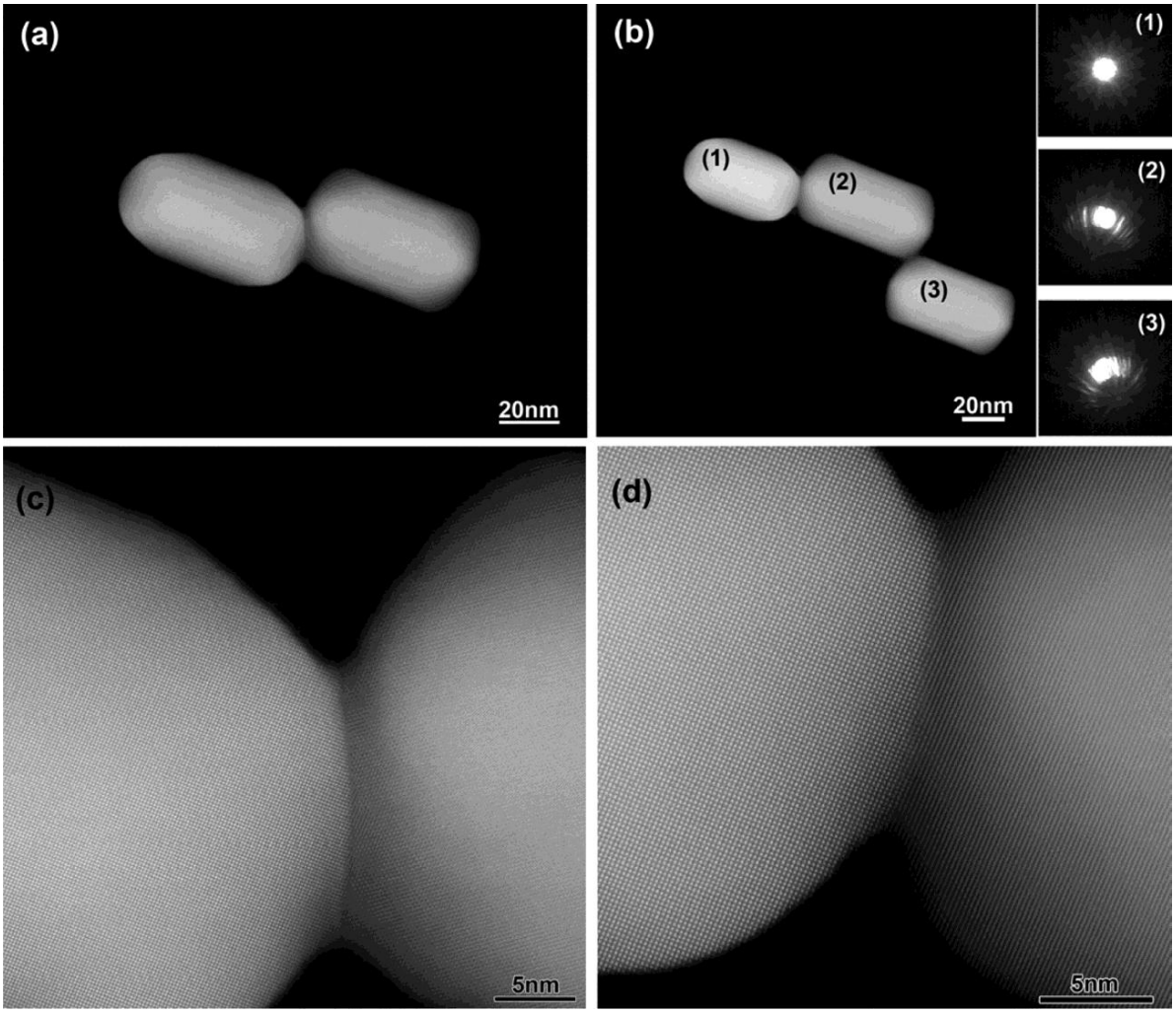

Figura 9. Imágenes de tomografía electrónica de campo oscuro de alto ángulo obtenidas por microscopía electrónica de transmisión en modo barrido (HAADF-STEM) de un dímero (a) y un trímero (b) fusionados por irradiación a 650 μJ/cm^2. Los recuadros (b) muestran los patrones de difracción obtenidos mediante difracción de electrones de haz convergente (CBED) de las AuNRs en el trímero. (c,d) Imágenes HAADF-STEM de alta resolución de las zonas de conexión en el dímero y en el trímero, respectivamente.

ENSAMBLAJE INTRACELULAR A TRAVÉS DE LAS PUNTAS DE NANOVARILLAS DE ORO MEDIADO POR pH PARA FOTOTERAPIA PLASMÓNICA MEJORADA.

El uso de nanopartículas de oro plasmónicas con fines biomédicos ha aumentado considerablemente en los últimos años debido a sus propiedades ópticas singulares y su elevada biocompatibilidad. En este contexto, la búsqueda de fototerapias térmicas plasmónicas (PPTT) eficientes mediante irradiación con láseres pulsados en el infrarrojo cercano (NIR) es fundamental para la investigación biomédica del cáncer. La PPTT utiliza AuNPs para convertir luz no dañina en energía térmica a través de la interacción de la radiación láser con los LSPRs de nanoestructuras plasmónicas.[76–78] Sin embargo, en general, los sistemas actuales necesitan irradiaciones con valores de fluencia todavía por encima del umbral de tolerancia de la piel para producir la destrucción óptima de las células cancerígenas.

Dentro de este contexto, hemos investigado el auto-ensamblaje de AuNRs para generar puntos calientes como vía eficaz para aumentar la eficiencia de la PPTT. Mediante la funcionalización de las AuNRs con un ligando (ácido lipoico) sensible al pH pudimos inducir su agregación dentro de los lisosomas celulares de cáncer de mama (Figura 10). Gracias al bajo pH del interior de estos compartimentos intracelulares, se forman enlaces de hidrógeno entre los grupos carboxilo del ácido lipoico que fuerzan el ensamblaje de las nanopartículas a través de sus puntas. La formación de oligómeros plasmónicos intracelulares, combinada con la irradiación láser en el NIR (800 nm Ti: zafiro 90 fs, 80 MHz), nos permitió optimizar las condiciones de PPTT, con irradiaciones de potencias mínimas (0,21 W/cm^2, por debajo del umbral de exposición de luz láser permitido para la piel), áreas de irradiación (20 mm^2) y concentraciones de AuNR extremadamente bajas (1 pM). Para obtener dichas eficiencias fue necesario maximizar el acoplamiento del LSPR de los agregados con el láser, para lo cual se empleó la misma premisa, y por tanto las mismas AuNRs utilizadas en el apartado anterior.

Podemos concluir que nuestras investigaciones han demostrado que las AuNRs, y en particular las estabilizadas con ácido lipoico, pueden formar auto-ensamblajes punta a punta dentro de los lisosomas de células cancerosas modelo, lo cual reduce considerablemente la densidad de irradiación del láser NIR de fs requerida para una PPTT eficiente.

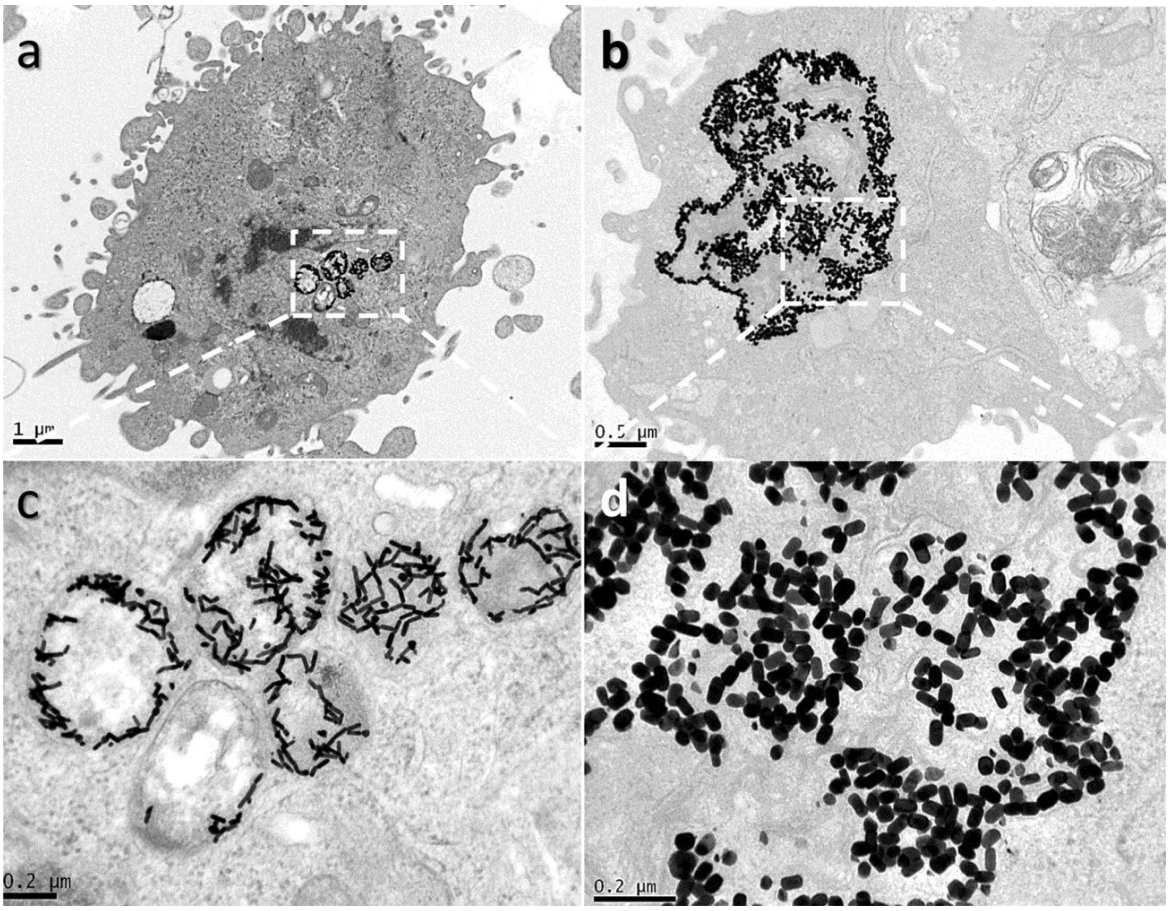

Figura 10. Imagen de TEM representativa de células cancerígenas MDA-MB-231 después de 24 h de incubación con 0,1 nM de AuNRs con su banda LSPR a (a) 803 nm y (b) 604 nm, funcionalizadas con ácido lipoico. (c) y (d) corresponden a magnificaciones de ciertas áreas de los lisosomas mostrados en (a) y (b), respectivamente.

CONCLUSIONES

Este trabajo se ha centrado en el diseño y síntesis de nanopartículas plasmónicas, su funcionalización racional y el control de su ensamblaje para obtener nuevas propiedades plasmónicas de valor en el estudio y/o tratamiento de enfermedades humanas.

Para cumplir dichos objetivos, primero se optimizó la síntesis de nanoesferas de oro y luego se procedió a su ensamblaje en estructuras piramidales altamente estructuradas con potencial uso en detección y análisis mediante espectroscopia SERS.

A continuación, se demostró la utilidad de las nanovarillas de oro como elementos para el estudio y detección de la formación de agregados oligoméricos amiloides de gran relevancia en el desarrollo de patologías tales como la enfermedad de Alzheimer.

De especial relevancia ha sido la implementación del uso de láseres pulsados de femtosegundos para controlar el auto-ensamblaje de nanopartículas de oro anisótropas, así como para su uso para terapia fototérmica. Primero llevamos a cabo una introducción a los usos más relevantes de los láseres pulsados como herramienta para la remodelación, fragmentación y ensamblaje de nanopartículas de oro, con énfasis en los mecanismos subyacentes.

A partir de dicha revisión, demostramos la utilidad de dichos láseres pulsados para controlar el ensamblaje de nanovarillas de oro en fase acuosa, y para formar nuevas especies plasmónicas con absorción en la región espectral del infrarrojo cercano.

Por último, hemos sido capaces de aumentar la eficacia de los láseres pulsados de femtosegundos para terapia fototérmica mediante el ensamblaje programado de nanovarillas de oro en el interior de lisosomas de células cancerígenas.

APORTACIONES FUNDAMENTALES DE LA TESIS

Se espera de la nanociencia y la nanotecnología que hagan frente a muchos de los retos que amenazan nuestro futuro, desde el almacenamiento de energía hasta la cura de enfermedades. En este contexto, las nanopartículas de oro se encuentran entre los sistemas que están a la cabeza de esta lucha, ofreciendo una combinación única de propiedades ópticas modulables (resonancias plasmónicas superficiales localizadas, LSPRs) y alta estabilidad química con reactividad controlable. Entre la gran variedad de campos de aplicación cubiertos

por las nanopartículas de oro, su uso en la detección, el diagnóstico y el tratamiento de enfermedades humanas pueden ser de las que produzcan un mayor impacto en la sociedad.

En esta tesis titulada "Síntesis y Ensamblaje de Nanoestructuras Plasmónicas de Oro Uniformes para Aplicaciones en Biomedicina", hemos trabajado en el desarrollo de enfoques novedosos para la síntesis de nanoestructuras plasmónicas que puedan utilizarse para el diagnóstico y tratamiento de diversas enfermedades humanas. Específicamente, los aspectos fundamentales de esta tesis son la síntesis de nanopartículas de oro con propiedades ópticas específicas y su subsiguiente funcionalización y/o auto-ensamblaje, con el objetivo de explotarlas para estudiar y detectar el proceso de amiloidogénesis, así como su aplicación en terapia fototérmica. Una de las principales innovaciones presentadas en este trabajo es la implementación de los láseres pulsados como herramientas valiosas para controlar algunos de los aspectos anteriormente mencionados.

Como primera estrategia se han sintetizado nanoesferas de oro con elevada monodispersidad y se han auto-ensamblado sobre sustratos usando plantillas piramidales, mediante funcionalización con polietilenglicol tiolado y en presencia de pequeñas concentraciones de un surfactante catiónico (Capítulo 2). Siguiendo con el concepto de síntesis y funcionalización racionales, se fabricaron nanovarillas de oro y se estabilizaron con el modelo prionoide RepA-WH (Capítulo 3). Este enfoque nos permitió inducir la formación de oligómeros amiloides, especies tóxicas que juegan un papel clave en la etiología de una serie de devastadoras enfermedades humanas degenerativas. Además, aprovechamos la sensibilidad de las LSPR y las propiedades de las nanopartículas plasmónicas para incrementar la señal Raman de moléculas (SERS) para monitorizarlo.

En una segunda aproximación, aprovechamos la fuerte interacción de las nanopartículas plasmónicas con pulsos láser de femtosegundos para el auto-ensamblaje de nanopartículas de oro anisótropas, así como para su uso en terapia fototérmica.

Se ha presentado una revisión crítica de los usos más relevantes de los láseres pulsados para la remodelación, fragmentación y ensamblaje de nanopartículas de oro, así como de su mecanismo de interacción (Capítulo 4). Posteriormente demostramos que mediante la irradiación con láseres pulsados de femtosegundo se puede controlar el auto-ensamblaje de las nanovarillas de oro utilizando un engarce molecular como mecanismo de ensamblaje (Capítulo 5). Además, a

altas fluencias se sintetizaron especies soldadas con LSPRs en el infrarrojo. Finalmente, se sintetizaron y funcionalizaron nanovarillas de oro de tal manera que se programaron para auto-ensamblarse dentro de los lisosomas de células cancerosas modelo, y de este modo formar especies adecuadas para una terapia fototérmica eficiente con láseres de femtosegundos (Capítulo 6).

En resumen, esta tesis presenta un avance significativo en la síntesis, funcionalización y auto-ensamblaje de diferentes nanopartículas plasmónicas para uso en biomedicina, fundamentalmente en el estudio del proceso de amiloidogénesis y para el tratamiento del cáncer mediante terapia fototérmica.

REFERENCIAS

(1) Pradeep, T.; Anshup. Noble Metal Nanoparticles for Water Purification: A Critical Review. *Thin Solid Films* **2009**, *517*, 6441–6478.

(2) Aćimović, S. S.; Ortega, M. A.; Sanz, V.; Berthelot, J.; Garcia-Cordero, J. L.; Renger, J.; Maerkl, S. J.; Kreuzer, M. P.; Quidant, R. LSPR Chip for Parallel, Rapid, and Sensitive Detection of Cancer Markers in Serum. *Nano Lett.* **2014**, *14*, 2636–2641.

(3) Huang, X.; El-Sayed, I. H.; El-Sayed, M. A. Applications of Gold Nanorods for Cancer Imaging and Photothermal Therapy. *Methods Mol. Biol.* **2010**, *624*, 343–357.

(4) Plass, R.; Pelet, S.; Krueger, J.; Grätzel, M.; Bach, U. Quantum Dot Sensitization of Organic−Inorganic Hybrid Solar Cells. *J. Phys. Chem. B* **2002**, *106*, 7578–7580.

(5) Bodelón, G.; Montes-García, V.; López-Puente, V.; Hill, E. H.; Hamon, C.; Sanz-Ortiz, M. N.; Rodal-Cedeira, S.; Costas, C.; Celiksoy, S.; Pérez-Juste, I.; *et al.* Detection and Imaging of Quorum Sensing in Pseudomonas Aeruginosa Biofilm Communities by Surface-Enhanced Resonance Raman Scattering. *Nat. Mater.* **2016**, *15*, 1203–1211.

(6) NSET. NSF's National Nanotechnology Initiative (NNI) - Nanotechnology definition https://www.nsf.gov/crssprgm/nano/reports/omb_nifty50.jsp (accessed Mar 21, 2017).

(7) Dong, X. *Discovering the Nanoscale*; Baird, D., Nordmann, A., Schummer, J., Ed.; Amsterdam, 2004; Vol. 3.

(8) Willets, K. A.; Van Duyne, R. P. Localized Surface Plasmon Resonance Spectroscopy and

Sensing. *Annu. Rev. Phys. Chem.* **2007**, *58*, 267–297.

(9) Liz-Marzán, L. M. Tailoring Surface Plasmons through the Morphology and Assembly of Metal Nanoparticles. *Langmuir* **2006**, *22*, 32–41.

(10) Myroshnychenko, V.; Rodríguez-Fernández, J.; Pastoriza-Santos, I.; Funston, A. M.; Novo, C.; Mulvaney, P.; Liz-Marzán, L. M.; García de Abajo, F. J. Modelling the Optical Response of Gold Nanoparticles. *Chem. Soc. Rev.* **2008**, *37*, 1792–1805.

(11) Jiang, L.; Liang, Z.; Sun, J.; Jiang, Y.; Jiang, L. Plasmonic Enhanced Optoelectronic Devices. *Plasmonics* **2014**, *9*, 859–866.

(12) Maier, S. A. *Plasmonics : Fundamentals and Applications*; Springer: New York, 2004; Vol. 677.

(13) Faraday, M. The Bakerian Lecture: Experimental Relations of Gold (and Other Metals) to Light. *Philos. Trans. R. Soc. London* **1857**, *147*, 145–181.

(14) Xia, Y.; Xiong, Y.; Lim, B.; Skrabalak, S. E. Shape-Controlled Synthesis of Metal Nanocrystals: Simple Chemistry Meets Complex Physics? *Angew. Chem. Int. Ed.* **2009**, *48*, 60–103.

(15) Xiong, Y.; Xia, Y. Shape-Controlled Synthesis of Metal Nanostructures: The Case of Palladium. *Adv. Mater.* **2007**, *19*, 3385–3391.

(16) Wiley, B.; Sun, Y.; Mayers, B.; Xia, Y. Shape-Controlled Synthesis of Metal Nanostructures: The Case of Silver. *Chem. Eur. J.* **2005**, *11*, 454–463.

(17) O'Brien, M. N.; Jones, M. R.; Brown, K. A.; Mirkin, C. A.; O'Brien, M. N.; Jones, M. R.; Brown, K. A.; Mirkin, C. A. Universal Noble Metal Nanoparticle Seeds Realized through Iterative Reductive Growth and Oxidative Dissolution Reactions. *J. Am. Chem. Soc.* **2014**, *136*, 7603–7606.

(18) Sánchez-Iglesias, A.; Winckelmans, N.; Altantzis, T.; Bals, S.; Grzelczak, M.; Liz-Marzán, L. M. High-Yield Seeded Growth of Monodisperse Pentatwinned Gold Nanoparticles through Thermally Induced Seed Twinning. *J. Am. Chem. Soc.* **2017**, *139*, 107–110.

(19) Niu, W.; Zhang, L.; Xu, G. Shape-Controlled Synthesis of Single-Crystalline Palladium

Nanocrystals. *ACS Nano* **2010**, *4*, 1987–1996.

(20) Kendrew, J. C.; Bodo, G.; Dintzis, H. M.; Parrish, R. G.; Wyckoff, H.; Phillips, D. C. Three-Dimensional Model of the Myoglobin Molecule Obtained by X-Ray Analysis. *Nature* **1958**, *181*, 662–666.

(21) Li, L.; Kolle, S.; Weaver, J. C.; Ortiz, C.; Aizenberg, J.; Kolle, M. A Highly Conspicuous Mineralized Composite Photonic Architecture in the Translucent Shell of the Blue-Rayed Limpet. *Nat. Commun.* **2015**, *6*, 6322.

(22) Alivisatos, A. P. Perspectives on the Physical Chemistry of Semiconductor Nanocrystals. *J. Phys. Chem.* **1996**, *100*, 13226–13239.

(23) Hamon, C.; Novikov, S.; Scarabelli, L.; Basabe-Desmonts, L.; Liz-Marzán, L. M. Hierarchical Self-Assembly of Gold Nanoparticles into Patterned Plasmonic Nanostructures. *ACS Nano* **2014**, *8*, 10694–10703.

(24) Guerrero-Martínez, A.; Auguié, B.; Alonso-Gómez, J. L.; Džolič, Z.; Gómez-Graña, S.; Žinić, M.; Cid, M. M.; Liz-Marzán, L. M. Intense Optical Activity from Three-Dimensional Chiral Ordering of Plasmonic Nanoantennas. *Angew. Chem. Int. Ed.* **2011**, *50*, 5499–5503.

(25) Le Ru, E. C.; Etchegoin, P. G. Single-Molecule Surface-Enhanced Raman Spectroscopy. *Annu. Rev. Phys. Chem.* **2012**, *63*, 65–87.

(26) Schlücker, S. Surface-Enhanced Raman Spectroscopy: Concepts and Chemical Applications. *Angew. Chem. Int. Ed.* **2014**, *53*, 4756–4795.

(27) Kraus, T.; Wolf, H. Templated Self-Assembly of Particles. In *Springer Handbook of Nanotechnology*; Springer Berlin Heidelberg: Berlin, Heidelberg, 2010; pp. 187–210.

(28) Grzelczak, M.; Vermant, J.; Furst, E. M.; Liz-Marzán, L. M. Directed Self-Assembly of Nanoparticles. *ACS Nano* **2010**, *4*, 3591–3605.

(29) Caswell, K. K.; Wilson, J. N.; Bunz, U. H. F.; Murphy, C. J. Preferential End-to-End Assembly of Gold Nanorods by Biotin−Streptavidin Connectors. *J. Am. Chem. Soc.* **2003**, *125*, 13914–13915.

(30) Macfarlane, R. J.; Lee, B.; Jones, M. R.; Harris, N.; Schatz, G. C.; Mirkin, C. A.

Nanoparticle Superlattice Engineering with DNA. *Science* **2011**, *334*, 204–208.

(31) Mirkin, C. A.; Letsinger, R. L.; Mucic, R. C.; Storhoff, J. J. A DNA-Based Method for Rationally Assembling Nanoparticles into Macroscopic Materials. *Nature* **1996**, *382*, 607–609.

(32) Ni, W.; Mosquera, R. A.; Pérez-Juste, J.; Liz-Marzán, L. M. Evidence for Hydrogen-Bonding-Directed Assembly of Gold Nanorods in Aqueous Solution. *J. Phys. Chem. Lett.* **2010**, *1*, 1181–1185.

(33) Wang, J.; Zhang, P.; Li, C. M.; Li, Y. F.; Huang, C. Z. A Highly Selective and Colorimetric Assay of Lysine by Molecular-Driven Gold Nanorods Assembly. *Biosens. Bioelectron.* **2012**, *34*, 197–201.

(34) Shibu Joseph, S. T.; Ipe, B. I.; Pramod, P.; Thomas, K. G. Gold Nanorods to Nanochains: Mechanistic Investigations on Their Longitudinal Assembly Using A,ω-Alkanedithiols and Interplasmon Coupling. *J. Phys. Chem. B* **2006**, *110*, 150–157.

(35) Scarabelli, L.; Coronado-Puchau, M.; Giner-Casares, J. J.; Langer, J.; Liz-Marzán, L. M. Monodisperse Gold Nanotriangles: Size Control, Large-Scale Self-Assembly, and Performance in Surface-Enhanced Raman Scattering. *ACS Nano* **2014**, *8*, 5833–5842.

(36) Sánchez-Iglesias, A.; Grzelczak, M.; Altantzis, T.; Goris, B.; Pérez-Juste, J.; Bals, S.; Van Tendeloo, G.; Donaldson, S. H.; Chmelka, B. F.; Israelachvili, J. N.; liz-Marzán, L. M.. Hydrophobic Interactions Modulate Self-Assembly of Nanoparticles. *ACS Nano* **2012**, *6*, 11059–11065.

(37) Thai, T.; Zheng, Y.; Ng, S. H.; Mudie, S.; Altissimo, M.; Bach, U. Self-Assembly of Vertically Aligned Gold Nanorod Arrays on Patterned Substrates. *Angew. Chem. Int. Ed.* **2012**, *51*, 8732–8735.

(38) Zhou, Y.; Zhou, X.; Park, D. J.; Torabi, K.; Brown, K. A.; Jones, M. R.; Zhang, C.; Schatz, G. C.; Mirkin, C. A. Shape-Selective Deposition and Assembly of Anisotropic Nanoparticles. *Nano Lett.* **2014**, *14*, 2157–2161.

(39) Greybush, N. J.; Liberal, I.; Malassis, L.; Kikkawa, J. M.; Engheta, N.; Murray, C. B.; Kagan, C. R. Plasmon Resonances in Self-Assembled Two-Dimensional Au Nanocrystal Metamolecules. *ACS Nano* **2016**, *11*, 2917-2927.

(40) Tebbe, M.; Mayer, M.; Glatz, B. A.; Hanske, C.; Probst, P. T.; Müller, M. B.; Karg, M.; Chanana, M.; König, T. A. F.; Kuttner, C.; Fery, A. Optically Anisotropic Substrates via Wrinkle-Assisted Convective Assembly of Gold Nanorods on Macroscopic Areas. *Faraday Discuss.* **2015**, *181*, 243–260.

(41) Ofir, Y.; Moran, I. W.; Subramani, C.; Carter, K. R.; Rotello, V. M. Nanoimprint Lithography for Functional Three-Dimensional Patterns. *Adv. Mater.* **2010**, *22*, 3608–3614.

(42) Hamon, C.; Postic, M.; Mazari, E.; Bizien, T.; Dupuis, C.; Even-Hernandez, P.; Jimenez, A.; Courbin, L.; Gosse, C.; Artzner, F.; Marchi-Artzner, V. Three-Dimensional Self-Assembling of Gold Nanorods with Controlled Macroscopic Shape and Local Smectic B Order. *ACS Nano* **2012**, *6*, 4137–4146.

(43) Hanske, C.; Tebbe, M.; Kuttner, C.; Bieber, V.; Tsukruk, V. V.; Chanana, M.; König, T. A. F.; Fery, A. Strongly Coupled Plasmonic Modes on Macroscopic Areas via Template-Assisted Colloidal Self-Assembly. *Nano Lett.* **2014**, *14*, 6863–6871.

(44) Zheng, Y.; Zhong, X.; Li, Z.; Xia, Y. Successive, Seed-Mediated Growth for the Synthesis of Single-Crystal Gold Nanospheres with Uniform Diameters Controlled in the Range of 5-150 Nm. *Part. Part. Syst. Charact.* **2014**, *31*, 266–273.

(45) Ruan, Q.; Shao, L.; Shu, Y.; Wang, J.; Wu, H. Growth of Monodisperse Gold Nanospheres with Diameters from 20 nm to 220 nm and Their Core/Satellite Nanostructures. *Adv. Opt. Mater.* **2014**, *2*, 65–73.

(46) Ma, Y.; Kuang, Q.; Jiang, Z.; Xie, Z.; Huang, R.; Zheng, L. Synthesis of Trisoctahedral Gold Nanocrystals with Exposed High-Index Facets by a Facile Chemical Method. *Angew. Chem. Int. Ed.* **2008**, *47*, 8901–8904.

(47) Rodríguez-Fernández, J.; Pérez-Juste, J.; Mulvaney, P.; Liz-Marzán, L. M. Spatially-Directed Oxidation of Gold Nanoparticles by Au(III)−CTAB Complexes. *J. Phys. Chem. B* **2005**, *109*, 14257–14261.

(48) Westermark, P.; Benson, M. D.; Buxbaum, J. N.; Cohen, A. S.; Frangione, B.; Ikeda, S.; Masters, C. L.; Merlini, G.; Saraiva, M. J.; Sipe, J. D. Amyloid Fibril Protein Nomenclature - 2002. *Amyloid* **2002**, *9*, 197–200.

(49) Knowles, T. P. J.; Vendruscolo, M.; Dobson, C. M. The Amyloid State and Its Association with Protein Misfolding Diseases. *Nat. Rev. Mol. Cell Biol.* **2014**, *15*, 496.

(50) Eichner, T.; Radford, S. E. A Diversity of Assembly Mechanisms of a Generic Amyloid Fold. *Mol. Cell* **2011**, *43*, 8–18.

(51) Gladytz, A.; Abel, B.; Risselada, H. J. Gold-Induced Fibril Growth: The Mechanism of Surface-Facilitated Amyloid Aggregation. *Angew. Chem. Int. Ed.* **2016**, *55*, 11242–11246.

(52) Walsh, D. M.; Klyubin, I.; Fadeeva, J. V; Cullen, W. K.; Anwyl, R.; Wolfe, M. S.; Rowan, M. J.; Selkoe, D. J. Naturally Secreted Oligomers of Amyloid Beta Protein Potently Inhibit Hippocampal Long-Term Potentiation in Vivo. *Nature* **2002**, *416*, 535–539.

(53) Cabaleiro-Lago, C.; Quinlan-Pluck, F.; Lynch, I.; Dawson, K. A.; Linse, S. Dual Effect of Amino Modified Polystyrene Nanoparticles on Amyloid β Protein Fibrillation. *ACS Chem. Neurosci.* **2010**, *1*, 279–287.

(54) Murphy, C. J.; Sau, T. K.; Gole, A. M.; Orendorff, C. J.; Gao, J.; Gou, L.; Hunyadi, S. E.; Li, T. Anisotropic Metal Nanoparticles: Synthesis, Assembly, and Optical Applications. *J. Phys. Chem. B* **2005**, *109*, 13857–13870.

(55) Oh, E.; Susumu, K.; Mäkinen, A. J.; Deschamps, J. R.; Huston, A. L.; Medintz, I. L. Colloidal Stability of Gold Nanoparticles Coated with Multithiol-Poly(ethylene Glycol) Ligands: Importance of Structural Constraints of the Sulfur Anchoring Groups. *J. Phys. Chem. C* **2013**, *117*, 18947–18956.

(56) Guerrero-Martínez, A.; Grzelczak, M.; Liz-Marzán, L. M. Molecular Thinking for Nanoplasmonic Design. *ACS Nano* **2012**, *6*, 3655–3662.

(57) K. K. Caswell; James N. Wilson; and Uwe H. F. Bunz; Murphy, C. J. Preferential End-to-End Assembly of Gold Nanorods by Biotin−Streptavidin Connectors. **2003**, *125*,13914-13915

(58) Fernández, C.; Núñez-Ramírez, R.; Jiménez, M.; Rivas, G.; Giraldo, R. RepA-WH1, the Agent of an Amyloid Proteinopathy in Bacteria, Builds Oligomeric Pores through Lipid Vesicles. *Sci. Rep.* **2016**, *6*, 23144.

(59) Costas, C.; López-Puente, V.; Bodelón, G.; González-Bello, C.; Pérez-Juste, J.; Pastoriza-Santos, I.; Liz-Marzán, L. M. Using Surface Enhanced Raman Scattering to Analyze the Interactions of Protein Receptors with Bacterial Quorum Sensing Modulators. *ACS Nano* **2015**, *9*, 5567–5576.

(60) Hamon, C.; Novikov, S. M.; Scarabelli, L.; Solís, D. M.; Altantzis, T.; Bals, S.; Taboada, J. M.; Obelleiro, F.; Liz-Marzán, L. M. Collective Plasmonic Properties in Few-Layer Gold Nanorod Supercrystals. *ACS Photonics* **2015**, *2*, 1482–1488.

(61) Logunov, S. L.; Ahmadi, T. S.; El-Sayed, M. A.; Khoury, J. T.; Whetten, R. L. Electron Dynamics of Passivated Gold Nanocrystals Probed by Subpicosecond Transient Absorption Spectroscopy. *J. Phys. Chem. B* **1997**, *101*, 3713–3719.

(62) Ahmadi, T. S.; Logunov, S. L.; El-Sayed, M. A. Picosecond Dynamics of Colloidal Gold Nanoparticles. *J. Phys. Chem.* **1996**, *100*, 8053–8056.

(63) Link, S.; El-Sayed, M. A. Optical Properties and Ultrafast Dynamics of Metallic Nanocrystals. *Annu. Rev. Phys. Chem.* **2003**, *54*, 331–366.

(64) Link, S.; Burda, C.; Mohamed, M. B.; Nikoobakht, B.; El-Sayed, M. A. Laser Photothermal Melting and Fragmentation of Gold Nanorods: Energy and Laser Pulse-Width Dependence. *J. Phys. Chem. A* **1999**, *103*, 1165–1170.

(65) Werner, D.; Furube, A.; Okamoto, T.; Hashimoto, S. Femtosecond Laser-Induced Size Reduction of Aqueous Gold Nanoparticles: In Situ and Pump-Probe Spectroscopy Investigations Revealing Coulomb Explosion. *J. Phys. Chem. C* **2011**, *115*, 8503–8512.

(66) Wang, Z. L.; Mohamed, M. B.; Link, S.; El-Sayed, M. A. Crystallographic Facets and Shapes of Gold Nanorods of Different Aspect Ratios. *Surf. Sci.* **1999**, *440*, L809-L814

(67) Kurita, H.; Takami, A.; Koda, S. Size Reduction of Gold Particles in Aqueous Solution by Pulsed Laser Irradiation. *Appl. Phys. Lett.* **1998**, *72*, 789.

(68) Pyatenko, A.; Yamaguchi, M.; Suzuki, M. Mechanisms of Size Reduction of Colloidal Silver and Gold Nanoparticles Irradiated by Nd:YAG Laser. *J. Phys. Chem. C* **2009**, *113*, 9078–9085.

(69) Liu, D.; Li, C.; Zhou, F.; Zhang, T.; Zhang, H.; Li, X.; Duan, G.; Cai, W.; Li, Y. Rapid

Synthesis of Monodisperse Au Nanospheres through a Laser Irradiation -Induced Shape Conversion, Self-Assembly and Their Electromagnetic Coupling SERS Enhancement. *Sci. Rep.* **2015**, *5*, 7686.

(70) Tomko, J.; Naddeo, J. J.; Jimenez, R.; Tan, Y.; Steiner, M.; Fitz-Gerald, J. M.; O'Malley, S. M.; Bubb, D. M. Size and Polydispersity Trends Found in Gold Nanoparticles Synthesized by Laser Ablation in Liquids. *Phys. Chem. Chem. Phys* **2015**, *17*, 16327–16333.

(71) Bueno-Alejo, C. J.; D'Alfonso, C.; Pacioni, N. L.; González-Béjar, M.; Grenier, M.; Lanzalunga, O.; Alarcon, E. I.; Scaiano, J. C. Ultraclean Derivatized Monodisperse Gold Nanoparticles through Laser Drop Ablation Customization of Polymorph Gold Nanostructures. *Langmuir* **2012**, *28*, 8183–8189.

(72) Herrmann, L. O.; Valev, V. K.; Tserkezis, C.; Barnard, J. S.; Kasera, S.; Scherman, O.; Aizpurua, J.; Baumberg, J. J. Threading Plasmonic Nanoparticle Strings with Light. *Nat. Commun.* **2014**, *5*, 1–6.

(73) Nordlander, P.; Oubre, C.; Prodan, E.; Li, K.; Stockman, M. I. Plasmon Hybridization in Nanoparticle Dimers. *Nano Lett.* **2004**, *4*, 899–903.

(74) Funston, A. M.; Novo, C.; Davis, T. J.; Mulvaney, P. Plasmon Coupling of Gold Nanorods at Short Distances and in Different Geometries. *Nano Lett.* **2009**, *9*, 1651–1658.

(75) Jain, P. K.; Huang, W.; El-Sayed, M. A. On the Universal Scaling Behavior of the Distance Decay of Plasmon Coupling in Metal Nanoparticle Pairs: A Plasmon Ruler Equation. *Nano Lett.* **2007**, *7*, 2080–2088.

(76) Abadeer, N. S.; Murphy, C. J. Recent Progress in Cancer Thermal Therapy Using Gold Nanoparticles. *J. Phys. Chem. C* **2016**, *120*, 4691–4716.

(77) Huang, X.; Jain, P. K.; El-Sayed, I. H.; El-Sayed, M. A. Plasmonic Photothermal Therapy (PPTT) Using Gold Nanoparticles. *Lasers Med. Sci.* **2008**, *23*, 217–228.

(78) Pérez-Hernández, M.; del Pino, P.; Mitchell, S. G.; Moros, M.; Stepien, G.; Pelaz, B.; Parak, W. J.; Gálvez, E. M.; Pardo, J.; de la Fuente, J. M. Dissecting the Molecular Mechanism of Apoptosis during Photothermal Therapy Using Gold Nanoprisms. *ACS Nano* **2015**, *9*, 52–61.

Publication List

(1) González-Rubio, G.; González-Izquierdo, J.; Bañares, L.; Tardajos, G.; Rivera, A.; Altantzis, T.; Bals, S.; Peña-Rodríguez, O.; Guerrero-Martínez, A.; Liz-Marzán, L. M. Femtosecond Laser-Controlled Tip-to-Tip Assembly and Welding of Gold Nanorods. *Nano Lett.* **2015**, *15*, 8282–8288.

(2) González-Rubio, G.; Guerrero-Martínez, A.; Liz-Marzán, L. M. Reshaping, Fragmentation, and Assembly of Gold Nanoparticles Assisted by Pulse Lasers. *Acc. Chem. Res.* **2016**, *49*, 678−686.

(3) Fernández, C.;† González-Rubio, G.;† Langer, J.; Tardajos, G.; Liz-Marzán, L. M.; Giraldo, R.; Guerrero-Martínez, A. Nucleation of Amyloid Oligomers by RepA-WH1-Prionoid-Functionalized Gold Nanorods. *Angew. Chem. Int. Ed.* **2016**, *55*, 11237–11241.

(4) Hanske, C.;† González-Rubio, G.;† Hamon, C.; Formentín, P.; Modin, E.; Chuvilin, A.; Guerrero-Martínez, A.; Marsal, L. F.; Liz-Marzán, L. M. Large-Scale Plasmonic Pyramidal Supercrystals via Templated Self-Assembly of Monodisperse Gold Nanospheres. *J. Phys. Chem. C* **2017**, acs.jpcc.6b12161.

(5) Ahijado-Guzmán, R.;† González-Rubio, G.;† Izquierdo, J. G.; Bañares, L.; López-Montero, I.; Calzado-Martín, A.; Calleja, M.; Tardajos, G.; Guerrero-Martínez, A. Intracellular pH-Induced Tip-to-Tip Assembly of Gold Nanorods for Enhanced Plasmonic Photothermal Therapy. *ACS Omega* **2016**, *1*, 388–395.

† These authors contributed equally to this work.

Other Related Publications

(6) Coelho, J. P.; González-Rubio, G.; Delices, A.; Barcina, J. O.; Salgado, C.; Ávila, D.; Peña-Rodríguez, O.; Tardajos, G.; Guerrero-Martínez, A. Polyrotaxane-Mediated Self-Assembly of Gold Nanospheres into Fully Reversible Supercrystals. *Angew. Chem. Int. Ed.* **2014**, *53*, 12751–12755.

(7) Gavilán-Rubio, H.; Coelho, J. P.; González-Rubio, G.; Tardajos, G.; Barcina, J. O.; Salgado, C.; Guerrero-Martínez, A. Thiol-Functionalized IGEPAL{®} Surfactants as

Novel Fluorescent Ligands for the Silica Coating of Gold Nanoparticles. *Isr. J. Chem.* **2016**, *56*, 249–256.

(8) Hamon, C.; Henriksen-Lacey, M.; La Porta, A.; Rosique, M.; Langer, J.; Scarabelli, L.; Montes, A. B. S.; González-Rubio, G.; de Pancorbo, M. M.; Liz-Marzán, L. M.; *et al.* Tunable Nanoparticle and Cell Assembly Using Combined Self-Powered Microfluidics and Microcontact Printing. *Adv. Funct. Mater.* **2016**, *26*, 8053–8061.

(9) González-Rubio, G.; Díaz-Núñez, P.; Rivera, A.; Tardajos, G.; González-Izquierdo, J.; Bañares, L.; Llombart, P.; González-Macdowell, L.; Liz-Marzán, L. M. Peña-Rodríguez, O.; Guerrero-Martínez, A. Femtosecond Laser-Controlled Reshaping of Uniform Gold Nanorod Colloids with Ultra-Narrow Localized Surface Plasmon Resonances. *In preparation*, **2017**.